

AD-A008 472

EVALUATION OF A PROPOSED INS KALMAN  
FILTER IN A DYNAMIC FLIGHT ENVIRONMENT

Jerry E. Hammett

Air Force Institute of Technology  
Wright-Patterson Air Force Base, Ohio

December 1974

DISTRIBUTED BY:

**NTIS**

National Technical Information Service  
U. S. DEPARTMENT OF COMMERCE

EVALUATION OF A PROPOSED  
INS KALMAN FILTER IN A  
DYNAMIC FLIGHT ENVIRONMENT

THESIS

Presented to the Faculty of the School of Engineering  
of the Air Force Institute of Technology

Air University  
in Partial Fulfillment of the  
Requirements for the Degree of  
Master of Science  
by

Jerry E. Hammett, B.S.E.E.  
Major USAF

Graduate Electrical Engineering  
December 1974

Approved for public release; distribution unlimited.

14

UNCLASSIFIED

SECURITY CLASSIFICATION OF THIS PAGE (When Data Entered)

REPORT DOCUMENTATION PAGE		READ INSTRUCTIONS BEFORE COMPLETING FORM
1. REPORT NUMBER GE/EE/74-45	2. GOVT ACCESSION NO.	3. RECIPIENT'S CATALOG NUMBER <b>AD-A008 472</b>
4. TITLE (and Subtitle) EVALUATION OF A PROPOSED INS KALMAN FILTER IN A DYNAMIC FLIGHT ENVIRONMENT		5. TYPE OF REPORT & PERIOD COVERED MS Thesis
7. AUTHOR(s) Jerry E. Hammett Major, USAF		6. PERFORMING ORG. REPORT NUMBER
9. PERFORMING ORGANIZATION NAME AND ADDRESS Air Force Institute of Technology (AFIT-EN) Wright-Patterson AFB, Ohio 45433		8. CONTRACT OR GRANT NUMBER(s)
11. CONTROLLING OFFICE NAME AND ADDRESS Navigation and Weapons Delivery Div. (NVE-2) Air Force Avionics Laboratory Wright-Patterson AFB, Ohio 45433		10. PROGRAM ELEMENT, PROJECT, TASK AREA & WORK UNIT NUMBERS
14. MONITORING AGENCY NAME & ADDRESS (if different from Controlling Office)		12. REPORT DATE December, 1974
		13. NUMBER OF PAGES 187
		15. SECURITY CLASS. (of this report) Unclassified
		15a. DECLASSIFICATION/DOWNGRADING SCHEDULE
16. DISTRIBUTION STATEMENT (of this Report) Approved for public release; distribution unlimited		
17. DISTRIBUTION STATEMENT (of the abstract entered in Block 20, if different from Report) Reproduced by NATIONAL TECHNICAL INFORMATION SERVICE US Department of Commerce Springfield, VA. 22151		
18. SUPPLEMENTARY NOTES Approved for public release; IAW AFR 190-17 <i>Jerry C. Hix</i> JERRY C. HIX, Captain, USAF Director of Information		
19. KEY WORDS (Continue on reverse side if necessary and identify by block number) Kalman Filter Inertial Navigation Optimal Aiding Navigation Covariance Analysis		
20. ABSTRACT (Continue on reverse side if necessary and identify by block number) This report is an evaluation of a proposed Kalman filter for an advanced manned aircraft. The evaluation is performed under simulated flight profiles which include straight and level and maneuvering flight. The aided inertial navigation system is represented by a 54-state linear system error model and the filter by a 17-state error model with decoupled horizontal and vertical channel mechanization. The simulated flight profiles include two hours of straight and level flight and one additional hour of either		

DD FORM 1 JAN 73 1473

EDITION OF 1 NOV 65 IS OBSOLETE

PRICES SUBJECT TO CHANGE  
UNCLASSIFIED

SECURITY CLASSIFICATION OF THIS PAGE (When Data Entered)

UNCLASSIFIED

SECURITY CLASSIFICATION OF THIS PAGE(When Data Entered)

straight and level or maneuvering flight. A comparison of filter effectiveness with the optimal filter is made for the two hour straight and level flight. The decoupled 17-state filter effectiveness is evaluated during one additional hour of maneuvering flight based on the filter performance in straight and level flight for the same time period. In addition, an error budget is determined for both flight profiles. The decoupled 17-state filter is found to provide adequate performance although the level channel velocity errors are twice those of the optimal filter. No consistent conclusions could be drawn from a comparison of the error budgets with the exception that the Doppler induced error increased during maneuvering flight.

1a UNCLASSIFIED

SECURITY CLASSIFICATION OF THIS PAGE(When Data Entered)

### Preface

In the early 1960's, R.E. Kalman presented his theories on optimal filtering and control techniques. The advent of the digital computer has provided the tool for implementation of Kalman's filtering theory. The recent trend toward the use of digital computers onboard advanced aircraft and a more stringent requirement on navigation and weapon delivery accuracy has resulted in the application of filtering techniques to aided inertial navigation systems.

I spent many weeks in pursuit of a competent understanding of Kalman's theory and several months with the CDC-6600 computer in order to obtain the CALCOMP plots of the system state variable error covariances presented throughout this report. The time was well spent in my opinion, but, I am sure there are those in my family who might question the premise.

I would like to express my sincere appreciation to Lt. Peter S. Maybeck, my thesis advisor as well as my instructor in the complexities of filtering theory. I also gratefully acknowledge the assistance of Mr. Richard M. Reeves and Mr. Ed Hamilton of the Air Force Avionics Laboratory for providing computer programs and other documents related to this study and for sharing their expertise and knowledge of Kalman filter design theory.

Jerry E. Hammett

Table of Contents

	<u>Page</u>
Preface . . . . .	ii
List of Figures . . . . .	v
List of Tables . . . . .	ix
List of Symbols . . . . .	xi
Abstract . . . . .	xvii
I. Introduction . . . . .	1
Aided-Inertial System . . . . .	2
Kalman Filter . . . . .	3
Basic Assumptions . . . . .	4
Type of Filter Employed. . . . .	5
Limitations of the Study . . . . .	7
II. Coordinate Systems, Transformation Matrices, and Angular Rates . . . . .	9
Coordinate Frame Definitions. . . . .	9
Inertial Reference Frame . . . . .	9
Earth-fixed Frame. . . . .	11
Navigation Frame . . . . .	11
Path Frame . . . . .	12
Alpha Wander Frame . . . . .	12
Transformation Matrices . . . . .	14
Inertial to Earth Transformation . . . . .	14
Earth to Navigation Frame. . . . .	15
Navigation to Path Frame . . . . .	17
Navigation to Alpha Wander Frame . . . . .	17
Angular Rates . . . . .	17
III. Kalman Filter Equations . . . . .	24
System Model Equations . . . . .	25
Filter Equations. . . . .	26
IV. System Model. . . . .	31
State Variable Definition and Initial Conditions . . . . .	31
Plant Error States . . . . .	39
Error Source Models . . . . .	40
Radar Position Error Equations . . . . .	45
Doppler Error Equations. . . . .	47
INS Error Source Models . . . . .	52
Altimeter Error Source Model . . . . .	59
System Measurement Equation . . . . .	61

Table of Contents

	<u>Page</u>
V. Filter Design . . . . .	66
The Optimal Filter . . . . .	67
Reduced Order Filters . . . . .	67
Decoupled 17-State Filter . . . . .	68
VI. Test Conditions . . . . .	77
Basic Flight Profile . . . . .	78
Flight Profile with Dynamic Maneuvers . .	102
Error Budget Determination . . . . .	129
VII. Conclusions and Recommendations . . . . .	163
Conclusions . . . . .	163
Recommendations . . . . .	163
Bibliography. . . . .	165
Vita. . . . .	167

List of Figures

<u>Figure</u>		<u>Page</u>
1	Indirect Feedback Kalman Filter . . . . .	6
2	Coordinate Systems. . . . .	10
3	Nav to Path Individual Coordinate Transformations . . . . .	16
4	Navigation to Alpha Wander Transformation . .	17
5	$F_{11}$ Matrix (Raides Error Model) . . . . .	41
6	Error Source Models for Random Variables . .	43
7	Doppler Error Source Model. . . . .	52
8	Gyro Error Source Model . . . . .	54
9	Accelerometer Error Source Model. . . . .	56
10	Altimeter Error Source Model. . . . .	60
11	System Measurement H Matrix . . . . .	64
12	Decoupled 17-State Filter $F_{11}$ Sub-matrix . .	73
13	Decoupled 17-State Filter $F_{12}$ and $F_{13}$ Sub-matrices. . . . .	74
14	Baseline Flight Profile . . . . .	79
15	Optimal Filter x RMS Position Error (ft). . .	81
16	Optimal Filter y RMS Position Error (ft). . .	82
17	Optimal Filter z RMS Position Error (ft). . .	83
18	Optimal Filter x RMS Velocity Error (ft/sec). .	84
19	Optimal Filter y RMS Velocity Error (ft/sec). .	85
20	Optimal Filter z RMS Velocity Error (ft/sec). .	86
21	Optimal Filter x RMS Tilt Error (rad) . . . .	87
22	Optimal Filter y RMS Tilt Error (rad) . . . .	88
23	Optimal Filter z RMS Tilt Error (rad) . . . .	89



List of Figures

<u>Figure</u>		<u>Page</u>
24	(13+4) Filter x RMS Position Error (ft). . .	90
25	(13+4) Filter y RMS Position Error (ft). . .	91
26	(13+4) Filter z RMS Position Error (ft). . .	92
27	(13+4) Filter x RMS Velocity Error (ft/sec). . .	93
28	(13+4) Filter y RMS Velocity Error (ft/sec). . .	94
29	(13+4) Filter z RMS Velocity Error (ft/sec). . .	95
30	(13+4) Filter x RMS Tilt Error (rad) . . . .	96
31	(13+4) Filter y RMS Tilt Error (rad) . . . .	97
32	(13+4) Filter z RMS Tilt Error (rad) . . . .	98
33	Dynamic Flight Profile . . . . .	103
34	Decoupled Filter Baseline x RMS Position Error. . . . .	106
35	Decoupled Filter Baseline y RMS Position Error. . . . .	107
36	Decoupled Filter Baseline z RMS Position Error. . . . .	108
37	Decoupled Filter Baseline x RMS Velocity Error. . . . .	109
38	Decoupled Filter Baseline y RMS Velocity Error. . . . .	110
39	Decoupled Filter Baseline z RMS Velocity Error. . . . .	111
40	Decoupled Filter Baseline x RMS Tilt Error .	112
41	Decoupled Filter Baseline y RMS Tilt Error .	113
42	Decoupled Filter Baseline z RMS Tilt Error .	114
43	Decoupled Filter Maneuvering x RMS Position Error . . . . .	118
44	Decoupled Filter Maneuvering y RMS Position Error . . . . .	119

List of Figures

<u>Figure</u>		<u>Page</u>
45	Decoupled Filter Maneuvering z RMS Position Error . . . . .	120
46	Decoupled Filter Maneuvering x RMS Velocity Error . . . . .	121
47	Decoupled Filter Maneuvering y RMS Velocity Error . . . . .	122
48	Decoupled Filter Maneuvering z RMS Velocity Error . . . . .	123
49	Decoupled Filter Maneuvering x RMS Tilt Error . . . . .	124
50	Decoupled Filter Maneuvering y RMS Tilt Error . . . . .	125
51	Decoupled Filter Maneuvering z RMS Tilt Error . . . . .	126
52	Straight and Level x RMS Position Error Budget . . . . .	131
53	Straight and Level y RMS Position Error Budget . . . . .	132
54	Straight and Level z RMS Position Error Budget . . . . .	133
55	Straight and Level x RMS Velocity Error Budget . . . . .	134
56	Straight and Level y RMS Velocity Error Budget . . . . .	135
57	Straight and Level z RMS Velocity Error Budget . . . . .	136
58	Straight and Level x RMS Tilt Error Budget . . . . .	137
59	Straight and Level y RMS Tilt Error Budget . . . . .	138
60	Straight and Level z RMS Tilt Error Budget . . . . .	139

List of Figures

<u>Figure</u>		<u>Page</u>
61	Maneuvering x RMS Position Error Budget . . .	140
62	Maneuvering y RMS Position Error Budget . . .	141
63	Maneuvering z RMS Position Error Budget . . .	142
64	Maneuvering x RMS Velocity Error Budget . . .	143
65	Maneuvering y RMS Velocity Error Budget . . .	144
66	Maneuvering z RMS Velocity Error Budget . . .	145
67	Maneuvering x RMS Tilt Error Budget . . . . .	146
68	Maneuvering y RMS Tilt Error Budget . . . . .	147
69	Maneuvering z RMS Tilt Error Budget . . . . .	148
70	Average Error Trend . . . . .	159

List of Tables

<u>Table</u>		<u>Page</u>
I	System 54-State Error Vector Definition. . .	32
II	Elements of $R_g$ Matrix. . . . .	65
III	Filter 17-State Error Vector Definition. . .	70
IV	Decoupled 17-State Filter $Q'$ Elements. . . .	72
V	RMS Errors of INS Plant States . . . . .	99
VI	RMS Errors of INS Plant States . . . . .	100
VII	Dynamic Flight Profile Data. . . . .	104
VIII	Straight and Level RMS Errors of INS Plant States . . . . .	116
IX	Maneuvering RMS Errors of INS Plant States .	127
X	Comparison of Decoupled 17-State Filter Average RMS Errors . . . . .	128
XI	Plant Error States Straight and Level RMS Errors . . . . .	149
XII	Plant + Gyro Error States Straight and Level RMS Errors . . . . .	150
XIII	Plant + Gyro + Accelerometer Error States Straight and Level RMS Errors . . . . .	151
XIV	Plant + Gyro + Accelerometer + Doppler Error States Straight and Level RMS Errors .	152
XV	Plant + Gyro + Accelerometer + Doppler + Altimeter Error States Straight and Level RMS Errors . . . . .	153
XVI	Plant Error States Maneuvering RMS Errors. .	154
XVII	Plant + Gyro Error States Maneuvering RMS Errors . . . . .	155
XVIII	Plant + Gyro + Accelerometer Error States Maneuvering RMS Errors . . . . .	156
XIX	Plant + Gyro + Accelerometer + Doppler Error States Maneuvering RMS Errors. . . .	157

List of Tables

<u>Table</u>		<u>Page</u>
XX	Plant + Gyro + Accelerometer + Doppler + Altimeter Error States Maneuvering RMS Errors . . . . .	158
XXI	Percent Contribution to Variable Error (Straight and Level Flight). . . . .	160
XXII	Percent Contribution to Variable Error (Maneuvering Flight) . . . . .	161

List of Symbols

<u>Symbol</u>	<u>Defined or First used</u>	<u>Symbol</u>	<u>Defined or First used</u>
$ V $	Page 2	$\underline{\omega}_{ie}$	Page 14
$\bar{\Omega}$	Figure 2	$\psi$	Page 15
$\mathcal{U}$	Figure 2	$\phi$	Page 15
$X_I$	Figure 2	$\theta$	Page 15
$X$	Figure 2	$\underline{c}_n^p$	Equation 4
$\Omega t$	Figure 2	$\underline{c}_n^{\cdot}$	Figure 3
$Z_I$	Figure 2	$\underline{c}_n^{\cdot\cdot}$	Figure 3
$Z$	Figure 2	$\underline{c}_n^p$	Figure 3
$Y_I$	Figure 2	$X_N$	Figure 4
$Y$	Figure 2	$X_W$	Figure 4
$l$	Figure 2	$\underline{\omega}_{ie}^e$	Equation 6
$L$	Figure 2	$\underline{\omega}_{ie}^n$	Equation 6
$L_c$	Figure 2	$\underline{\omega}_{en}$	Equation 7
$X_n$	Figure 2	$\dot{L}$	Equation 8
$Y_n$	Figure 2	$V_N$	Equation 8
$Z_n$	Figure 2	$\dot{l}$	Equation 9
$h$	Figure 2	$V_W$	Equation 9
$Z_a$	Figure 2	$\bar{e}_x$	Page 19
$\alpha$	Figure 2	$\bar{e}_z$	Page 19
$\underline{c}_a^b$	Page 12	$\underline{\omega}_{en}^n$	Equation 10
$\underline{c}_e^n$	Page 13	$\rho_x^n$	Equation 11
$\underline{c}_i^e$	Page 13	$\rho_y^n$	Equation 12
$\underline{c}_n^a$	Page 13	$\rho_z^n$	Equation 13
$\underline{c}_i^n$	Page 13	$\dot{\omega}_{en}^n$	Equation 14

List of Symbols

<u>Symbol</u>	<u>Defined or First used</u>	<u>Symbol</u>	<u>Defined or First used</u>
$\dot{\rho}_x^n$	Equation 15	$\underline{P}$	Page 24
$A_W$	Equation 15	$\dot{\underline{x}}_s$	Equation 32
$\dot{\rho}_y^n$	Equation 16	$\underline{x}_s$	Page 25
$A_N$	Equation 16	$\underline{F}_s$	Page 25
$\dot{\rho}_z^n$	Equation 17	$\underline{G}_s$	Page 25
$\underline{\omega}_{in}^n$	Equation 18	$\underline{w}_s$	Page 25
$\omega_x$	Equation 18	$\underline{Q}_s$	Equation 33
$\omega_y$	Equation 18	$\underline{Z}_s$	Page 26
$\omega_z$	Equation 18	$\underline{H}_s$	Page 26
$\underline{\omega}_{ie}^a$	Equation 19	$\underline{v}_s$	Page 26
$\Omega_x$	Equation 19	$\underline{R}_s$	Equation 35
$\Omega_y$	Equation 19	$\dot{\underline{x}}_f$	Equation 37
$\Omega_z$	Equation 19	$\underline{x}_f$	Page 27
$\underline{\omega}_{en}^a$	Equation 20	$\underline{F}_f$	Page 27
$\dot{\underline{\omega}}_{en}^a$	Equation 21	$\underline{G}_f$	Page 27
$\underline{\omega}_{in}^a$	Equation 22	$\underline{w}_f$	Page 27
$\underline{\omega}_{ea}^a$	Equation 23	$\underline{Q}_f$	Equation 38
$\underline{\omega}_{na}^a$	Equation 24	$\underline{Z}_f$	Page 27
$\rho_x^a$	Equation 25	$\underline{H}_f$	Page 27
$\rho_y^a$	Equation 26	$\underline{V}_f$	Page 27
$\rho_z^a$	Equation 27	$\underline{R}_f$	Equation 40
$\dot{\underline{\omega}}_{na}^a$	Equation 28	$\hat{\underline{x}}_f$	Equation 41
$\dot{\underline{\omega}}_{ea}^a$	Equation 29	$\hat{\underline{x}}_f$	Equation 41
$\underline{\omega}_{ia}^a$	Equation 30	$\dot{\underline{P}}_f$	Equation 42

List of Symbols

<u>Symbol</u>	<u>Defined or First used</u>	<u>Symbol</u>	<u>Defined or First used</u>
$\underline{P}_f$	Equation 42	$\epsilon_{x_1}$	Table I
-	Page 28	$\epsilon_{y_1}$	Table I
+	Page 28	$\epsilon_{z_1}$	Table I
$\underline{K}_f$	Page 28	$b_x$	Table I
$\sum_s$	Page 28	$b_y$	Table I
$( )^T$	Page 28	$b_z$	Table I
$\hat{x}_0$	Equation 46	$K_1$	Table I
$\underline{P}_0$	Equation 47	$K_2$	Table I
$\mu$	Page 29	$\delta_1$	Table I
$E(x)$	Equation 48	$\delta_2$	Table I
$\sigma^2$	Page 29	$\delta_h$	Table I
$\text{Var}(x)$	Equation 49	$\epsilon_{x_2}$	Table I
$E(x)$	Equation 50	$\epsilon_{y_2}$	Table I
$\text{Cov}(x)$	Equation 51	$\epsilon_{x_2}$	Table I
$\delta_x$	Table I	$DX_x$	Table I
$\delta_y$	Table I	$DX_y$	Table I
$\delta_z$	Table I	$DY_x$	Table I
$\delta_{v_x}$	Table I	$DY_y$	Table I
$\delta_{v_y}$	Table I	$DZ_y$	Table I
$\delta_{v_z}$	Table I	$DZ_z$	Table I
$\delta\phi_x$	Table I	$DX_{xy}$	Table I
$\delta\phi_y$	Table I	$DY_{xy}$	Table I
$\delta\phi_z$	Table I	$DZ_{xy}$	Table I
$\delta\theta_z$	Table I	$GSF_x$	Table I



List of Symbols

<u>Symbol</u>	<u>Defined or First used</u>	<u>Symbol</u>	<u>Defined or First used</u>
$GSF_y$	Table I	$\sigma_{V_x K_2}^2$	Equation 54
$GSF_z$	Table I	$\sigma_{V_y K_1}^2$	Equation 55
$XG_y$	Table I	$\sigma_{V_y K_2}^2$	Equation 56
$XG_z$	Table I	$\sigma_{V_x}^2 \delta_1$	Equation 57
$YG_x$	Table I	$\sigma_{V_x}^2 \delta_2$	Equation 58
$YG_z$	Table I	$\sigma_{V_y}^2 \delta_1$	Equation 59
$ZG_x$	Table I	$\sigma_{V_y}^2 \delta_2$	Equation 60
$ZG_y$	Table I	$q'$	Equation 61
$ASF_x$	Table I	$q_i$	Page 39
$ASF_y$	Table I	$w(t)$	Page 40
$ASF_z$	Table I	$F_{11}$	Figure 5
$XA_y$	Table I	$\beta$	Figure 6
$XA_z$	Table I	$\tau$	Page 44
$YA_x$	Table I	$\Delta \hat{x}_n$	Page 45
$YA_z$	Table I	$\Delta \hat{x}_w$	Page 45
$ZA_x$	Table I	$\delta \hat{x}$	Equation 68
$ZA_y$	Table I	$\delta \hat{y}$	Equation 68
$\delta_{ge}$	Table I	$\Delta \hat{R}_N$	Equation 70
$\delta_{gn}$	Table I	$\Delta \hat{R}_E$	Equation 70
$\delta_{gz}$	Table I	$\Delta \hat{L}$	Equation 71
$\sigma_{V_x V_y}^2$	Equation 52	$r$	Page 46
$V_{x_0}$	Equation 52	$R_0$	Page 46

List of Symbols

<u>Symbol</u>	<u>Defined or First used</u>	<u>Symbol</u>	<u>Defined or First used</u>
$v_{yo}$	Equation 52	$e$	Page 46
$\sigma^2_{v_x K_1}$	Equation 53	$\hat{L}_{true}$	Equation 72
$\Delta \hat{l}$	Equation 73	$\Phi$	Page 50
$\hat{l}_{true}$	Equation 74	$\delta v$	Equation 88
$\Delta \hat{\alpha}$	Equation 75	$v_c$	Equation 88
$\delta \hat{\theta}_z$	Equation 75	$v_T$	Equation 88
$\hat{\alpha}_{true}$	Equation 76	$T$	Page 51
$c_e^a$	Equation 77	$\delta$	Page 51
$v$	Page 48	$K$	Page 51
$\Delta$	Page 48	$v_x$	Equation 91
$v_{Dx}$	Equation 78	$v_y$	Equation 91
$v_{Dy}$	Equation 79	$\beta_1$	Figure 7
$\theta_s$	Page 48	$\beta_2$	Figure 7
$\Delta v_x$	Equation 80	$\beta_g$	Figure 8
$\Delta v_y$	Equation 81	$F_{12}$	Equation 93
$\Delta v_{xm}$	Equation 82	$F_{13}$	Equation 94
$\Delta v_{ym}$	Equation 83	$\beta_a$	Figure 9
$v_c^c$	Page 49	$F_{14}$	Equation 95
$v_D^P$	Page 49	$F_{15}$	Equation 96
$v_D$	Page 49	$F_{16}$	Equation 97
$v_T$	Page 49	$F_{33}$	Equation 98
$\delta v_D$	Page 49	$F_{66}$	Equation 105
$v_D^P$	Equation 85	$d_x$	Equation 105

List of Symbols

<u>Symbol</u>	<u>Defined or First used</u>	<u>Symbol</u>	<u>Defined or First used</u>
$V_T^P$	Equation 85	$d_y$	Equation 105
$\delta V_D^P$	Equation 85	$d_a$	Equation 105
$V_T^T$	Equation 86	$\beta_h$	Equation 113
$\eta(t)$	Equation 113		
$F_{22}$	Equation 114		
$\beta_k$	Equation 114		
$\beta_d$	Equation 114		
$\delta \hat{z}$	Equation 123		
$\hat{h}$	Equation 123		
$\sigma_x^2$	Equation 126		
$\sigma_y^2$	Equation 126		
$\sigma_z^2$	Equation 126		
$\sigma_v^2$	Equation 126		
$\sigma_{v_y}^{2x}$	Equation 126		
$q'_f$	Equation 128		
$\sigma_{v_x}^2$	Equation 132		
$\sigma_{v_y}^2$	Equation 133		
$\sigma_{v_x}^2 \delta$	Equation 134		
$\sigma_{v_y}^2 \delta$	Equation 135		
H	Table V		
L	Table V		

Abstract

This report is an evaluation of a proposed Kalman filter for an advanced manned aircraft. The evaluation is performed under simulated flight profiles which include straight and level and maneuvering flight. The aided inertial navigation system is represented by a 54-state linear system error model and the filter by a 17-state error model with decoupled horizontal and vertical channel mechanization. The simulated flight profiles include two hours of straight and level flight and one additional hour of either straight and level or maneuvering flight. A comparison of filter effectiveness with the optimal filter is made for the two hour straight and level flight. The decoupled 17-state filter effectiveness is evaluated during one additional hour of maneuvering flight based on the filter performance in straight and level flight for the same time period. In addition, an error budget is determined for both flight profiles. The decoupled 17-state filter is found to provide adequate performance although the level channel velocity errors are twice those of the optimal filter. No consistent conclusions could be drawn from a comparison of the error budgets with the exception that the Doppler induced error increased during maneuvering flight.

EVALUATION OF A PROPOSED  
INS KALMAN FILTER IN A  
DYNAMIC FLIGHT ENVIRONMENT

I. Introduction

This report is an evaluation of a Kalman filter design proposed for use with navigation and weapons delivery systems of advanced aircraft. The evaluation is a subproblem of a current research and development topic of interest to the Navigation Division of the Air Force Avionics Laboratory at Wright-Patterson Air Force Base as well as other government and civilian agencies. A tentative reduced order filter was designed previously to meet performance requirements and computer loading constraints, but was only evaluated in a benign flight environment. Thus, an evaluation of filter performance during a maneuvering aircraft mission profile was desired. A CDC-6600 digital computer and covariance analysis techniques were used to obtain the required data.

The development of this study is presented by chapters in the following sequence. Preliminary information such as reference frames, coordinate transformations, and angular rates are presented in the second chapter. Chapter III is a development of the Kalman filter equations required to solve the navigation problem. The fifty-four state system model selected for the study is presented in chapter IV while the proposed filter design of the decoupled seventeen

8  
state filter is defined in chapter V. Chapter VI delineates the basic and dynamic test flight conditions and the error budget determination. The results and conclusions comprise the final chapter of this study.

### Aided-Inertial System

The basic idea of the aided-inertial system is to combine external navigation and attitude information (such as position, velocity, and attitude) received from radar, doppler, and a central air data computer with the inertial navigation system (INS) data to provide highly accurate position and velocity information. Since the INS generally presents accurate short term or high frequency information and the aiding systems generally provide more accurate long term or low frequency information, Kalman filtering theory applies to this combination of data quite readily yielding a profound improvement in navigation system accuracy.

The navigation sensors considered in this study include an inertial measurement unit (IMU), a Doppler radar, a position fix radar, and a central air data computer (CADC) which provides barometric altitude. The basic IMU is considered to be of the type currently operational in the Air Force with navigation accuracy of 0.5 nautical mile per hour. The position fix radar is assumed to have an accuracy of  $\pm 500$  feet. The Doppler radar accuracy is dependent on the aircraft velocity with a relationship of  $3.48 \times 10^{-3} |V|$  where  $|V|$  is the magnitude of the aircraft path velocity in feet per second. The altimeter is assumed

to have an accuracy of  $\pm 20$  feet (Ref 1.). An on-board computer is used to apply the Kalman filter equations, i.e., to compute the Kalman gains or weighting coefficients, to estimate the state variables, and to apply the control to the INS.

#### Kalman Filter

The Kalman filter is an optimal recursive data processing algorithm located in the on-board computer or central processor. The filter combines all available measurement data, plus prior knowledge of the system and measuring devices to produce an estimate of the system states in such a manner as to minimize the resulting errors statistically. In more easily understood terms, the filter provides the best estimate possible subject to certain modeling assumptions.

The filter will act to optimize the attitude, position, and velocity information accuracy by weighting each data source heavily in the frequency ranges where it provides more accurate information, and suppressing it in the region where it is less accurate. The inertial system provides good high frequency information, but it drifts slowly and therefore exhibits poor low frequency performance. On the other hand, the external aids generally exhibit good low frequency information but are subject to high frequency noise. Therefore, the filter will use the good low frequency external information to damp out the slowly growing errors in the inertial system.

Basic Assumptions. The Kalman filter can be shown to be the best filter of any possible form based on three assumptions. These assumptions are system linearity, white noise drivers, and Gaussian noise distribution.

Although the system itself may be nonlinear, formulation of an approximate linear error state space model make possible linear analysis. The justification for the linear model is based on two points. In the case of aided INS systems, the use of linear error state space models has proven to yield very adequate representations. The techniques of linear systems analysis are well developed and better understood than those of nonlinear analysis.

The white noise assumption implies that the noise is not correlated in time and also has equal power at all frequencies. If, in fact, a time-correlated noise is required to adequately model the system, it can be produced by passing a white noise through a linear shaping filter. The system can then be modeled with an augmented state vector as a linear system driven by white noise.

Gaussianity pertains to the distribution of amplitudes of the noise and implies that at any single point in time the probability density function of the amplitude takes on the shape of a normal bell-shaped curve. The assumption of Gaussian noise amplitude is justified by the fact that system or measurement noise is typically caused by a number of sources. It can be shown mathematically that when a number of independent random variables are added the



resultant effect is very nearly a Gaussian probability density even though the individual densities are not Gaussian. (Ref 2:8-21 and Ref 9:4-6).

Under the assumptions of a white Gaussian noise, the entire shape of the density describing the noise is specified by its first two moments. These three assumptions greatly simplify the mathematics of the problem and, in fact, make them tractable. (Ref 2:3-11 and Ref 3:132).

Type of Filter Employed. An indirect filter estimates the errors in the navigation information using the difference between the INS and external sensor data to drive the filter. This is in contrast to the direct Kalman filter which uses the total state space formulation. The indirect filter is implemented in a feedback configuration which minimizes the INS errors by applying the weighted estimates as a control or correcting signal. (See Figure 1). Since the INS is corrected after each measurement sample, the predicted error states and measurement differences at the next sample time will be zero. Therefore, there is no need to propagate the error state variable estimates.

A discussion of the relative merits of both feed forward and feed back and direct versus indirect Kalman filter implementation is found in Reference 4 pages 1-10. It is not the intent of this study to explore the development of Kalman filter theory but to evaluate a proposed filter design. The reader who is unfamiliar with Kalman filter theory or who seeks more detailed information is

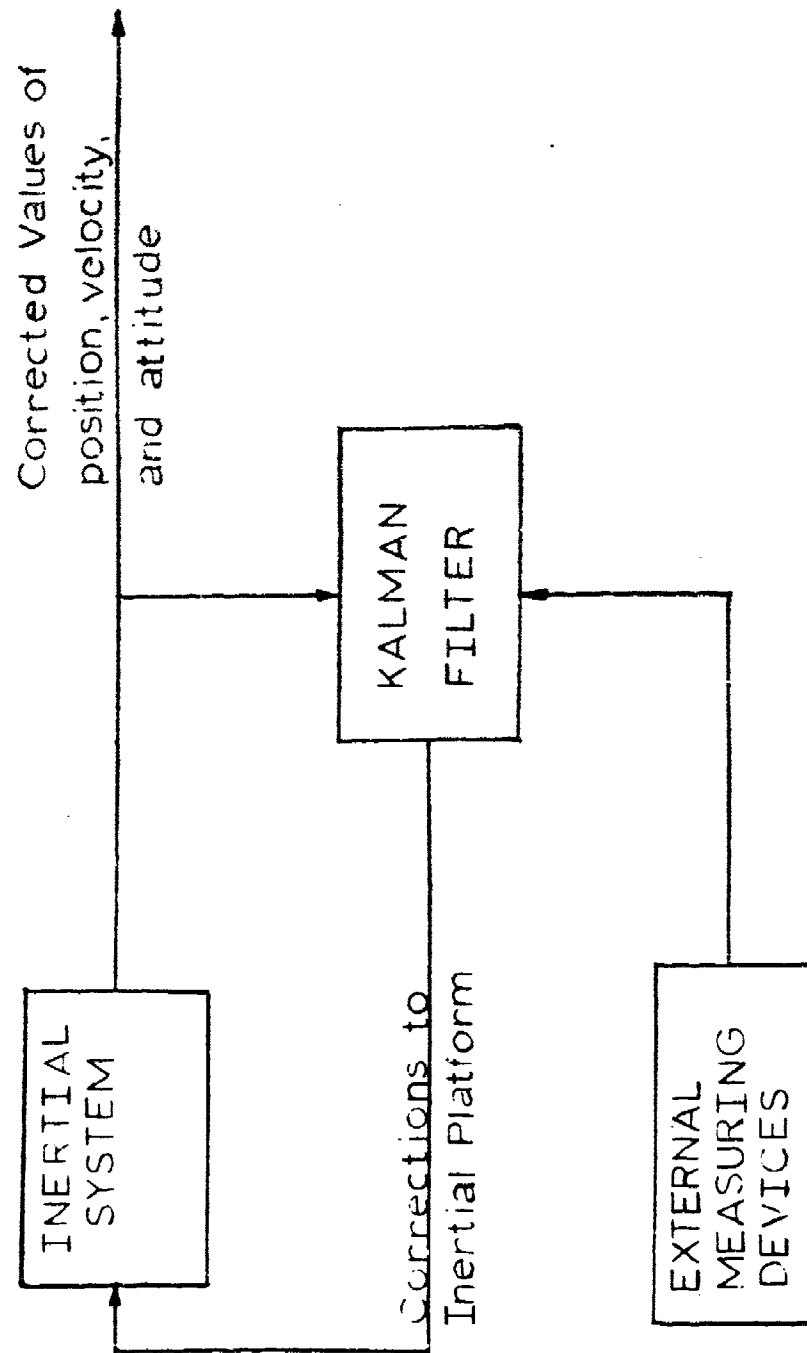


Figure 1. Indirect Feedback Kalman Filter

referred to References 1 through 5 of the bibliography.

### Limitations of the Study

It is recognized that no matter what system reference model is selected, it will only be an approximation since the complex real world dynamics are not modeled exactly. The evaluation of the filter design is sensitive to erroneous reference system models and statistics; thus great care was used to model the reference system as accurately as possible in the computer simulation in order to yield meaningful results.

The system reference model was provided by the Air Force Avionics Laboratory and contains fifty-four error state variables. This reference model was used for the evaluation in both the "baseline" or straight and level flight regime and the highly dynamic or maneuvering flight environment.

Two flight profiles were chosen to simulate the aircraft environment during filter evaluation. The baseline data utilized a two hour (7200 sec) straight and level unaccelerated flight profile and allowed the system errors to reach approximate "steady state" conditions. The second flight profile simulated a maneuvering aircraft environment including horizontal and vertical accelerations, turns, climbs, dives, and sinusoidal heading changes. This dynamic portion of the flight had a duration of one hour (3600 sec) and utilized the baseline data at 6300 seconds for steady state initial conditions.

9  
C  
An exceptional amount of time was spent in interfacing the three computer programs required to complete the evaluation. The computer resources required for each data run required two to four day turn-around times thus extending the data collection time.

## II. Coordinate Systems, Transformation Matrices, and Angular Rates

### Coordinate Frame Definitions

Five different coordinate frames are defined to describe the problem graphically and conveniently. These are the inertial reference frame, the Earth-fixed frame, the navigation frame, the path frame, and the alpha wander frame. (See Figure 2).

Inertial Reference Frame. The inertial coordinate system is fixed with its origin at the center of the earth and is nonrotating with respect to inertial space. The coordinate system thus defined is not truly an inertial system, but for the error analysis of a vehicle moving near the earth, the errors introduced by this definition of inertial space are negligible. The axes of the coordinate system form a right hand set with the z-axis pointing from the center of the Earth through the North Pole in alignment with the Earth's spin axis and the +x-axis pointing to Ares (Ref 6:32).

Earth-fixed Frame. The Earth-fixed reference frame is identical to the inertial reference system except that it is nonrotating with respect to the Earth. The axes of this coordinate system are oriented with the z-axis directed outward through the North Pole, the x-axis directed through the intersection of the Greenwich meridian and the equator, and the y-axis forms the third member of the right hand set.

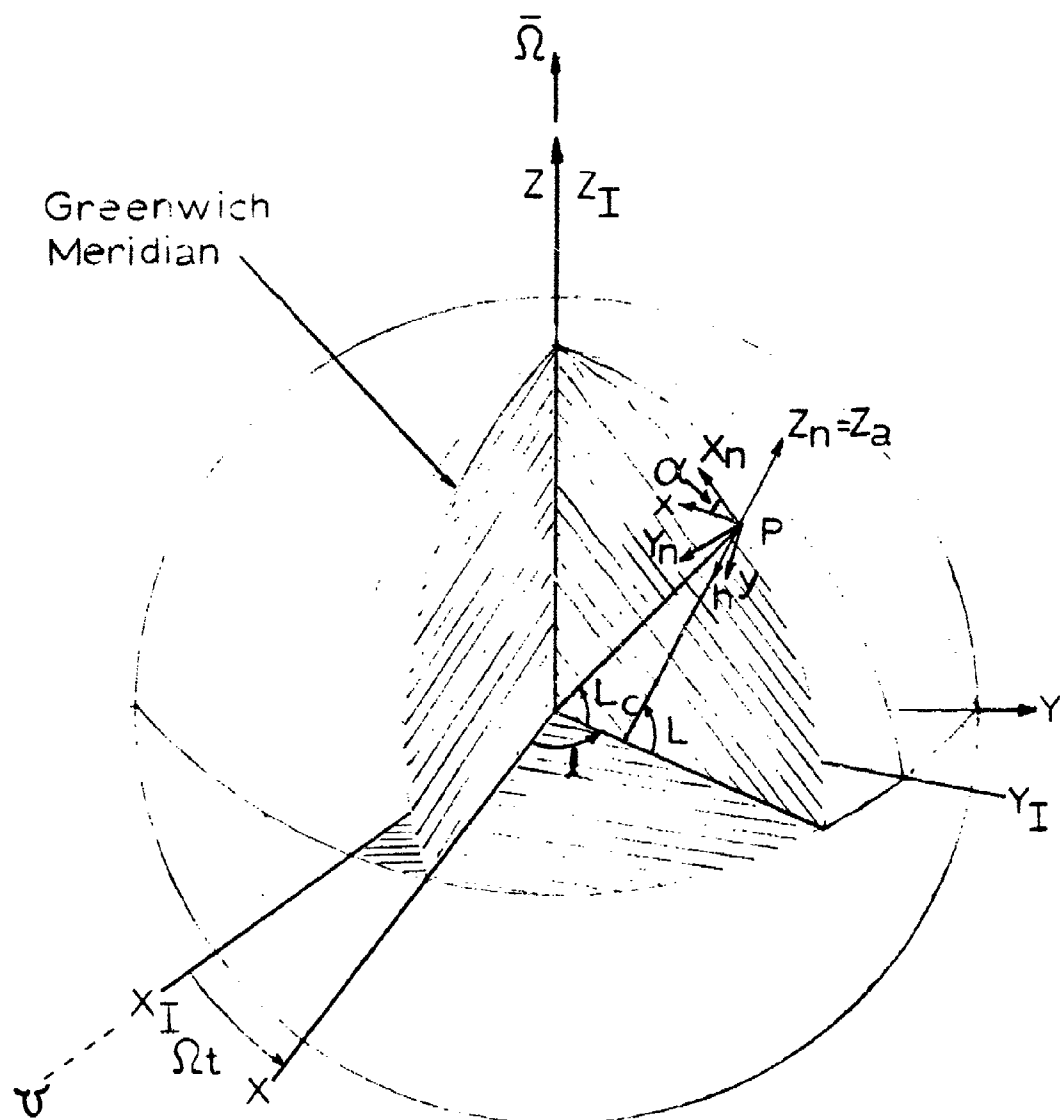


Figure 2. Coordinate Systems

Since this frame is nonrotating with respect to the Earth, any point on the Earth's surface can be specified by a set of Euler angle rotations in the Earth fixed frame,  $L$  about the x-axis (latitude) and  $l$  about the z-axis (longitude). (Ref 6:32).

Navigation Frame. The navigation frame is the frame in which the navigation problem is solved. The position, velocity, and attitude errors are expressed in navigation coordinates. Since the problem involves a gimballed platform which remains essentially locally level at all times, the z-axis of the navigation frame ( $Z_n$ ) remains perpendicular to the Earth (positive upward). The x-axis ( $X_n$ ) always points North and the y-axis ( $Y_n$ ) points West to complete the right-handed orthogonal set (Ref 6:33).

It should be noted that although the INS performs computations based on an elliptical Earth model, utilizing a rotation about the Earth centered x-axis through an Euler angle of geographic latitude ( $L$ ), the Kalman filter has been shown to provide reasonable accuracy utilizing a spherical Earth model with Euler angle rotation through the geocentric latitude ( $L_c$ ).

Path Frame. The path frame is defined with its origin at the center of gravity of the vehicle and is aligned such that the x-axis coincides with the total vehicle velocity. The y-axis is aligned with the right wing of the vehicle, and the z-axis ( $h$ ) forms the third member of the right-hand orthogonal triad and points down with the aircraft

in level upright flight (Ref 7:2).

Alpha Wander Frame. The alpha wander frame is defined to be centered at the navigation frame origin. The z-axis coincides with the z-axis of the navigation frame (positive upward). The x-axis and y-axis are in the plane of the x and y axes of the navigation frame, but are rotated about the z-axis by the angle alpha. Alpha is defined as positive when rotation is counterclockwise as seen from above. The alpha wander frame and navigation frame are identical when alpha is zero.

#### Transformation Matrices

First, a description of the notation to be used in the transformation of matrices is in order. The transformation matrices will all be designated as  $\underline{C}_a^b$  matrices where the transformation is from the a-reference frame to the b-reference frame. Thus  $\underline{C}_a^b$  is read as "the transformation matrix from a to b." This matrix is a direction cosine matrix which transforms the components of a vector in the a-reference frame to a corresponding set of components in the b-reference frame through from one to several rotations about primary axes. Each set of primary axes will usually change after a rotation is completed.

The transformation matrices derived may be utilized in various ways to accomplish the desired result. The mathematics involved in these manipulations can be shown to be sound theoretically.

Typical examples of the matrices used include such



transformations as  $\underline{C}_e^n$ , which is the transformation from Earth to navigation frame,  $\underline{C}_1^e$  - the transformation from inertial to navigation frame, and  $\underline{C}_n^a$  - the transformation from navigation to the alpha wander coordinate system.

These transformation matrices may be applied to vectors, which may be coordinatized in any frame, as well as other matrices. A typical example would be to apply  $\underline{C}_e^i$  to  $\underline{V}_{en}^e$  which gives the velocity of the navigation frame with respect to the Earth centered frame transformed from Earth to inertial frame coordinates.

In order to transform vector quantities such as positions and velocities from one of the above coordinate frames to another it is convenient to derive a set of time varying transformation matrices. These transformation matrices will be used in the development of the simulation equations. To obtain the inverse transformations the inverse matrix is used which is equal to the transpose for direction cosine matrices and their products. Total transformations from one reference frame through a second frame to a third reference frame are made by multiplying the individual transformation matrices in the proper order. The convention used here is that the transformation operates from the subscripted reference frame to the superscripted frame. The proper multiplication order is such that the subscripts and superscripts can be thought of as a cancellation:

$$\underline{C}_1^n = \underline{C}_e^n \underline{C}_1^e \quad (1)$$

Inertial to Earth Transformation. The transformation from the inertial reference frame to the Earth-fixed frame simply involves a rotation of the Earth-fixed axes about the z-axis through an angle equal to the Earth angular rate, which is constant, multiplied by the time of rotation from some arbitrary time  $t=0$ . By projecting vector components of the inertial frame along the axes of the Earth-fixed frame and utilizing the direction cosines in the transformation matrix we obtain

$$\underline{C}_i^e = \begin{bmatrix} \cos \Omega t & \sin \Omega t & 0 \\ -\sin \Omega t & \cos \Omega t & 0 \\ 0 & 0 & 1 \end{bmatrix} \quad (2)$$

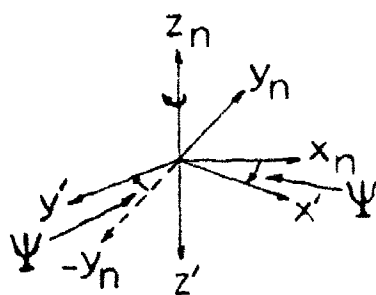
where  $\Omega = \omega_{ie}$ , the angular velocity of the Earth with respect to the inertial reference frame.

Earth to Navigation Frame. The transformation from the Earth-fixed to navigation reference frame involves two rotations. The initial alignment of the navigation frame is such that the  $X_n$ -axis is coincident with the  $Z_e$ -axis and the  $Z_n$ -axis is coincident with the  $X_e$ -axis. The rotation sequence used for the study was to first rotate about the  $Z_e$ -axis through an angle  $l$  (longitude) followed by a second rotation about the rotated  $Y_n'$ -axis through an angle  $L$  (latitude).

$$\begin{aligned}
 \underline{C}_e^n &= \begin{bmatrix} \cos L & 0 & -\sin L \\ 0 & 1 & 0 \\ \sin L & 0 & \cos L \end{bmatrix} \begin{bmatrix} 0 & 0 & 1 \\ \sin l & -\cos l & 0 \\ \cos l & \sin l & 0 \end{bmatrix} \\
 &= \begin{bmatrix} -\sin l \cos L & -\sin L \sin l & \cos L \\ \sin l & -\cos l & 0 \\ \cos L \cos l & \cos L \sin l & \sin L \end{bmatrix} \quad (3)
 \end{aligned}$$

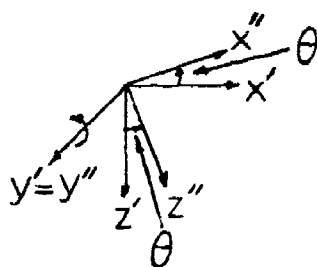
Navigation to Path Frame. The derivation of the transformation matrix from the navigation to the path frame involves three rotations. The first rotation is performed about the z-axis through the angle  $\psi$  (the aircraft heading angle measured clockwise from North) followed by a rotation about the y'-axis through the angle  $\theta$  (the aircraft pitch angle). The third rotation is about the x''-axis through an angle  $\phi$  (the aircraft roll angle). See Figure 3. The resultant transformation matrix is shown below. (Ref 1:121-123 and Ref 6:37)

$$\begin{aligned}
 \underline{C}_n^p &= \begin{bmatrix} 1 & 0 & 0 \\ 0 & \cos \phi & \sin \phi \\ 0 & -\sin \phi & \cos \phi \end{bmatrix} \begin{bmatrix} \cos \theta & 0 & -\sin \theta \\ 0 & 1 & 0 \\ \sin \theta & 0 & \cos \theta \end{bmatrix} \begin{bmatrix} \cos \psi & -\sin \psi & 0 \\ -\sin \psi & -\cos \psi & 0 \\ 0 & 0 & -1 \end{bmatrix} \\
 &= \begin{bmatrix} \cos \theta \cos \psi & \sin \theta \cos \psi & -\sin \psi \\ \sin \phi \sin \theta \cos \psi - \cos \phi \sin \psi & \cos \phi \sin \theta \cos \psi + \sin \phi \sin \psi & \sin \theta \sin \psi \\ -\cos \theta \sin \psi & -\sin \phi \sin \theta \sin \psi - \cos \phi \cos \psi & \sin \phi \cos \theta \sin \psi - \cos \phi \sin \theta \sin \psi \end{bmatrix} \begin{bmatrix} \sin \theta \\ -\sin \phi \cos \theta \\ -\cos \phi \cos \theta \end{bmatrix} \quad (4)
 \end{aligned}$$



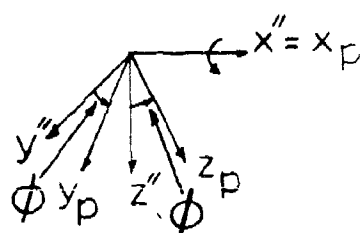
YAW

$$\underline{C}'_n = \begin{bmatrix} \cos \Psi & -\sin \Psi & 0 \\ \sin \Psi & \cos \Psi & 0 \\ 0 & 0 & 1 \end{bmatrix}$$



PITCH

$$\underline{C}''_i = \begin{bmatrix} \cos \theta & 0 & -\sin \theta \\ 0 & 1 & 0 \\ \sin \theta & 0 & \cos \theta \end{bmatrix}$$



ROLL

$$\underline{C}''_p = \begin{bmatrix} 1 & 0 & 0 \\ 0 & \cos \phi & \sin \phi \\ 0 & -\sin \phi & \cos \phi \end{bmatrix}$$

Figure 3. Nav to Path Individual Coordinate Transformations

Navigation to Alpha Wander Frame. The navigation to alpha wander transformation matrix is obtained by a single positive rotation about the z-axis of the navigation frame through the wander angle alpha (See Figure 4).

$$C_n^a = \begin{bmatrix} \cos\alpha & \sin\alpha & 0 \\ -\sin\alpha & \cos\alpha & 0 \\ 0 & 0 & 1 \end{bmatrix} \quad (5)$$

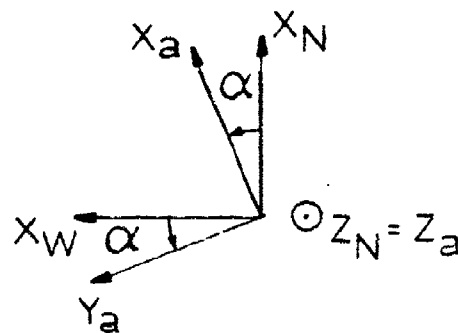


Figure 4. Navigation to Alpha Wander Transformation

#### Angular Rates

The angular rates are obtained and coordinatized in the alpha wander frame, since this is the frame in which the computations will be made. The values required for propagation of the Raides inertial system error model (explained in chapter IV) in the alpha wander frame are

obtained from the navigation frame rates utilizing the navigation to alpha wander transformation. A flight profile generating computer program which will be discussed in detail in Chapter VI is used to compute and store values related to the dynamics of the aircraft at each time increment of numerical integration. The profile generator program was modified to compute the required velocities and accelerations, as well as other pertinent values, in the alpha wander frame. Note that the aircraft's distance from the Earth's center is approximated as being equal to the radius of the Earth. This approximation is justified by the fact that the altitude of the aircraft is 2000 feet as compared to an Earth radius of approximately 4000 miles as well as the fact that although the INS uses an elliptical earth model the Kalman filter can use a constant value of R for earth radius. The angular velocity of the Earth with respect to the inertial frame coordinatized in the navigation frame is

$$\underline{\omega}_{ie}^n = \underline{C}_e^n \underline{\omega}_{ie}^e = \underline{C}_e^n \begin{bmatrix} 0 \\ 0 \\ \Omega \end{bmatrix} = \begin{bmatrix} \Omega \cos L \\ 0 \\ \Omega \sin L \end{bmatrix} \quad (6)$$

The angular velocity of the navigation frame with respect to the Earth-fixed frame is obtained using the stored values of aircraft velocity coordinatized in the navigation frame. The eastward angular velocity is the

time rate of change of longitude,  $\dot{\lambda}$ , and the northward angular velocity is the time rate of change of latitude,  $\dot{L}$ . Then

$$\underline{\omega}_{en} = \dot{L} \bar{e}_x + \dot{\lambda} \bar{e}_z \quad (7)$$

$$\text{and} \quad \dot{L} = V_N / R \quad (8)$$

$$\text{and} \quad \dot{\lambda} = -V_W / R \cos L \quad (9)$$

where  $\bar{e}_x$  and  $\bar{e}_z$  are unit vectors along the axes about which rotation occurs and  $R$  is the Earth's radius. The angular velocity of the navigation frame with respect to the Earth in navigation coordinates becomes

$$\underline{\omega}_{en}^n \triangleq \begin{bmatrix} \rho_x \\ \rho_y \\ \rho_z \end{bmatrix}^n \quad (10)$$

$$\rho_x^n = \dot{\lambda} \cos L = -V_W / R \quad (11)$$

$$\rho_y^n = V_N / R \quad (12)$$

$$\rho_z^n = \dot{L} \sin L = (V_W / R) \tan L \quad (13)$$

The angular accelerations are now obtained by taking the time derivatives of the angular velocities.

$$\dot{\underline{\omega}}_{en}^n = \begin{bmatrix} \dot{\rho}_x \\ \dot{\rho}_y \\ \dot{\rho}_z \end{bmatrix}^n \quad (14)$$

$$\dot{\rho}_x^n = \frac{d}{dt}(-V_W/R) = -A_W/R \quad (15)$$

$$\dot{\rho}_y^n = \frac{d}{dt}(V_N/R) = A_N/R \quad (16)$$

$$\dot{\rho}_z^n = \frac{d}{dt} \left( -\frac{V_W}{R} \tan L \right) = -\frac{A_W \tan L}{R} - \frac{V_W L \sec^2 L}{R} \quad (17)$$

The angular velocity of the navigation frame with respect to the inertial frame expressed in navigation coordinates is then

$$\underline{\omega}_{in}^n = \underline{\omega}_{ie}^n + \underline{\omega}_{en}^n = \begin{bmatrix} \Omega \cos L \\ 0 \\ \Omega \sin L \end{bmatrix} + \begin{bmatrix} -\frac{V_W}{R} \\ \frac{V_N}{R} \\ -\frac{V_W \tan L}{R} \end{bmatrix} = \begin{bmatrix} \omega_x \\ \omega_y \\ \omega_z \end{bmatrix} \quad (18)$$

In order to obtain the angular velocities and accelerations in the alpha wander frame first premultiply each vector coordinatized in the navigation frame by the navigation to alpha wander transformation matrix. Then

$$\underline{\omega}_{ie}^a = \underline{C}_{n \rightarrow a}^a \underline{\omega}_{ie}^n = \begin{bmatrix} \Omega \cos L \cos \alpha \\ -\Omega \cos L \sin \alpha \\ \Omega \sin L \end{bmatrix} = \begin{bmatrix} \Omega_x \\ \Omega_y \\ \Omega_z \end{bmatrix} \quad (19)$$



$$\underline{\omega}_{en}^a = \underline{C}_n^a \underline{\omega}_{en}^n = \begin{bmatrix} (-V_W/R)\cos\alpha + (V_N/R)\sin\alpha \\ (V_W/R)\sin\alpha + (V_N/R)\cos\alpha \\ (-V_W/R)\tan L \end{bmatrix} \quad (20)$$

$$\dot{\underline{\omega}}_{en}^a = \underline{C}_n^a \dot{\underline{\omega}}_{en}^n + \dot{\underline{C}}_n^a \underline{\omega}_{en}^n$$

$$= \begin{bmatrix} (-A_W/R)\cos\alpha + (A_N/R)\sin\alpha \\ (A_W/R)\sin\alpha + (A_N/R)\cos\alpha \\ (-A_W/R)\tan L - (V_W/R)L\sec^2 L \end{bmatrix} + \begin{bmatrix} (V_W/R)\sin\alpha + (V_N/R)\cos\alpha \\ (V_W/R)\cos\alpha - (V_N/R)\sin\alpha \\ 0 \end{bmatrix} \quad (21)$$

$$\underline{\omega}_{in}^a = \underline{C}_n^a \underline{\omega}_{in}^n = \begin{bmatrix} (\Omega\cos L - V_W/R)\cos\alpha + (V_N/R)\sin\alpha \\ (V_W/R - \Omega\cos L)\sin\alpha + (V_N/R)\cos\alpha \\ \Omega\sin L - (V_W/R)\tan L \end{bmatrix} \quad (22)$$

Thus, to get the required angular velocities and accelerations as measured in the alpha wander frame and coordinatized in that frame:

$$\underline{\omega}_{ea}^a = \underline{C}_n^a \underline{\omega}_{en}^n + \underline{\omega}_{na}^a = \begin{bmatrix} \rho_x \\ \rho_y \\ \rho_z \end{bmatrix}^a \quad (23)$$

$$= \begin{bmatrix} (-V_W/R)\cos\alpha + (V_N/R)\sin\alpha \\ (V_W/R)\sin\alpha + (V_N/R)\cos\alpha \\ (-V_W/R)\tan L \end{bmatrix} + \begin{bmatrix} 0 \\ 0 \\ (V_W/R)\tan L \end{bmatrix} \quad (24)$$

which gives

$$\rho_x^a = (-V_W/R)\cos\alpha + (V_N/R)\sin\alpha \quad (25)$$

$$\rho_y^a = (V_W/R)\sin\alpha + (V_N/R)\cos\alpha \quad (26)$$

$$\rho_z^a = 0 \quad (27)$$

for the alpha wander frame mechanization.

Now

$$\begin{aligned} \dot{\omega}_{ea}^a = \dot{\omega}_{en}^a + \dot{\omega}_{na}^a = & \begin{bmatrix} (V_N/R - A_W/R)\cos\alpha + (V_W/R + A_N/R)\sin\alpha \\ (V_W/R + A_N/R)\cos\alpha - (V_N/R - A_W/R)\sin\alpha \\ -(A_W/R)\tan L - (V_W/R)\dot{L}\sec^2 L \end{bmatrix} \\ & + \begin{bmatrix} 0 \\ 0 \\ (A_W/R)\tan L + (V_W/R)\dot{L}\sec^2 L \end{bmatrix} \end{aligned} \quad (28)$$

thus,

$$\dot{\omega}_{ea}^a = \begin{bmatrix} (V_N/R - A_W/R)\cos\alpha + (V_W/R + A_N/R)\sin\alpha \\ -(V_N/R - A_W/R)\sin\alpha + (V_W/R + A_N/R)\cos\alpha \\ 0 \end{bmatrix} \quad (29)$$

Finally

$$\underline{\omega}_{ia}^a = \underline{C}_n^a \underline{\omega}_{in}^n + \underline{\omega}_{na}^a$$

$$= \begin{bmatrix} (\Omega \cos L - V_W/R) \cos \alpha + (V_N/R) \sin \alpha \\ -(\Omega \cos L - V_W/R) \sin \alpha + (V_N/R) \cos \alpha \\ \Omega \sin L - (V_W/R) \tan L \end{bmatrix} + \begin{bmatrix} 0 \\ 0 \\ (V_W/R) \tan L \end{bmatrix} \quad (30)$$

$$\underline{\omega}_{ia}^a = \begin{bmatrix} (\Omega \cos L - V_W/R) \cos \alpha + (V_N/R) \sin \alpha \\ -(\Omega \cos L - V_W/R) \sin \alpha + (V_N/R) \cos \alpha \\ \Omega \sin L \end{bmatrix} \quad (31)$$

(Ref 8:Chap 4)

### III. Kalman Filter Equations

This chapter includes a discussion of the equations required not only for the mechanization of the Kalman filter but also those required to simulate the aircraft dynamics and driving error sources required in the complete system reference model. The basic system model equations will be discussed first and the Kalman filter equations discussed for a given system reference model.

The method of covariance analysis will be the principal tool used in solution of the problem. Physically derived initial conditions are specified on the elements of the covariance matrix  $\underline{P}$ . These conditions include both diagonal and off-diagonal elements of the matrix. The covariance, i.e. variances of scalar variables and cross-variances among different variables, is a measure of the uncertainty in the knowledge of true values of the components of the state vector. In the simulation, both the filter and system covariance matrices are propagated forward in time using numerical integration techniques. When a specified update time is reached, the best estimate of the states is determined, and control is applied to the system to adjust the values of the state variables. The square root of the individual diagonal elements of the system covariance matrix (RMS values) are then plotted as a function of time to provide a basis for comparison of filter performance. For this study, the plots are also utilized to determine

the error contribution from each modeled error source.

In the simulation, the error statistics are propagated; i.e. the standard deviation of the noise value is supplied when a noise is required. One attribute of covariance analysis is that, under the assumptions of linearity and white Gaussian noise, the covariance is independent of the actual measurement values and can be computed without generating a sample sequence of measurements. Thus this method is easier to handle than a Monte Carlo type simulation.

#### System Model Equations

The basic equations used are the differential equations which describe how the aided-inertial navigation system errors propagate with time. The equations are formulated into a set of first order, linear differential equations, driven by white Gaussian noise. Linear measurements are made upon the actual system variables, corrupted by white Gaussian noise. The equations representing a detailed model of the system can be formulated as follows:

$$\dot{\underline{x}}_s = \underline{F}_s \underline{x}_s + \underline{G}_s \underline{w}_s \quad (32)$$

where

$\underline{x}_s$  is an  $n_1$  vector denoting the true states

$\underline{F}_s$  is an  $n_1 \times n_1$  system dynamics matrix

$\underline{G}_s$  is an  $n_1 \times m_1$  gain matrix

$\underline{w}_s$  is an  $m_1$  vector of white noise inputs with zero mean and variance

$$E[\underline{w}(i)\underline{w}(j)^T] = \begin{bmatrix} \underline{Q}_0(i) & i = j \\ 0 & i \neq j \end{bmatrix} \quad (33)$$

where  $i$  and  $j$  are instants in time. The observations obtained from external references can be described by the linear measurement vector equation

$$\underline{z}_s = \underline{H}_s \underline{x}_s + \underline{v}_s \quad (34)$$

where

$\underline{z}_s$  is an  $r$  vector of measurements

$\underline{H}_s$  is an  $r \times n_1$  measurement matrix

$\underline{v}_s$  is an  $r$  vector of white noise inputs with zero mean and variance

$$E[\underline{v}(i)\underline{v}(j)^T] = \begin{bmatrix} \underline{R}_0(i) & i = j \\ 0 & i \neq j \end{bmatrix} \quad (35)$$

It is assumed that the system noise and measurement noise are uncorrelated for all time.

$$E[\underline{w}(i)\underline{v}(j)^T] = 0 \quad \text{for all } i, j \quad (36)$$

### Filter Equations

The set of equations discussed above are assumed to be a complete and accurate mathematical description of the aided-inertial system dynamics and measurement equations for the purpose of simulation. This set of equations is also used to model the full scale optimal Kalman filter. Due to the requirement to lessen the computational burden on the aircraft computer, the suboptimal filter equations are obtained by reducing the dimension of the state vector. The states which are eliminated are those that least affect

the ability of the mathematical model to represent the time system dynamics adequately.

The reduced order filter equations are then described by

$$\dot{\underline{x}}_f = \underline{F}_f \underline{x}_f + \underline{G}_f \underline{w}_f \quad (37)$$

where

$\underline{x}_f$  is an  $n_2$  vector

$\underline{F}_f$  is an  $n_2 \times n_2$  filter dynamics matrix

$\underline{G}_f$  is an  $n_2 \times m_2$  gain matrix

$\underline{w}_f$  is an  $m_2$  vector of white noise inputs with zero mean and variance

$$E[\underline{w}_f(i)\underline{w}_f(j)^T] = \begin{bmatrix} Q_f(i) & i = j \\ 0 & i \neq j \end{bmatrix} \quad (38)$$

The filter measurement equation is then

$$\underline{z}_f = \underline{H}_f \underline{x}_f + \underline{v}_f \quad (39)$$

where

$\underline{z}_f$  is an  $r$  vector

$\underline{H}_f$  is an  $r \times n_2$  measurement matrix

$\underline{v}_f$  is an  $r$  vector of white noise inputs with zero mean and variance

$$E[\underline{v}_f(i)\underline{v}_f(j)^T] = \begin{bmatrix} R_f(i) & i = j \\ 0 & i \neq j \end{bmatrix} \quad (40)$$

The filter propagation and update equations based on the models above are as given below. Between measurements

$$\dot{\hat{\mathbf{x}}}_f = \mathbf{F}_f \hat{\mathbf{x}}_f \quad (41)$$

$$\dot{\mathbf{P}}_f = \mathbf{F}_f \mathbf{P}_f + \mathbf{P}_f \mathbf{F}_f^T + \mathbf{G}_f \mathbf{Q}_f \mathbf{G}_f^T \quad (42)$$

starting from the values of  $\hat{\mathbf{x}}_f^+$  and  $\mathbf{P}_f^+$  achieved after the most recent measurement incorporation.

At measurement times

$$\mathbf{K}_f = \mathbf{P}_f^- \mathbf{H}_f^T [\mathbf{H}_f \mathbf{P}_f^- \mathbf{H}_f^T + \mathbf{R}_f]^{-1} \quad (43)$$

$$\mathbf{P}_f^+ = \mathbf{P}_f^- - \mathbf{K}_f \mathbf{H}_f \mathbf{P}_f^- \quad (44)$$

$$\hat{\mathbf{x}}_f^+ = \hat{\mathbf{x}}_f^- + \mathbf{K}_f [\zeta_s - \mathbf{H}_f \hat{\mathbf{x}}_f^-] \quad (45)$$

where

$\hat{\mathbf{x}}_f$  is an  $n_2$  vector denoting the best estimate

$\mathbf{P}_f$  is the filter covariance matrix

- superscript indicates the time instant just prior to update

+ superscript indicates the time instant just after update

$\mathbf{K}_f$  is the matrix of Kalman gains

$\zeta_s$  are the actual values of the measurements taken

( )<sup>T</sup> - is the transpose of the matrix or vector represented by the parenthesis

The filter takes the actual value of the measurements,  $\zeta_s$ , and subtracts from it the best estimate of them before the actual measurement is taken,  $\mathbf{H}_f \hat{\mathbf{x}}_f^-$ . The difference is then optimally weighted by the Kalman gain matrix,  $\mathbf{K}_f$ , and used to correct  $\hat{\mathbf{x}}_f^-$ , the best estimate of the state prior



to measurement. This estimate is then propagated to the next measurement time by the equations for  $\hat{\underline{x}}_f$  and  $\hat{\underline{p}}$  where the process is repeated.

These recursive relationships are solved based on initial conditions from an assumed Gaussian density which describe the apriori knowledge of the states.

$$\hat{\underline{x}}(0) = \hat{\underline{x}}_0 \quad (46)$$

$$\underline{P}(0) = \underline{P}_0 \quad (47)$$

The Kalman filter propagates the conditional probability density of the desired states, conditioned on the actual measurements taken. The first and second order statistics; i.e. the mean and variance, completely determine a Gaussian density. Thus, the Kalman filter, which propagates the first and second order statistics, completely describes the condition probability density (Ref 10:4-6 and 2:8-21).

The expectation or mean,  $\mu$ , of a random variable is defined as

$$E[X] = \mu = \int_{-\infty}^{\infty} \xi f(\xi) d\xi \quad (48)$$

which is the weighted average of the values of  $x$ , using the probability density function  $f(x)$  as the weighting function. The mean is assumed to be zero for all Gaussian white driving noises used in the simulation.

The variance,  $\sigma^2$ , of a random variable  $X$  is defined as

$$\text{Var}[X] = \sigma^2 = \int_{-\infty}^{\infty} (\xi - \mu)^2 f(\xi) d\xi \quad (49)$$

where  $\sigma^2$  is the weighted average of the values of  $(X - \mu)^2$ , which makes  $\sigma^2$  a measure of the spread of the density (Ref 11:136-146). Thus  $\sigma$  is a direct measure of the uncertainty in that the larger the value of  $\sigma$ , the broader the probability density peak spreading the probability weight over a larger range of values of  $X$ . For a Gaussian density, 68.3% of the probability weight is concentrated within a band  $1\sigma$  units to either side of the mean ( $\mu$ ) while 95.4% of the weight is within  $2\sigma$  and 99.7% within  $3\sigma$  of the mean.

The equations for the mean and variance of  $\underline{X}$  give the first and second order statistics for the scalar case. These equations are easily extended to the vector case, as required for this evaluation, and are

$$E[\underline{X}] = \underline{\mu} = \int_{-\infty}^{\infty} \cdots \int_{-\infty}^{\infty} \underline{\xi} f(\underline{\xi}) d\xi_1 \cdots d\xi_n \quad (50)$$

$$\text{Cov}[\underline{X}] = \underline{P} = \int_{-\infty}^{\infty} \cdots \int_{-\infty}^{\infty} (\underline{\xi} - \underline{\mu})(\underline{\xi} - \underline{\mu})^T f(\underline{\xi}) d\xi_1 \cdots d\xi_n \quad (51)$$

#### IV. System Model

To apply the Kalman filter equations developed in the previous chapter, a reference system model, which is the most complete linear model to describe the real world, is needed. This chapter outlines the reference system model used for the evaluation. The first section defines the 54 error states incorporated in the system model along with the assumed initial conditions. The system dynamics matrix,  $F_s$ , is presented in partitioned form. The second section discusses the modeling of the plant INS error states. Section three presents the Doppler radar, position fix radar and barometric altimeter error source models as linear systems driven by white Gaussian noise. The last section describes the measurement equation (34) explicitly in matrix form.

##### State Variable Definition and Initial Conditions

Table I presents a detailed listing of the 54 states used in the reference system model. The initial conditions on the INS error states have been chosen based on values used in similar studies. The initial conditions on the accelerometer and gyro error states are typical of an inertial navigation system in the 0.5 nautical mile per hour class. The initial conditions on the Doppler and altimeter system are extracted from documents reflecting typical values for currently operational systems (Ref 1). The actual initial conditions for the position fix radar

Table I

System 54 State Error Vector Definition

Error State	Symbol	Definition	RMS Initial Condition
<u>INS Plant Error States</u>			
1	$\delta x$	x position error	50,000 ft
2	$\delta y$	y position error	50,000 ft
3	$\delta z$	z position error	1,000 ft
4	$\delta v_x$	x velocity error	10 ft/sec
5	$\delta v_y$	y velocity error	10 ft/sec
6	$\delta v_z$	z velocity error	5 ft/sec
7	$\delta \phi_x$	x attitude error	.0175 rad (1 deg)
8	$\delta \phi_y$	y attitude error	.0175 rad (1 deg)
9	$\delta \phi_z$	z attitude error	0.000 rad
10	$\delta \theta_z$	computer axes to true axes compu- tation error	.0349 rad (2 deg)
<u>INS, Doppler, and Altimeter Errors</u>			
11	$\epsilon_{x_1}$	x gyro fixed bias	.03 deg/hr
12	$\epsilon_{y_1}$	y gyro fixed bias	.03 deg/hr
13	$\epsilon_{z_1}$	z gyro fixed bias	.045deg/hr
14	$b_z$	z accelerometer fixed bias	250 $\mu g$
15	$K_1$	Doppler scale factor error; Exponentially correlated $T=900$ sec	.12%
16	$\delta_1$	Doppler drift angle Exponentially correlated $T=900$ sec	1.8 millirad

Table I

System 54 State Error Vector Definition  
(Cont.)

Error State	Symbol	Definition	RMS Initial Condition
17	$\delta h$	Altimeter error Exponentially correlated $T = 1800$ sec	250 ft
18	$\epsilon_{x2}$	x gyro random bias Exponentially correlated $T = 10,800$ sec	.003 deg/hr
19	$\epsilon_{y2}$	y gyro random bias Exponentially correlated $T = 10,800$ sec	.003 deg/hr
20	$\epsilon_{z2}$	z gyro random bias Exponentially correlated $T = 10,800$ sec	.005 deg/hr
21	$b_x$	x accelerometer fixed bias	25 $\mu g$
22	$b_y$	y accelerometer fixed bias	25 $\mu g$
23	$K_2$	Doppler sea state scale factor error	.16 %
24	$\delta_2$	Doppler sea state drift angle error	2.4 millirad
25	$DX_x$	x gyro input axis G sensitivity	.3 deg/hr/g
26	$DX_y$	x gyro spin axis G sensitivity	.3 deg/hr/g
27	$DY_x$	y gyro spin axis G sensitivity	.3 deg/hr/g
28	$DY_y$	y gyro input axis G sensitivity	.3 deg/hr/g

Table I

System 54 States Error Vector Definition  
(Cont.)

Error State	Symbol	Definition	RMS Initial Condition
29	DZ <sub>y</sub>	z gyro spin axis G sensitivity	.3 deg/hr/g
30	DZ <sub>z</sub>	z gyro input axis G sensitivity	.3 deg/hr/g
31	DX <sub>xy</sub>	x gyro spin-input G <sup>2</sup> sensitivity	.04 deg/hr/g
32	DY <sub>xy</sub>	y gyro spin-input G <sup>2</sup> sensitivity	.04 deg/hr/g
33	DZ <sub>yz</sub>	z gyro spin-input G <sup>2</sup> sensitivity	.04 deg/hr/g
34	GSF <sub>x</sub>	x gyro scale factor error	$3 \times 10^{-4}$
35	GSF <sub>y</sub>	y gyro scale factor error	$3 \times 10^{-4}$
36	GSF <sub>z</sub>	z gyro scale factor error	$3 \times 10^{-4}$
37	XG <sub>y</sub>	x gyro input axis misalignment about the y axis	40 sec
38	XG <sub>z</sub>	x gyro input axis misalignment about the z axis	40 sec
39	YG <sub>x</sub>	y gyro input axis misalignment about x axis	40 sec
40	YG <sub>z</sub>	y gyro input axis misalignment about the z axis	40 sec

Table I

System 54 States Error Vector Definition  
(Cont.)

Error State	Symbol	Definition	RMS Initial Condition
41	$ZG_x$	z gyro input axis misalignment about the x axis	40 $\widehat{\text{sec}}$
42	$ZG_y$	z gyro input axis misalignment about the y axis	40 $\widehat{\text{sec}}$
43	$ASF_x$	x accelerometer scale factor error	$1.5 \times 10^{-4}$
44	$ASF_y$	y accelerometer scale factor error	$1.5 \times 10^{-4}$
45	$ASF_z$	z accelerometer scale factor error	$1.5 \times 10^{-4}$
46	$XA_y$	x accel. input axis misalign. about y	30 $\widehat{\text{sec}}$
47	$XA_z$	x accel. input axis misalign. about z	180 $\widehat{\text{sec}}$
48	$YA_x$	y accel. input axis misalign. about x	30 $\widehat{\text{sec}}$
49	$YA_z$	y accel. input axis misalign. about z	180 $\widehat{\text{sec}}$
50	$ZA_x$	z accel. input axis misalign. about x	30 $\widehat{\text{sec}}$
51	$ZA_y$	z accel. input axis misalign. about y	30 $\widehat{\text{sec}}$
52	$\delta g_e$	East-West gravity deflection; exp. correlated $\mathcal{T} = d_x/V = 10\text{nm/V}$	26 $\mu\text{g}$
53	$\delta g_n$	North-South gravity deflection; exp. correlated	17 $\mu\text{g}$

Table I

System 54 States Error Vector Definition  
(Cont.)

Error State	Symbol	Definition	RMS Initial Condition
54	$\delta g_z$	$\tau = d_y/V = 10\text{nm/V}$ Gravity anomaly exp. correlated $\tau = d_a/V = 60\text{nm/V}$	35 $\mu\text{g}$



is classified; therefore numbers of a reasonable order of magnitude were selected to maintain the unclassified status of the report. It should be noted that when an integrator is required in the simulation diagram the output of the integrator becomes a system state variable. Thus, the addition of an integrator to the error model increases the dimension of the error state variable vector by one. The x, y, and z axes for the elements of the F matrix are alpha wander reference frame axes.

The value of the elements of the  $\underline{P}(0)$  matrix are specified in Table I for each of the reference system states. The values actually used in  $\underline{P}(0)$  are the squared values of the RMS initial conditions and these are located along the principal diagonal of the matrix. Eighteen off-diagonal elements enter into the  $\underline{P}(0)$  matrix for airborne alignment. These are cross correlation terms between  $V_x$  and  $V_y$  and between the doppler bias, drift, and sea states. Due to symmetry of the  $\underline{P}(0)$  matrix (i.e.  $\sigma_{V_x V_y}^2 = \sigma_{V_y V_x}^2$ ) only the equation for nine of the off-diagonal elements are shown below.

$$\sigma_{V_x V_y}^2 = (\sigma_{K_1 K_1}^2 + \sigma_{K_2 K_2}^2 - \sigma_{\delta_1 \delta_1}^2 - \sigma_{\delta_2 \delta_2}^2) V_{x0} V_{y0} \quad (52)$$

$$\sigma_{V_x K_1}^2 = \sigma_{K_1 K_1}^2 V_{x0} \quad (53)$$

$$\sigma_{V_x K_2}^2 = \sigma_{K_2 K_2}^2 V_{x0} \quad (54)$$

$$\sigma_{V_y K_1}^2 = \sigma_{K_1 K_1}^2 V_{y0} \quad (55)$$

$$\sigma_{V_y K_2}^2 = \sigma_{K_2 K_2}^2 V_{y0} \quad (56)$$

$$\sigma_{V_x \delta_1}^2 = -\sigma_{\delta_1 \delta_1}^2 V_{y0} \quad (57)$$

$$\sigma_{V_x \delta_2}^2 = -\sigma_{\delta_2 \delta_2}^2 V_{y0} \quad (58)$$

$$\sigma_{V_y \delta_1}^2 = \sigma_{\delta_1 \delta_1}^2 V_{x0} \quad (59)$$

$$\sigma_{V_y \delta_2}^2 = \sigma_{\delta_2 \delta_2}^2 V_{x0} \quad (60)$$

Propagation of the variance equation (42) requires additional knowledge of the matrices  $\underline{F}$  and  $\underline{Q}'$  where

$$\underline{Q}' = \underline{G}\underline{Q}\underline{G}^T \quad (61)$$

The  $\underline{F}_s$  matrix is partitioned as follows:

$$\underline{F}_s = \begin{matrix} & \begin{matrix} 1-10 & 11-17 & 18-24 & 25-42 & 43-51 & 52-54 \end{matrix} \\ \begin{matrix} 1-10 \\ 11-17 \\ 18-24 \\ 25-42 \\ 43-51 \\ 52-54 \end{matrix} & \left[ \begin{array}{cccccc} F_{11} & F_{12} & F_{13} & F_{14} & F_{15} & F_{16} \\ 0 & F_{22} & 0 & 0 & 0 & 0 \\ 0 & 0 & F_{33} & 0 & 0 & 0 \\ 0 & 0 & 0 & 0 & 0 & 0 \\ 0 & 0 & 0 & 0 & 0 & 0 \\ 0 & 0 & 0 & 0 & 0 & F_{66} \end{array} \right] \end{matrix} \quad (62)$$

8

The submatrices of equation (62) are displayed in explicit form as they are encountered in the following sections. The only non-zero elements of  $\underline{Q}'$  are all diagonal and are given in the following sections as  $q_i$  where the  $i$  subscript denotes the row and column of the element. For example,  $q_6$  indicates that this is the element located at the intersection of the 6th row and 6th column of the  $\underline{Q}'$  matrix corresponding to a white noise input on the 6th state variable. There are nine non-zero elements in the reference system  $\underline{Q}'$  matrix corresponding to states 15, 16, 17, 18, 19, 20, 52, 53, and 54:

$$\underline{Q}'_s = \begin{matrix} & \begin{matrix} 1-10 & 11-17 & 18-24 & 25-42 & 43-51 & 52-54 \end{matrix} \\ \begin{matrix} 1-10 \\ 11-17 \\ 18-24 \\ 25-42 \\ 43-51 \\ 52-54 \end{matrix} & \left[ \begin{array}{cccccc} 0 & 0 & 0 & 0 & 0 & 0 \\ 0 & q'_{22} & 0 & 0 & 0 & 0 \\ 0 & 0 & q'_{33} & 0 & 0 & 0 \\ 0 & 0 & 0 & 0 & 0 & 0 \\ 0 & 0 & 0 & 0 & 0 & 0 \\ 0 & 0 & 0 & 0 & 0 & q'_{66} \end{array} \right] \end{matrix} \quad (63)$$

### Plant Error States

The plant error state equations are the linear differential equations that describe the natural unforced dynamic response of the errors in the inertial navigation system. These include ten states:  $x$ ,  $y$ , and  $z$  position, velocity and attitude in the alpha wander frame and the angular error between the computer axes and the true axes. Additional states added to compensate for gyro sensitivity

to axis misalignment, both fixed and random bias errors for gyros and accelerometers, gravity and gravity squared terms which were ignored in the basic plant equations, and gravity anomaly terms. The barometric altimeter is added to damp the inherently unstable vertical channel of the inertial navigation system. Doppler velocity and drift angle are used to provide external velocity data for inertial navigation system tuning and oscillation damping.

There are various models for the nine basic INS plant states. The model used by the contractor for the plant error states is the RAIDES inertial system error model which requires one more integrator than the Pinson error model. A complete derivation of the Pinson error model is given in Chapter 4 of Reference 9 while a derivation of the RAIDES model is the subject of Reference 10. This model comprises the  $F_{11}$  matrix shown in Figure 5.

#### Error Source Models

The error propagation equations given in Chapter IV were developed under the assumption that the system disturbances,  $w(t)$ , are not correlated in time. The estimation of disturbances which have significant time correlation is done by means of state vector augmentation. Thus, the dimension of the system state vector is increased by including the correlated disturbances as well as descriptions of their dynamic response in the appropriate rows of the enlarged  $F$  matrix. Since these quantities are random or are unknown values (constant biases) that are

	1	2	3	4	5	6	7	8	9	10
1	$\frac{V_z}{R}$	$-\rho_z$	$-\frac{V_x}{R}$	1	0	0	0	0	0	$-V_y$
2	$\rho_z$	$\frac{V_z}{R}$	$-\frac{V_y}{R}$	0	1	0	0	0	0	$V_x$
3	0	0	0	0	0	1	0	0	0	0
4	$\frac{2V_y\Omega_x}{R}$	$\frac{2(V_y\Omega_y + V_z\Omega_z)}{R}$	$\frac{V_zV_x}{R^2}$	$-\frac{V_z}{R}$	$\rho_z + 2\Omega_z$	$-(\omega_y + \Omega_y)$	0	$-A_z$	$A_y$	$2V_z\Omega_x$
5	$\frac{-2(V_x\Omega_x + V_z\Omega_z)}{R}$	$\frac{-2V_x\Omega_y}{R}$	$\frac{V_zV_y}{R^2}$	$-\rho_z - 2\Omega_z$	$-\frac{V_z}{R}$	$\omega_x + \Omega_x$	$A_z$	0	$-A_x$	$2V_z\Omega_y$
6	$\frac{2V_y\Omega_z}{R}$	$\frac{-2V_x\Omega_z}{R}$	$\frac{29(R - V_x^2 + V_y^2)}{R^2}$	$2(\rho_y + \Omega_y) - 2(\rho_x + \Omega_x)$	0	0	$-A_y$	$A_x$	0	$-2(V_y\Omega_y + V_x\Omega_x)$
7	$\frac{\Omega_z}{R}$	0	$\frac{V_y}{R^2}$	0	$-\frac{1}{R}$	0	0	$\rho_z + \Omega_z$	$-\omega_y$	$\Omega_y$
8	0	$-\frac{\Omega_z}{R}$	$-\frac{V_x}{R^2}$	$\frac{1}{R}$	0	0	$-\rho_z - \Omega_z$	0	$\omega_x$	$-\Omega_x$
9	$\frac{\Omega_x}{R}$	$\frac{\Omega_y}{R}$	0	0	0	0	$\omega_y$	$-\omega_x$	0	0
10	$\frac{V_y}{R^2}$	$-\frac{V_x}{R^2}$	0	0	0	0	0	0	0	0

Figure 5.  $F_{11}$  Matrix (RAIDES Error Model)

modeled as random variables, they cannot be described deterministically and are modeled as state variables of a fictitious linear dynamic system driven by white noise. This model provides proper autocorrelation characteristics through specification of the linear system and strength of the driving noise while also providing a random signal from its random excitation (Ref 13).

The correlated noises in the reference system model are obtained from one or more of the basic errors models described in Figure 6. Specification of the block diagram models of these error sources implies the structure of the corresponding element of the  $\underline{F}$  and  $\underline{Q}'$  matrices.

The random constant or fixed bias is a non-dynamic quantity meant to model a constant of unknown amplitude. It is simulated as the output of an integrator with a random initial condition and no input. The constant nature of this model is indicated by zeros in the corresponding row and column of both the  $\underline{F}$  and  $\underline{Q}'$  matrices.

The random walk or varying bias gets its name from the illustration of a man who takes fixed-length steps in an arbitrary direction. It is modeled as an integrator with a white noise input. In this case the row and column of the augmented  $\underline{F}$  matrix contains a zero with a non-zero element,  $q$ , at the intersection of the corresponding row and column of the  $\underline{Q}'$  matrix.

The exponentially correlated random variable, whose autocorrelation function is a decreasing exponential,

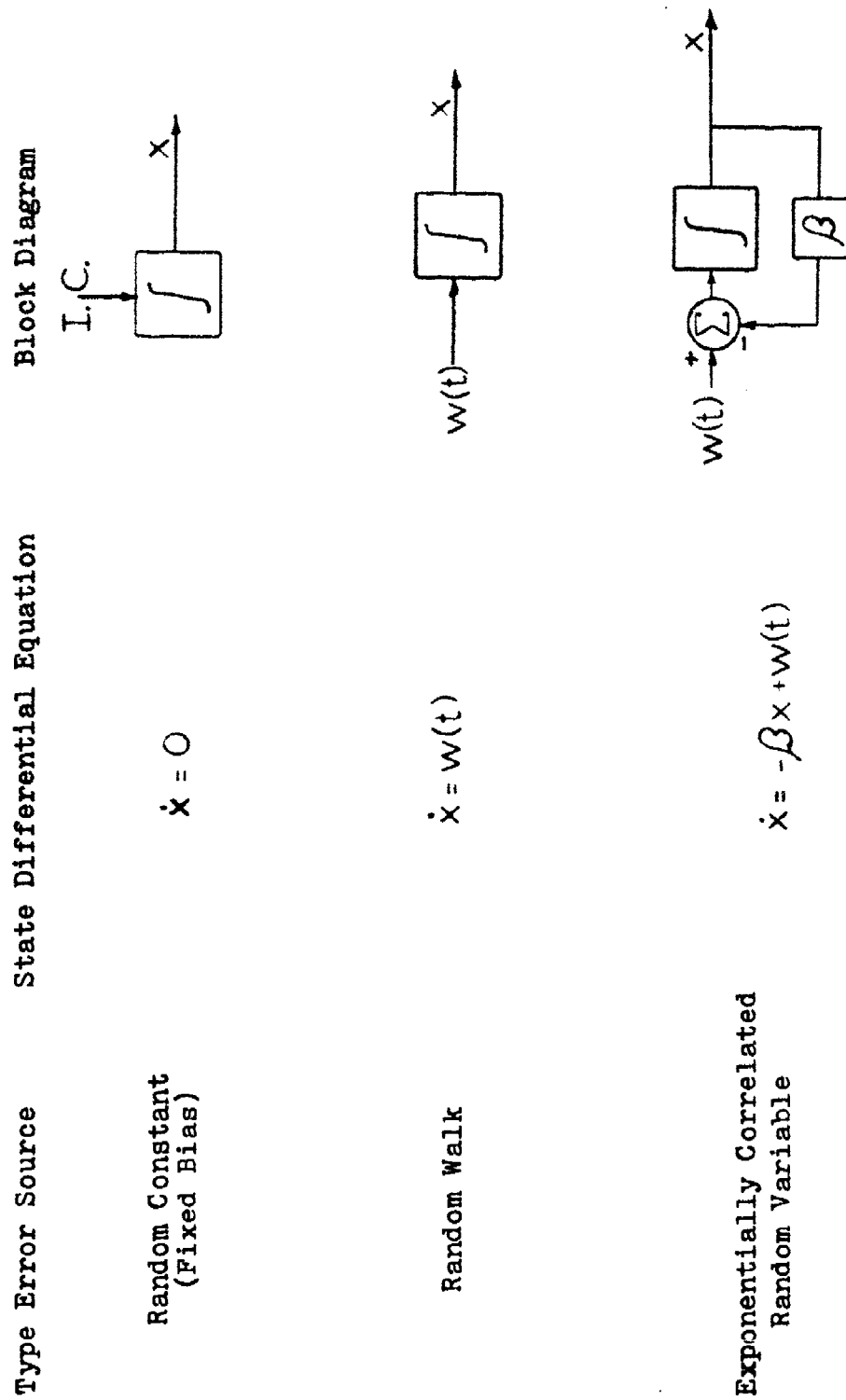


Figure 6. Error Source Models for Random Variables

provides a reasonable approximation to a band limited signal. The power spectral density is approximately flat for a finite bandwidth. This model introduces a single non-zero element,  $-\beta$ , into the  $\underline{F}$  matrix where

$$\beta = \frac{1}{\tau} \quad (64)$$

and  $\tau$  is the correlation time constant of the exponentially decaying function. If the corresponding element of the  $P(0)$  matrix is specified, then the noise value required to drive the linear model is determined by assuming stationary statistics and solving the  $\dot{\underline{P}}$  equation for steady state conditions. In steady state  $\dot{\underline{P}} = \underline{0}$  so that the linear variance equation becomes

$$\underline{0} = \underline{F}\underline{P} + \underline{P}\underline{F}^T + \underline{Q} \quad (65)$$

or, for the scalar case

$$0 = -\beta P - \beta P + Q \quad (66)$$

$$Q = 2\beta P = 2P/\tau \quad (67)$$

Therefore, if the initial covariance equals the steady state (stationary) value of the variance, the exponentially correlated random variable requires a diagonal element in  $\underline{Q}$  whose value is two times the initial covariance divided



by the correlation time. (Ref 5:3-36 thru 3-49).

Radar Position Error Equations. Assume  $\Delta\hat{x}_N$  and  $\Delta\hat{x}_W$  represent the range deviations derived from position fixing in the north and west coordinate set. In order to use these measurements in the Kalman filter, the computer first transforms them to platform coordinates (See Figure 4).

$$\begin{bmatrix} \delta\hat{x} \\ \delta\hat{y} \end{bmatrix} = \begin{bmatrix} \cos\alpha & \sin\alpha \\ -\sin\alpha & \cos\alpha \end{bmatrix} \begin{bmatrix} \Delta\hat{x}_N \\ \Delta\hat{x}_W \end{bmatrix} \quad (68)$$

The distances  $\delta\hat{x}$  and  $\delta\hat{y}$  in the expression above provide the actual position measurement error components  $\zeta$  in the state vector update equation

$$\hat{x}_f^+ = \hat{x}_f^- + K_f [\zeta - H_f \hat{x}_f^-] \quad (69)$$

The  $H_f \hat{x}_f^-$  portion of this expression is the predicted position measurement error. The difference between  $\zeta$  and  $H_f \hat{x}_f^-$  is called the residual. The updated state error vector  $\hat{x}_f^+$  is used to correct the navigation direction cosines.

The proposed implementation makes corrections to the direction cosine matrix elements based on the estimated linear position errors ( $\delta\hat{x}$  and  $\delta\hat{y}$ ) in platform coordinates. The manner in which the direction cosine matrix is updated depends on whether the update is derived from Doppler measurements or from a position fix. When position fix

data is used and the state vector is updated, the direction cosine matrix is reinitialized using updated values of latitude, longitude, and wander angle as follows:

$$\begin{bmatrix} \Delta \hat{R}_N \\ \Delta \hat{R}_E \end{bmatrix} = \begin{bmatrix} \cos \alpha_c & -\sin \alpha_c \\ -\sin \alpha_c & -\cos \alpha_c \end{bmatrix} \begin{bmatrix} \delta \hat{x} \\ \delta \hat{y} \end{bmatrix} \quad (70)$$

where  $\delta \hat{x}$  and  $\delta \hat{y}$  are position error estimates supplied by the filter in platform coordinates and  $\alpha_c$  is the computed value of the wander angle  $\alpha$ .

The latitude error is then computed from

$$\Delta \hat{L} = \frac{\Delta \hat{R}_N}{r} \quad (71)$$

where  $r = R_0 (1 + e \sin^2 L_c)$ ,  $R_0$  = spherical Earth radius,  $e$  = Earth ellipticity, and the latitude is corrected to be

$$\hat{L}_{\text{true}} = L_c - \Delta \hat{L} \quad (72)$$

The longitude error is computed using the updated values of latitude as

$$\Delta \hat{\lambda} = \frac{\Delta \hat{R}_E}{r \cos \hat{L}_{\text{true}}} \quad (73)$$

The longitude is updated to be

$$\hat{l}_{\text{true}} = l_c - \Delta \hat{l} \quad (74)$$

The wander angle error  $\Delta \hat{\alpha}$  is computed using

$$\Delta \hat{\alpha} = \delta \hat{\theta}_z - \Delta \hat{l} \sin \hat{l}_{\text{true}} \quad (75)$$

and the wander angle corrected to be

$$\hat{\alpha}_{\text{true}} = \alpha_c - \Delta \hat{\alpha} \quad (76)$$

It should be noted that the filter estimate ( $\delta \hat{\theta}_z$ ) of  $\delta \theta_z$ , the error between computer axes and true axes, is used in the computation of the wander angle correction. (Ref 12)

The updated values of the latitude, longitude, and wander angle are then used to reset the Earth to wander azimuth direction cosine matrix as shown below:

$$\underline{C}_e^a = \begin{bmatrix} s\hat{l}s\hat{\alpha} - s\hat{l}c\hat{l}c\hat{\alpha} & -s\hat{l}s\hat{l}c\hat{\alpha} - c\hat{l}s\hat{\alpha} & c\hat{l}c\hat{\alpha} \\ s\hat{l}c\hat{\alpha} + s\hat{l}c\hat{l}s\hat{\alpha} & s\hat{l}s\hat{l}s\hat{\alpha} - c\hat{l}c\hat{\alpha} & -c\hat{l}s\hat{\alpha} \\ c\hat{l}c\hat{l} & c\hat{l}s\hat{l} & s\hat{l} \end{bmatrix} \quad (77)$$

where C = cosine and S = sine of an angle.

Doppler Error Equations. Velocity updates require more measurement processing than position updates. First the Doppler velocities are expressed in platform wander azimuth coordinates; next the measured velocities are differenced with computer or inertial navigation system

velocities; finally, for this system, the velocity differences are accumulated and averaged over a velocity update cycle before they are used by the filter.

The accumulation and averaging is performed for two reasons. The Doppler output is available each 0.5 seconds (i.e. a faster rate than required) and only seven of the twelve possible values are required for computation of the average value of the accumulated velocity differences.

The Doppler outputs groundspeed ( $V$ ) and drift angle ( $\Delta$ ). It is stabilized in pitch and roll using IMU synchro outputs. The Doppler radar nulls the cross track velocity by rotating the antenna about the z-axis. Thus the Doppler antenna centerline is parallel to and aligned along the groundspeed vector. Doppler drift angle is proportional to cross wind.

The expressions in the airborne computer for resolving Doppler groundspeed in platform coordinates are:

$$V_{D_x} = V \cos(\theta_s - \Delta) \quad (78)$$

$$V_{D_y} = V \sin(\theta_s - \Delta) \quad (79)$$

where  $\theta_s$  is the platform azimuth synchro readout.

The difference between these velocities and the velocities computed from the IMU outputs are:

$$\Delta V_x = V_{C_x} - V_{D_x} \quad (80)$$

$$\Delta V_y = V_{Cy} - V_{Dy} \quad (81)$$

The differences are computed each 0.5 seconds. Since Doppler outputs are available at this rate, accumulated, averaged, and tested for reasonableness. The average value of the accumulated velocity differences is then used in the Kalman filter to update the state error vector at a six second update rate.

From the discussion above, it can be seen that the measured velocity difference is of the form

$$\Delta V_{xm} = V_{Cx}^C - V_{Dx}^P \quad (82)$$

$$\Delta V_{ym} = V_{Cy}^C - V_{Dy}^P \quad (83)$$

where the  $V_{C\_}$ 's for x and y axes are computed (or system) velocity components in computer coordinates and the  $V_{D\_}^P$ 's represent the Doppler velocity resolved in platform coordinates.

The Doppler velocity ( $V_D$ ) is basically the true velocity ( $V_T$ ) plus inherent or apparent (terrain/sea state) Doppler errors ( $\delta V_D$ ). Let

$$V_D = V_T + \delta V_D \quad (84)$$

represent the Doppler velocity in ideal platform coordinates.

Then the Doppler velocity in actual (misaligned) platform coordinates is

$$\underline{v}_D^P = \underline{v}_T^P + \delta \underline{v}_D^P \quad (85)$$

or, since

$$\underline{v}_T^P = \underline{v}_T^T - \underline{\phi} \times \underline{v}_T^T \quad (86)$$

where  $\underline{\phi}$  is the vector of platform misalignment angles (tilts), then

$$\underline{v}_C^C - \underline{v}_D^P = \underline{v}_C^C - (\underline{v}_T^T - \underline{\phi} \times \underline{v}_T^T + \delta \underline{v}_D^P) \quad (87)$$

For the error dynamics modeled in the filter, the navigation system errors are defined as the difference between computed values and true or error-free values. Therefore vehicle velocity error is defined as

$$\delta \underline{v} = \underline{v}_C - \underline{v}_T \quad (88)$$

In component form

$$v_{C_x}^C - v_{D_x}^P = \delta v_x - \phi_z v_y - \delta v_{D_x} \quad (89)$$

$$V_{C_y}^C - V_{D_y}^P = \delta V_y + \phi_z V_x - \delta V_{D_y} \quad (90)$$

where the superscript/subscript T has been dropped from the true velocity and the superscript P from the Doppler error ( $\delta V_D^P = \delta V_D$ ).

The Doppler error  $\delta V_D$  in platform coordinates is derived from equations (78) and (79). Let T represent the transformation angle  $T = \theta_S - \Delta$  from Doppler axes to platform axes. Let  $\delta$  represent the error in this transformation caused by Doppler drift angle error and synchro readout error, and let K represent Doppler scale factor error.

The complete Doppler to platform axes transformation including Doppler and synchro errors becomes

$$\begin{bmatrix} V_x \\ V_y \end{bmatrix} = \begin{bmatrix} \cos(T+\delta) & \sin(T+\delta) \\ -\sin(T+\delta) & \cos(T+\delta) \end{bmatrix} \begin{bmatrix} V \\ 0 \end{bmatrix} \quad (91)$$

It can be shown by expanding the expression above that the Doppler errors  $\delta V_D$  in platform coordinates are

$$\begin{bmatrix} \delta V_{D_x} \\ \delta V_{D_y} \end{bmatrix} = \begin{bmatrix} V_x & -V_y \\ V_y & V_x \end{bmatrix} \begin{bmatrix} K \\ \delta \end{bmatrix} \quad (92)$$

where K and  $\delta$  are the Doppler scale factor and drift angle errors in Doppler coordinates.

The Doppler scale factor ( $K_1$ ) and drift angle ( $\delta_1$ ) errors are modeled as exponentially correlated random variables generated by passing white Gaussian noise through

a first order linear shaping filter. The Doppler sea state errors ( $K_2, \delta_2$ ) are modeled differently depending on the aircraft flight condition. Over land they are modeled as fixed biases while for flight over water they are modeled as exponentially correlated random variables. The block diagram for the Doppler error source model is shown below.

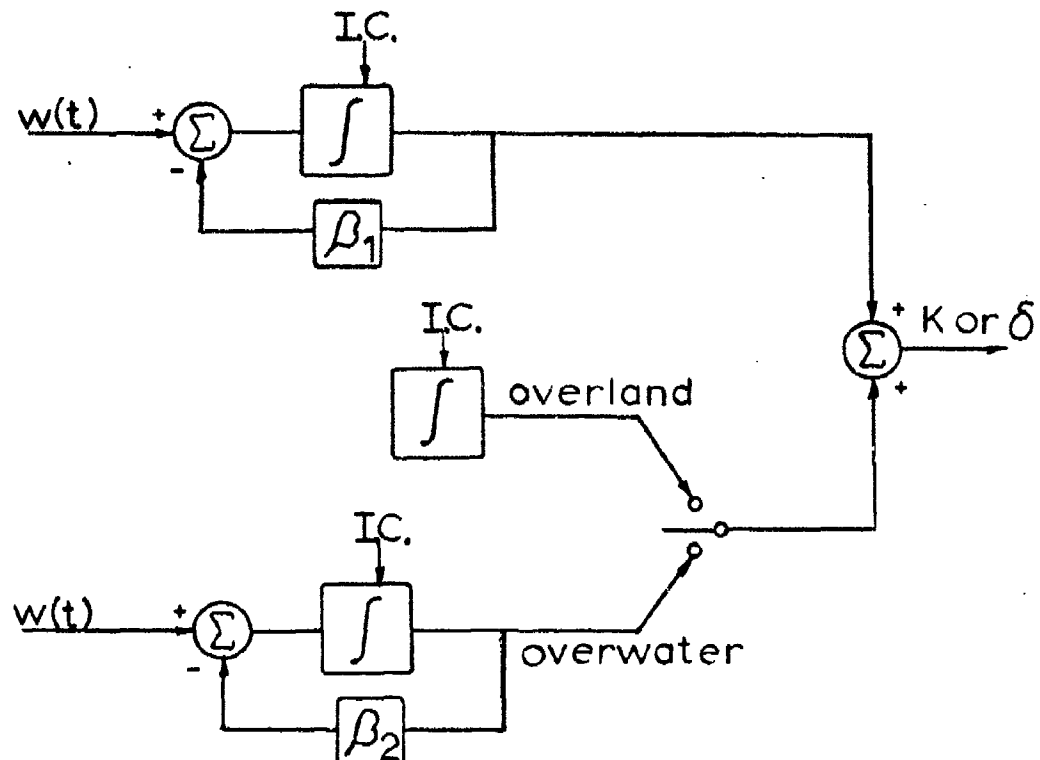


Figure 7. Doppler Error Source Model

Since the  $F_{22}$  and  $Q_{22}$  submatrices also contain elements determined by the INS and altimeter error source models, they will be shown after the complete error sources have been discussed.

INS Error Source Models. Through extensive testing and



and detailed knowledge of sensor dynamics many imperfections and errors of inertial navigation systems are removed by careful design. However, there still remain errors whose source defies compensation. The statistical behavior of these sensor errors can be obtained through testing and fitting curves to laboratory experimental data. The error models chosen for the gyros and accelerometers are typical of an INS in the one-half nautical mile per hour class. The gyro and accelerometer errors are modeled as a linear combination of fixed biases and exponentially correlated random variables as shown in the block diagram, Figure 8. Note the coupling between the gyro error sources and the tilt angles ( $\phi$ ) of the plant error source model as exemplified in submatrices  $F_{12}$ ,  $F_{13}$ , and  $F_{14}$ . Note also the coupling between the accelerometer error sources and the velocities as shown by submatrices  $F_{15}$  and  $F_{16}$ .

The eight gyro errors include long and short term drifts modeled as a fixed bias and an exponentially correlated random variable respectively. Gravity sensitive gyro errors in both the spin axis and input axis directions are modeled as fixed biases, as is the spin-input axes gravity squared sensitive error source. Gyro scale factor error and input axis misalignment about the other two axes complete the list of errors and are also modeled as fixed biases. Note that each gyro adds eight states to the state error vector, requiring 24 additional states in the system state error vector for the complete gyro error model.

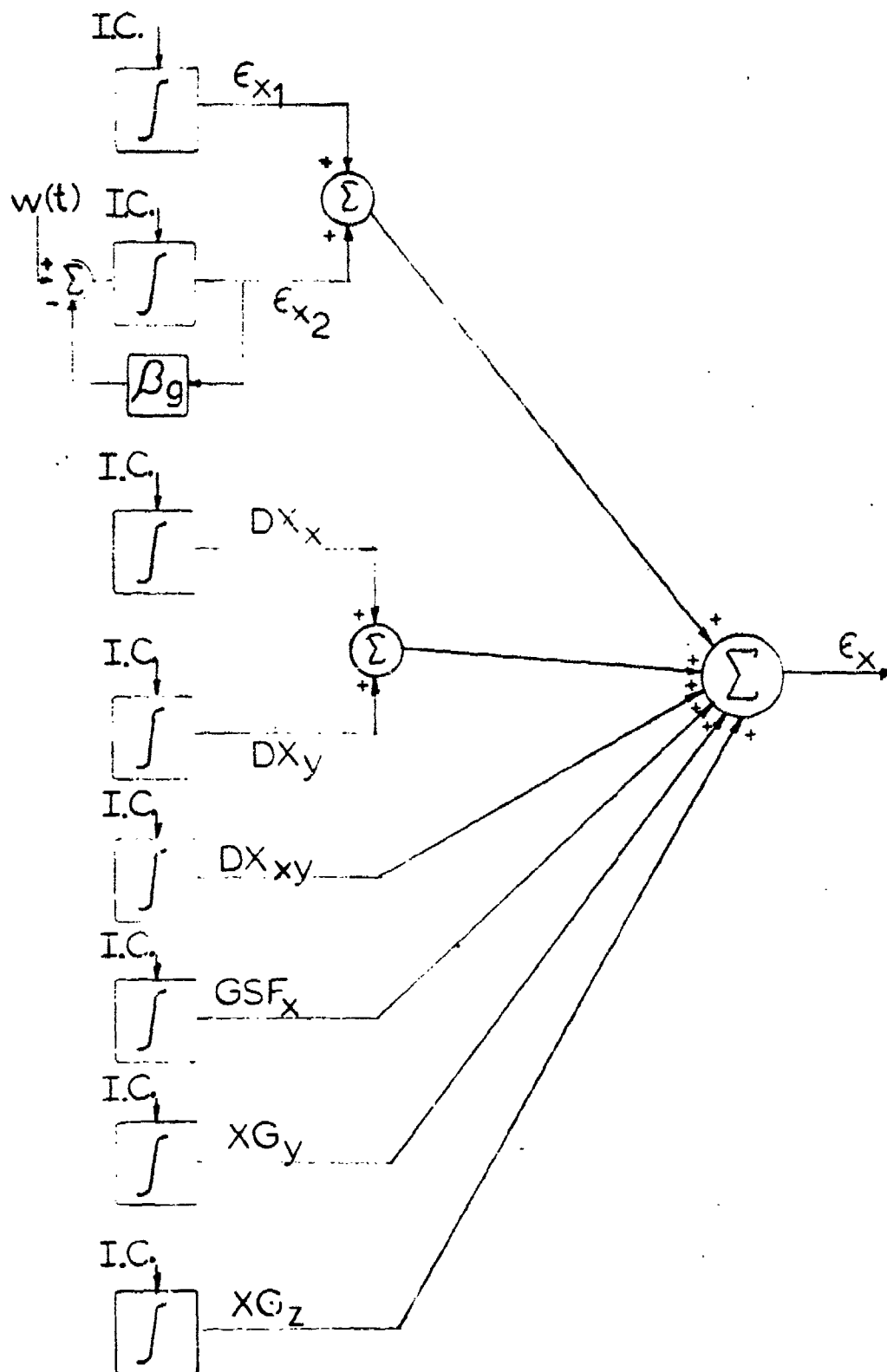


Figure 8. Gyro Error Source Model (Typical)

There are four accelerometer errors modeled as fixed biases. They include accelerometer bias, scale factor error, and input axis-misalignment about the other two axes. In addition, gravity anomaly is modeled as an exponentially correlated random variable. Since each accelerometer adds five states to the state error vector, an additional 15 states are required in the system state error vector for the complete accelerometer error model (See Figure 9).

The  $\underline{F}_s$  and  $\underline{Q}_s$  matrix terms, recalling the definition of states 1 to 54 from the Table I, are

$$\underline{F}_{12} = \begin{array}{c} \begin{array}{ccccc} & 11 & 12 & 13 & 14 & 15-17 \\ \begin{array}{c} 1-5 \\ 6 \\ 7 \\ 8 \\ 9 \\ 10 \end{array} & \left[ \begin{array}{ccccc|c} & & & & & 0 \\ \hline 0 & 0 & 0 & 1 & & \\ 1 & 0 & 0 & 0 & & \\ 0 & 1 & 0 & 0 & & 0 \\ 0 & 0 & 1 & 0 & & \\ \hline & & 0 & & & 0 \end{array} \right] \end{array} \quad (93)$$

$$\underline{F}_{13} = \begin{array}{c} \begin{array}{ccccc} & 18 & 19 & 20 & 21 & 22 & 23-24 \\ \begin{array}{c} 1-3 \\ 4 \\ 5 \\ 6 \\ 7 \\ 8 \\ 9 \\ 10 \end{array} & \left[ \begin{array}{ccccc|c} & & & & & 0 \\ \hline 0 & 0 & 0 & 1 & 0 & \\ 0 & 0 & 0 & 0 & 1 & \\ 0 & 0 & 0 & 0 & 0 & 0 \\ 1 & 0 & 0 & 0 & 0 & \\ 0 & 1 & 0 & 0 & 0 & \\ 0 & 0 & 1 & 0 & 0 & \\ \hline & & 0 & & & 0 \end{array} \right] \end{array} \quad (94)$$

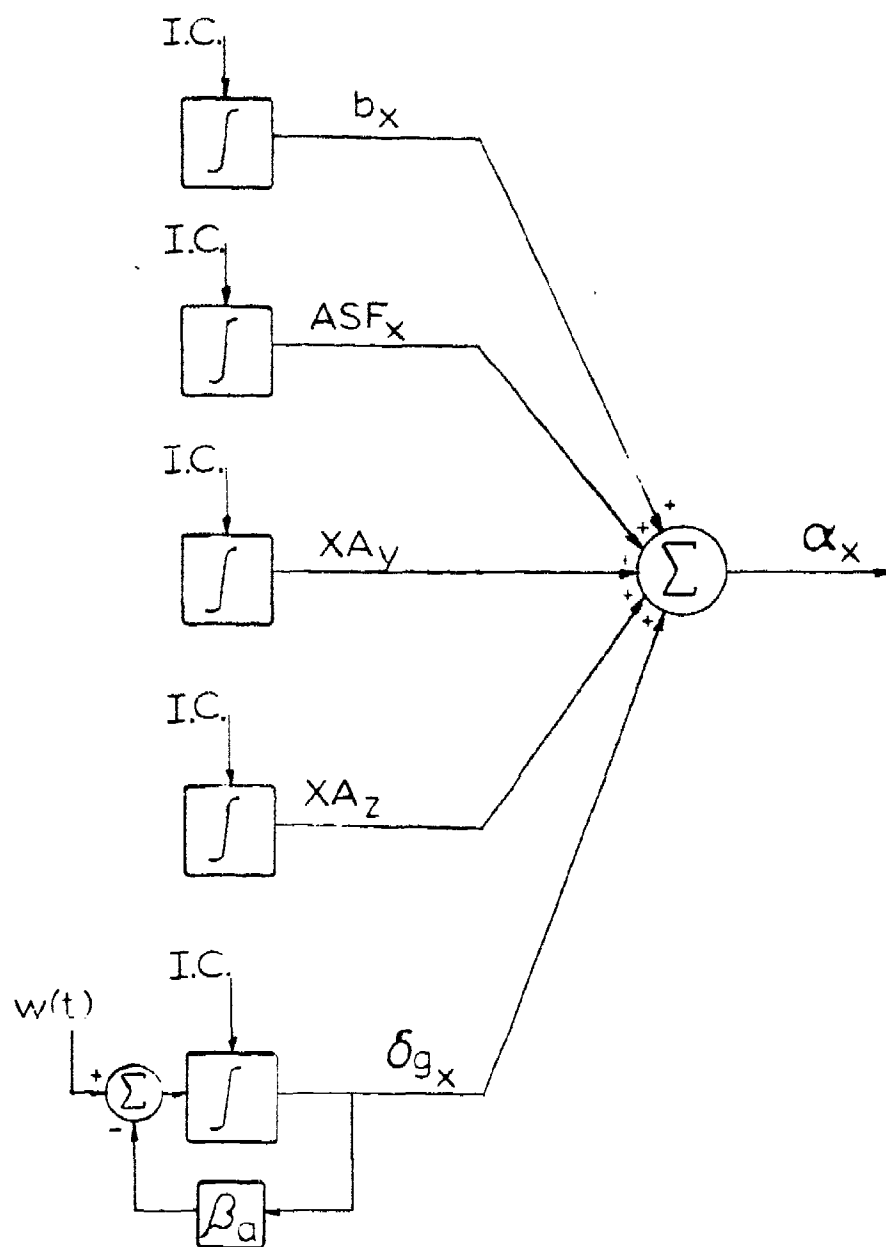


Figure 9. Accelerometer Error Source Model (Typical)

$$\underline{F}_{14} = \begin{array}{c} \begin{matrix} 1-6 \\ 7 \\ 8 \\ 9 \\ 10 \end{matrix} \end{array} \begin{array}{c} \begin{matrix} 25 & 26 & 27 & 28 & 29 & 30 \end{matrix} \\ \left[ \begin{array}{cccccc|cccc} & & & 0 & & & & & 0 & \\ \hline A_x & A_y & 0 & 0 & 0 & 0 & A_x A_y & 0 & 0 \\ 0 & 0 & A_x & A_y & 0 & 0 & 0 & A_x A_y & 0 \\ 0 & 0 & 0 & 0 & A_y & A_z & 0 & 0 & A_y A_z \\ \hline & & & 0 & & & & & 0 \end{array} \right] \end{array} \begin{array}{c} \begin{matrix} 31 & 32 & 33 \end{matrix} \end{array}$$

$$\underline{F}_{14} = \begin{array}{c} \begin{matrix} 1-6 \\ 7 \\ 8 \\ 9 \\ 10 \end{matrix} \end{array} \begin{array}{c} \begin{matrix} 34 & 35 & 36 & 37 & 38 & 39 & 40 & 41 & 42 \end{matrix} \\ \left[ \begin{array}{cccccc|cccc} & & & & & & 0 & & \\ \hline \omega_x & 0 & 0 & \omega_z & -\omega_y & 0 & 0 & 0 & 0 \\ 0 & \omega_y & 0 & 0 & 0 & -\omega_z & \omega_x & 0 & 0 \\ 0 & 0 & \omega_z & 0 & 0 & 0 & 0 & \omega_y & -\omega_x \\ \hline & & & & & & & & 0 \end{array} \right] \end{array} \begin{array}{c} \begin{matrix} 43 & 44 & 45 & 46 & 47 & 48 & 49 & 50 & 51 \end{matrix} \end{array} \quad (95)$$

(cont.)

$$\underline{F}_{15} = \begin{array}{c} \begin{matrix} 1-3 \\ 4 \\ 5 \\ 6 \\ 7-10 \end{matrix} \end{array} \begin{array}{c} \begin{matrix} 43 & 44 & 45 & 46 & 47 & 48 & 49 & 50 & 51 \end{matrix} \\ \left[ \begin{array}{cccccc|cccc} & & & & & & 0 & & \\ \hline A_x & 0 & 0 & -A_z & A_y & 0 & 0 & 0 & 0 \\ 0 & A_y & 0 & 0 & 0 & A_z & -A_x & 0 & 0 \\ 0 & 0 & A_z & 0 & 0 & 0 & 0 & -A_y & A_x \\ \hline & & & & & & & & 0 \end{array} \right] \end{array} \begin{array}{c} \begin{matrix} 52 & 53 & 54 \end{matrix} \end{array} \quad (96)$$

$$\underline{F}_{16} = \begin{array}{c} \begin{matrix} 1-3 \\ 4 \\ 5 \\ 6 \\ 7-10 \end{matrix} \end{array} \begin{array}{c} \begin{matrix} 52 & 53 & 54 \end{matrix} \\ \left[ \begin{array}{ccc|c} & & & 0 \\ \hline 1 & 0 & 0 & \\ 0 & 1 & 0 & \\ 0 & 0 & 1 & \\ \hline & & & 0 \end{array} \right] \end{array} \quad (97)$$

$$\underline{F}_{33} = \begin{matrix} & \begin{matrix} 18 & 19 & 20 & 21-24 \end{matrix} \\ \begin{matrix} 18 \\ 19 \\ 20 \\ 21-24 \end{matrix} & \left[ \begin{array}{ccc|c} -\beta_g & 0 & 0 & \\ 0 & -\beta_g & 0 & 0 \\ 0 & 0 & -\beta_g & \\ \hline & 0 & & 0 \end{array} \right] \end{matrix} \quad (98)$$

$$q_{18} = 2\beta_g P_{18} \quad (99)$$

$$q_{18} = 2(1/10,800 \text{ sec}) \left[ .003 \text{ deg/hr} \times \pi \text{ rad/180 deg} \times \frac{1 \text{ hr}}{3600 \text{ sec}} \right]^2 \quad (100)$$

$$q_{18} = 3.9174 \times 10^{-20} \text{ rad}^2/\text{sec}^3 \quad (101)$$

$$q_{18} = q_{19} \quad (102)$$

$$q_{20} = 2(1/10,800 \text{ sec}) \left[ .005 \text{ deg/hr} \times \pi \text{ rad/180 deg} \times \frac{1 \text{ hr}}{3600 \text{ sec}} \right]^2 \quad (103)$$

$$q_{20} = 1.0882 \times 10^{-19} \text{ rad}^2/\text{sec}^3 \quad (104)$$

$$\underline{F}_{66} = \begin{matrix} & \begin{matrix} 52 & 53 & 54 \end{matrix} \\ \begin{matrix} 52 \\ 53 \\ 54 \end{matrix} & \left[ \begin{array}{ccc} -\frac{v}{d_x} & 0 & 0 \\ 0 & -\frac{v}{d_y} & 0 \\ 0 & 0 & -\frac{v}{d_a} \end{array} \right] \end{matrix} \quad (105)$$

For the baseline data in straight and level unaccelerated flight at  $V=710$  feet per second

$$q_{52} = \frac{2VP}{d_x} 52 \quad (106)$$

$$q_{52} = \frac{2(710 \text{ ft/sec}) \left[ (26 \times 10^{-6} g) (32.2 \text{ ft/sec}^2 - g) \right]}{(10 \text{ nm} \times 6080 \text{ ft/nm})} 2 \quad (107)$$

$$q_{52} = 1.637 \times 10^{-8} \text{ ft}^2/\text{sec}^5 \quad (108)$$

Similarly

$$q_{53} = \frac{2(710 \text{ ft/sec}) \left[ (17 \times 10^{-6} \text{ g}) (32.2 \text{ ft/sec}^2\text{-g}) \right]^2}{(10\text{nm} \times 6080 \text{ ft/nm})} \quad (109)$$

$$q_{53} = 6.998 \times 10^{-9} \text{ ft}^2/\text{sec}^5 \quad (110)$$

and

$$q_{54} = \frac{2(710 \text{ ft/sec}) \left[ (35 \times 10^{-6} \text{ g}) (32.2 \text{ ft/sec}^2\text{-g}) \right]^2}{(60\text{nm} \times 6080 \text{ ft/nm})} \quad (111)$$

$$q_{54} = 4.944 \times 10^{-9} \text{ ft}^2/\text{sec}^5 \quad (112)$$

Altimeter Error Source Model. The inertial navigation system vertical position is derived by integration of vertical velocity. This output is inherently divergent but is damped with measurements of elevation above mean sea level obtained from Central Air Data Computer (CADC) outputs.

The altitude is initialized either by radar altimeter measurement or with altitude derived from the CADC using a standard atmosphere model. After initialization, CADC static pressure and free air temperature are used to adjust the altitude output for non-standard atmospheric conditions. Altitude calibrations may be obtained when the aircraft is over terrain/sea of known elevation using radar measurement techniques. The altitude is updated

every one minute in this mechanization.

The altimeter error is modeled as an exponentially correlated random variable. The differential equation and block diagram are:

$$\dot{\delta h} = -\beta_h \delta h + \eta \quad (113)$$

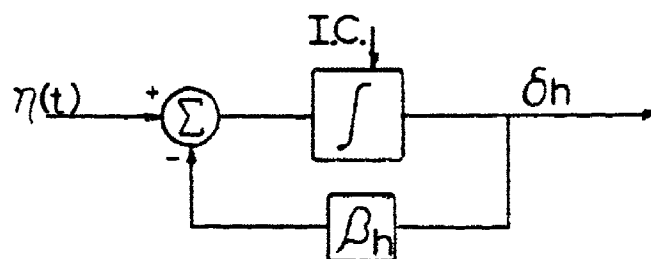


Figure 10. Altimeter Error Source Model

The non-standard atmosphere algorithm output is differenced once each minute with the IMU altitude output to four as an altitude observation for the Kalman filter. When altitude is calibrated the non-standard atmosphere algorithm is reinitialized to the sum of the height above terrain plus terrain height above mean sea level. A vertical position update is made within six seconds after altitude calibration.

The contributions made to the system  $\underline{F}$  and  $\underline{Q}$  matrices from the gyro long and short term drifts, the z-axis accelerometer bias, the Doppler scale factor and drift angle errors, and the altimeter error are, again referring to



Table I for the definition of pertinent state variable:

$$\underline{F}_{22} = \begin{matrix} & \begin{matrix} 11 & 12 & 13 & 14 & 15 & 16 & 17 \end{matrix} \\ \begin{matrix} 11 \\ 12 \\ 13 \\ 14 \\ 15 \\ 16 \\ 17 \end{matrix} & \left[ \begin{array}{cccccc} 0 & 0 & 0 & 0 & 0 & 0 & 0 \\ 0 & 0 & 0 & 0 & 0 & 0 & 0 \\ 0 & 0 & 0 & 0 & 0 & 0 & 0 \\ 0 & 0 & 0 & 0 & 0 & 0 & 0 \\ 0 & 0 & 0 & 0 & \beta_k & 0 & 0 \\ 0 & 0 & 0 & 0 & 0 & \beta_h & 0 \\ 0 & 0 & 0 & 0 & 0 & 0 & \beta_h \end{array} \right] \end{matrix} \quad (114)$$

$$q_{15} = 2\beta_k P_{15} (\text{no. of samples}) \quad (115)$$

$$q_{15} = 2(1/900 \text{ sec}) [0.0012]^2 (6) \quad (116)$$

$$q_{15} = 1.92 \times 10^{-8} / \text{sec} \quad (117)$$

Similarly,

$$q_{16} = 2(1/900 \text{ sec}) [(1.8 \times 10^{-3}) \text{ rad}]^2 (6) \quad (118)$$

$$q_{16} = 4.32 \times 10^{-8} \text{ rad}^2 / \text{sec} \quad (119)$$

and

$$q_{17} = 2\beta_h P_{17} \quad (120)$$

$$q_{17} = 2(1/1800 \text{ sec}) [250 \text{ ft}]^2 \quad (121)$$

$$q_{17} = 69.444 \text{ ft}^2 / \text{sec} \quad (122)$$

### System Measurement Equation

The system measurement equation consists of a set of five linear equations incorporating x and y axis position error, altitude error, and x and y velocity error and is

of the form derived in Chapter III (Equation 34).

The  $\underline{H}$  matrix maps the state error vector into predicted position, altitude, and velocity measurement errors. The predicted errors,  $\underline{H}\hat{\delta\mathbf{x}}$ , are differenced with the observed errors to form the residuals. Since the position error observation is formed in platform coordinates and no position measurement biases are estimated by the filter, the position error mapping elements are unity. The altitude observation is formed along the z-axis with a predicted altitude divergence of

$$\delta\hat{z} - \hat{h} \quad (123)$$

where  $\hat{h}$  is the filter's estimate of the barometric altimeter bias. The third row of the  $\underline{H}$  matrix therefore contains a one and a minus one in the appropriate positions to yield the above relation.

The rows of the  $\underline{H}$  matrix that relate to velocity measurements reflect the fact that the system velocity error estimate must be corrected for the Doppler error estimate in forming the residual with the observed velocity difference. The Doppler error correction modeled in the  $\underline{H}$  matrix represents the substitution of equation 92 into equations 89 and 90.

The system measurement equation is equation 34 repeated here

$$\underline{z}_S = \underline{H}_S \underline{x}_S + \underline{v}_S \quad (124)$$

where the 54 variables of  $\underline{x}_S$  are listed in Table I and

$$\underline{z}_S = \begin{bmatrix} \delta_x \\ \delta_y \\ \delta_z \\ \delta_{v_x} \\ \delta_{v_y} \end{bmatrix} \quad (125)$$

$\underline{H}_S$  is the 5 by 54 matrix shown in Figure 11. The white Gaussian noise vector  $\underline{v}_S$  is described by the covariance matrix  $\underline{R}_S$  where

$$\underline{R}_S = \begin{bmatrix} \sigma_x^2 & 0 & 0 & 0 & 0 \\ 0 & \sigma_y^2 & 0 & 0 & 0 \\ 0 & 0 & \sigma_z^2 & 0 & 0 \\ 0 & 0 & 0 & \sigma_{v_x}^2 & 0 \\ 0 & 0 & 0 & 0 & \sigma_{v_y}^2 \end{bmatrix} \quad (126)$$

The values chosen for the elements of  $\underline{R}_S$  are shown in Table II.

	1	2	3	4	5	6	8	9	10	14	15	16	17	25	54
1	1	0	0	0	0	0	0	0	0	0	0	0	0	0	0
2	0	1	0	0	0	0	0	0	0	0	0	0	0	0	0
3	0	0	1	0	0	0	0	0	0	0	0	0	-1	0	0
4	0	0	0	1	0	0	0	-V <sub>y</sub>	0	0	-V <sub>x</sub>	V <sub>y</sub>	0	0	0
5	0	0	0	0	1	0	0	V <sub>x</sub>	0	0	V <sub>y</sub>	-V <sub>x</sub>	0	0	0

Figure 11. System Measurement H Matrix

Table II

Elements of  $R_s$  Matrix

Element	Value
$\sigma_x^2$	$(500 \text{ ft})^2$
$\sigma_y^2$	$(500 \text{ ft})^2$
$\sigma_z^2$	$(20 \text{ ft})^2$
$\sigma_{v_x}^2$	$3.48 \times 10^{-3}  v $
$\sigma_{v_y}^2$	$3.48 \times 10^{-3}  v $

## V. Filter Design

This chapter discusses the filter design chosen for mechanization as well as several preliminary filters which led to this choice. None of the preliminary filter designs are presented in detail but merely as outlines to show the process of filter reduction. The filter designs discussed include: (1) the 54-state optimal filter, (2) various reduced order filters, and (3) the decoupled 17-state filter.

Selection of the number and type of state variables to be included in the reduced order Kalman filter is based on a trade-off between desired accuracy and computational time required by the onboard computer. Obviously, the most accurate filter would be the optimal 54-state filter; however, the burden this mechanization would place on the computer is unacceptable. Therefore, filter designs are proposed which eliminate second order effects and weak cross-couplings in an attempt to reduce the dimension of the error state vector while maintaining reasonable filtering accuracy. Many of the stronger cross-coupling terms affect filter performance only during highly dynamic flight conditions, while the majority of time is spent in relatively straight and level unaccelerated flight. In this case, it is often presupposed that the cross-coupling effects in this category may be ignored for short periods of time to further reduce the complexity of the onboard computer calculations. This study investigates the effects of a

highly dynamic flight regime on filter accuracy and attempts to determine the major contributing error sources in this environment.

#### The Optimal Filter

The optimal filter system model is simply an exact replica of the reference system model (i.e. the same 54-state system and measurement model given in Chapter IV). This optimal 54-state filter will yield the most accurate performance possible for the given set of reference system error state and measurement equations. Thus the error covariances obtained using the optimal filter are often used as the standard against which to compare the performance of sub-optimal filter designs. This is the technique utilized for the initial portion of this study (i.e. evaluation of the decoupled 17-state filter performance in straight and level flight).

#### Reduced Order Filters

The first attempt to design a sub-optimal or reduced order filter was made by eliminating the state variables numbered 25 through 54 listed in the reference system state vector definition (Table I) in Chapter IV. The result was a 24-state Kalman filter design with new values for the elements of the  $Q$  matrix. Elimination of the fixed biases and exponentially correlated random variables modeled in reference system states 25 through 54 were compensated in filter model by adding new values or increasing existing

values in the filter  $Q'$  matrix for states 1 through 24.

Next the error state vector was reduced to 19 states by eliminating the short term gyro drifts and the x and y axes accelerometer bias terms. This mechanization was found to be unsatisfactory and the accelerometer bias terms were reinserted while the Doppler sea state variables were combined with the Doppler scale factor and drift angle errors, thereby achieving a second 19-state design. Again compensation was made in the  $Q'$  matrix by computing new values for appropriate elements.

A 17-state fully coupled sub-optimal filter design was derived by eliminating the x and y axes accelerometer bias terms and decoupling the horizontal (level) and vertical channels. The changes made to the elements of the  $Q'$  matrix to compensate for elimination of the two level axis accelerometer bias terms will be discussed in the section on the decoupled 17-state filter.

#### Decoupled 17-State Filter

The decoupled 17-state (13+4) filter mechanization includes the 10 states of the Raides inertial navigation system error model, three gyro fixed biases, the z-axis accelerometer bias, Doppler scale factor and drift angle errors, and the barometric altimeter error as the filter error state vector elements. In the navigation software, the level axis (x and y) errors are decoupled from the vertical axis (z) errors. The theory behind the decoupled equations will not be discussed here but a thorough



treatment may be found in Reference 14. The elements of 17-state error vector are shown in Table III along with the initial condition on each of the error states.

The decoupled 17-state filter mechanization combines state variables numbered 3, 6, 14, and 17 into the four element vertical channel error state vector. The remaining error state variables make up the decoupled 13 element level channel error state vector. For this evaluation the filter model was treated as one 17-state error vector with appropriate cross-coupling elements set to zero.

Incorporating the Raides INS error model into the decoupled 17-state filter requires the computation of only 33 non-zero terms in the filter  $\underline{F}$  matrix as compared to 53 non-zero terms required in the fully coupled 17-state plant error model. The simplified  $\underline{F}$  matrix along with the  $\underline{Q}$ ,  $\underline{H}$ , and  $\underline{R}$  matrices for the decoupled 17-state filter are given in Equations 127 through 130 and Tables II and IV. The submatrices of the filter  $\underline{F}$  matrix are shown in Figures 12 and 13.

$$\underline{F} = \begin{matrix} & \begin{matrix} 1-10 & 11-13 & 14 & 15 & 16 & 17 \end{matrix} \\ \begin{matrix} 1-10 \\ 11-13 \\ 14 \\ 15 \\ 16 \\ 17 \end{matrix} & \left[ \begin{array}{c|c|c|c|c|c} \hline F_{11} & F_{12} & F_{13} & 0 & 0 & 0 \\ \hline 0 & 0 & 0 & 0 & 0 & 0 \\ \hline 0 & 0 & 0 & 0 & 0 & 0 \\ \hline 0 & 0 & 0 & -\beta_k & 0 & 0 \\ \hline 0 & 0 & 0 & 0 & -\beta_d & 0 \\ \hline 0 & 0 & 0 & 0 & 0 & -\beta_h \\ \hline \end{array} \right] \end{matrix} \quad (127)$$

Table III

Filter 17 State Error Vector Definition

Error State	Symbol	Definition	RMS Initial Condition
<u>INS Plant Error States</u>			
1	$\delta x$	x position error	50,000 ft
2	$\delta y$	y position error	50,000 ft
3	$\delta z$	z position error	1,000 ft
4	$\delta v_x$	x velocity error	10 ft/sec
5	$\delta v_y$	y velocity error	10 ft/sec
6	$\delta v_z$	z velocity error	5 ft/sec
7	$\delta \phi_x$	x attitude error	.0175 rad (1 deg)
8	$\delta \phi_y$	y attitude error	.0175 rad (1 deg)
9	$\delta \phi_z$	z attitude error	0.000 rad
10	$\delta \theta_z$	computer axes to true axes compu- tation error	.0349 rad (2 deg)
<u>INS, Doppler and Altimeter Errors</u>			
11	$\epsilon_{x1}$	x gyro random bias	.03 deg/hr
12	$\epsilon_{y1}$	y gyro random bias	.03 deg/hr
13	$\epsilon_{z1}$	z gyro random bias	.045deg/hr
14	$b_z$	z accelerometer random bias	250 $\mu g$
15	K	Doppler Scale factor error exp. correlated $\tau = 900\text{sec}$	.15 %

Table III

Filter 17-State Error Vector Definition  
(Cont.)

Error State	Symbol	Definition	RMS Initial Condition
16	$\delta$	Doppler drift angle error exp. correlated $T = 900$ sec	6.0 millirad
17	$\delta h$	altimeter error exp. correlated $T = 1800$ sec	250 ft

Table IV  
Decoupled 17-State Filter  $Q'$  Elements

Element	Value
$q_4$	$2.7 \times 10^{-6} \text{ ft}^2/\text{sec}^3$
$q_5$	$2.7 \times 10^{-6} \text{ ft}^2/\text{sec}^3$
$q_7$	$2.76 \times 10^{-12} \text{ rad}^2/\text{sec}$
$q_8$	$2.76 \times 10^{-12} \text{ rad}^2/\text{sec}$
$q_{11}$	$1.2 \times 10^{-19} \text{ rad}^2/\text{sec}^3$
$q_{12}$	$1.2 \times 10^{-19} \text{ rad}^2/\text{sec}^3$
$q_{13}$	$1.2 \times 10^{-19} \text{ rad}^2/\text{sec}^3$
$q_{14}$	$4.15 \times 10^{-9} \text{ ft}^2/\text{sec}^3$
$q_{15}$	$3.0 \times 10^{-8} / \text{sec}$
$q_{16}$	$4.8 \times 10^{-7} \text{ rad}^2/\text{sec}$
$q_{17}$	$69.44 \text{ ft}^2/\text{sec}$

	1	2	3	4	5	6	7	8	9	10
1	0	0	0	1	0	0	0	0	0	$-V_y$
2	0	0	0	0	1	0	0	0	0	$V_x$
3	0	0	0	0	0	1	0	0	0	0
4	$\frac{2V_y\Omega_x}{R}$	$\frac{2V_y\Omega_y}{R}$	0	0	$\rho_z + 2\Omega_z$	0	0	$-A_z$	$A_y$	0
5	$-\frac{2V_x\Omega_x}{R}$	$-\frac{2V_x\Omega_y}{R}$	0	$\rho_z - 2\Omega_z$	0	0	$A_z$	0	$-A_x$	0
6	0	0	$\frac{2q}{R}$	0	0	0	0	0	0	0
7	$-\frac{\Omega_z}{R}$	0	0	0	$-\frac{1}{R}$	0	0	$\omega_z$	$-\omega_y$	$\Omega_y$
8	0	$-\frac{\Omega_z}{R}$	0	$\frac{1}{R}$	0	0	$-\omega_z$	0	$\omega_x$	$-\Omega_x$
9	$\frac{\Omega_x}{R}$	$\frac{\Omega_y}{R}$	0	0	0	0	$\omega_y$	$-\omega_x$	0	0
10	$\frac{V_y}{R^2}$	$-\frac{V_x}{R^2}$	0	0	0	0	0	0	0	0

Figure 12. Decoupled 17-State Filter  $\underline{F}_{11}$  Sub-Matrix

$$\underline{E}_{12} =$$

	11	12	13
1-6	0	0	0
7	1	0	0
8	0	1	0
9	0	0	1
10	0	0	0

$$\underline{E}_{13} =$$

	14
1-5	0
6	1
7-10	0

Figure 13. Decoupled 17-State Filter  $\underline{E}_{12}$  and  $\underline{E}_{13}$  Submatrices

$$\underline{Q}_f = \begin{matrix} & \begin{matrix} 1-3 & 4 & 5 & 6 & 7 & 8 & 9-10 & 11-17 \end{matrix} \\ \begin{matrix} 1-3 \\ 4 \\ 5 \\ 6 \\ 7 \\ 8 \\ 9-10 \\ 11-17 \end{matrix} & \left[ \begin{array}{cccccccc} 0.0 & & & & & & & \\ & q_4 & & & & & & \\ & & q_5 & & & & & \\ & & & 0.0 & & & & \\ & & & & q_7 & & & \\ & & & & & q_8 & & \\ & & & & & & 0.0 & \\ & & & & & & & q_{11} \\ & & & & & & & & q_{17} \end{array} \right] \end{matrix} \quad (128)$$

$$\underline{H}_f = \begin{matrix} & \begin{matrix} 1 & 2 & 3 & 4 & 5 & 6-8 & 9 & 10-14 & 15 & 16 & 17 \end{matrix} \\ \begin{matrix} 1 \\ 2 \\ 3 \\ 4 \\ 5 \end{matrix} & \left[ \begin{array}{ccccccccccc} 1 & 0 & 0 & 0 & 0 & & 0 & & 0 & 0 & 0 \\ 0 & 1 & 0 & 0 & 0 & & 0 & & 0 & 0 & 0 \\ 0 & 0 & 1 & 0 & 0 & 0 & & 0 & 0 & 0 & -1 \\ 0 & 0 & 0 & 1 & 0 & & -v_y & & -v_x & v_y & 0 \\ 0 & 0 & 0 & 0 & 1 & & v_x & & -v_y & -v_x & 0 \end{array} \right] \end{matrix} \quad (129)$$

$$\underline{R}_f = \begin{matrix} & \begin{matrix} 1 & 2 & 3 & 4 & 5 \end{matrix} \\ \begin{matrix} 1 \\ 2 \\ 3 \\ 4 \\ 5 \end{matrix} & \left[ \begin{array}{ccccc} \sigma_x^2 & 0 & 0 & 0 & 0 \\ 0 & \sigma_y^2 & 0 & 0 & 0 \\ 0 & 0 & \sigma_z^2 & 0 & 0 \\ 0 & 0 & 0 & \sigma_{v_x}^2 & 0 \\ 0 & 0 & 0 & 0 & \sigma_{v_y}^2 \end{array} \right] \end{matrix} \quad (130)$$

The values of the elements in the  $R_f$  matrix are given in Table II, Chapter IV.

The value of the elements for the filter  $\underline{P}(0)$  matrix are specified in Table III for each of the filter states. The values actually used are the squared values of the RMS initial conditions and are located along the principal diagonal of the  $\underline{P}(0)$  matrix. Ten off-diagonal elements enter into the filter  $\underline{P}(0)$  matrix for airborne alignment of the INS. The relationships governing these initial conditions are given in Equations (131) through (135). Only five equations are given since the off-diagonal terms are identical both above and below the principal diagonal of the  $\underline{P}(0)$  matrix (i.e.  $\sigma^2_{V_x V_y} = \sigma^2_{V_y V_x}$ , etc.)

$$\sigma^2_{V_x V_y} = (\sigma^2_{KK} - \sigma^2_{\delta\delta}) V_{x0} V_{y0} \quad (131)$$

$$\sigma^2_{V_x K} = \sigma^2_{KK} V_{x0} \quad (132)$$

$$\sigma^2_{V_y K} = \sigma^2_{KK} V_{y0} \quad (133)$$

$$\sigma^2_{V_x \delta} = -\sigma^2_{\delta\delta} V_{y0} \quad (134)$$

$$\sigma^2_{V_y \delta} = \sigma^2_{\delta\delta} V_{x0} \quad (135)$$



VI. Test Conditions

The performance evaluation of the decoupled 17-state filter was based on two test conditions. The first test condition simulated a straight and level unaccelerated aircraft flight profile of approximately two hours duration. Comparison of the decoupled 17-state filter with the 54-state optimal filter utilizes this straight and level test condition. The decoupled filter and reference system RMS initial conditions were taken as the values listed in Tables I and III respectively. The RMS initial conditions for the optimal filter duplicate those of the reference system.

The second test condition simulated one additional hour of flight. The additional hour was obtained by inserting the final values of all elements of both the filter and reference system  $P$  matrices after two hours of flight, as obtained from the first test condition, into the initial  $P$  matrices for one hour of flight. The performance of the decoupled 17-state filter in straight and level unaccelerated flight under the second test condition was used as a baseline for both the maneuvering flight evaluation and error budget determination. The second test condition also included a highly dynamic flight profile over the same additional hour with the initial conditions on the filter and reference system  $P$  matrices described above. The flight profile was highly dynamic to simulate aircraft maneuvers such as might be encountered during low altitude flight.

Basic Flight Profile

The basic flight profile used in this evaluation is a straight and level flight path at an altitude of 2000 feet and a true heading (aircraft heading referenced from True North) of 30 degrees with an aircraft velocity of 710 feet per second. The initial position chosen was 45 degrees North latitude and 60 degrees West longitude. The course flown was a rhumb line; i.e. a path of constant heading. The altitude was chosen to be compatible with a low altitude flight environment but has little or no effect on the results for a vehicle operating near the surface of the Earth due to the large value of Earth radius. The heading of 30 degrees was chosen based on preliminary data indicating that this heading approximates "worst case" conditions on navigation circular error probability. The velocity of 710 feet per second is consistent with low altitude subsonic flight and converts to 420 nautical miles per hour (knots).

The basic flight profile was generated by a subroutine in the covariance analysis computer program and provided both translational and rotational velocity and acceleration, Earth radius, and gravity data in the alpha wander coordinate frame. This data was then used during computation of the values to be inserted into the elements of both the filter and the reference system  $F$  matrices. The basic flight profile is shown in Figure 14.

Plots of the RMS value of nine of the ten plant error states (position, velocity, and attitude) error covariances

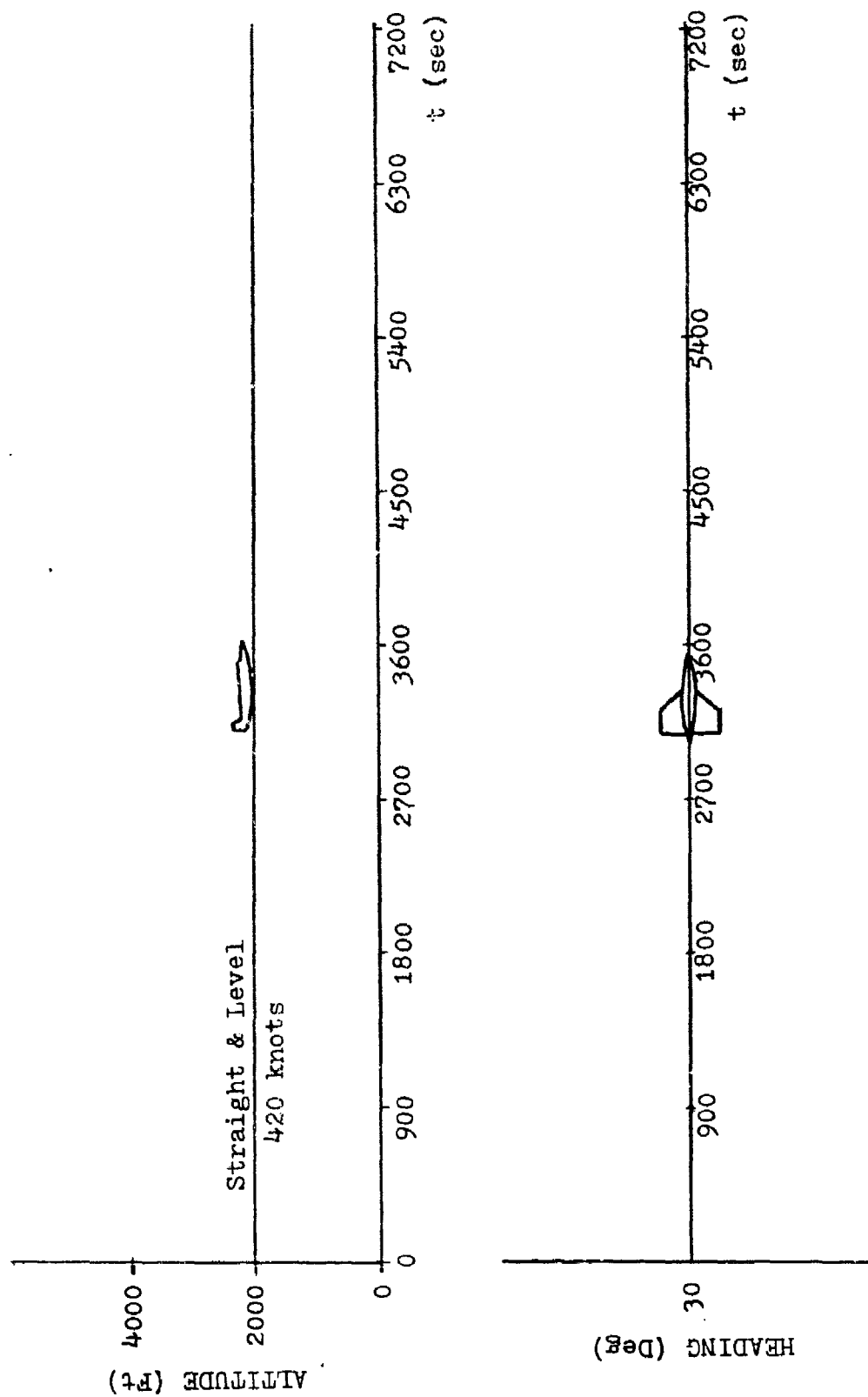


Figure 14. Baseline Flight Profile

for the optimal filter during straight and level flight are shown in Figures 15 through 23. These plots provide the basis against which sub-optimal filter performance will be compared. Note that the time of flight differs slightly between plots (7000 seconds for the optimal filter and 7200 seconds for the reduced filter). Also, the vertical axis is automatically scaled in the computer plotting routine and may vary from one case to the next except for the error budget plots. For example, the optimal filter z axis attitude error (Figure 23) is scaled from 0.0 to  $0.40 \times 10^{-2}$  radians whereas the plot of this same variable for the decoupled 17-state filter (Figure 32) is scaled from 0.0 to  $0.80 \times 10^{-2}$  radians. For the error budget plots, a constant maximum value was specified for the vertical axis for each state variable making all the plots consistent.

The reference system RMS position, velocity, and attitude error plots for the decoupled 17-state filter during straight and level flight are given in Figures 24 through 32 and should be compared with those for the optimal filter. Tables V and VI following these plots compare the reference system plant x, y, and z position, velocity, and tilt error values for both the optimal and decoupled 17-state filter at 3600 (mid-time update) and 6300 seconds (last recorded update) with the initial values to provide a quick comparison of performance.

Note that the decoupled 17-state filter most closely approaches the accuracy of the optimal filter after

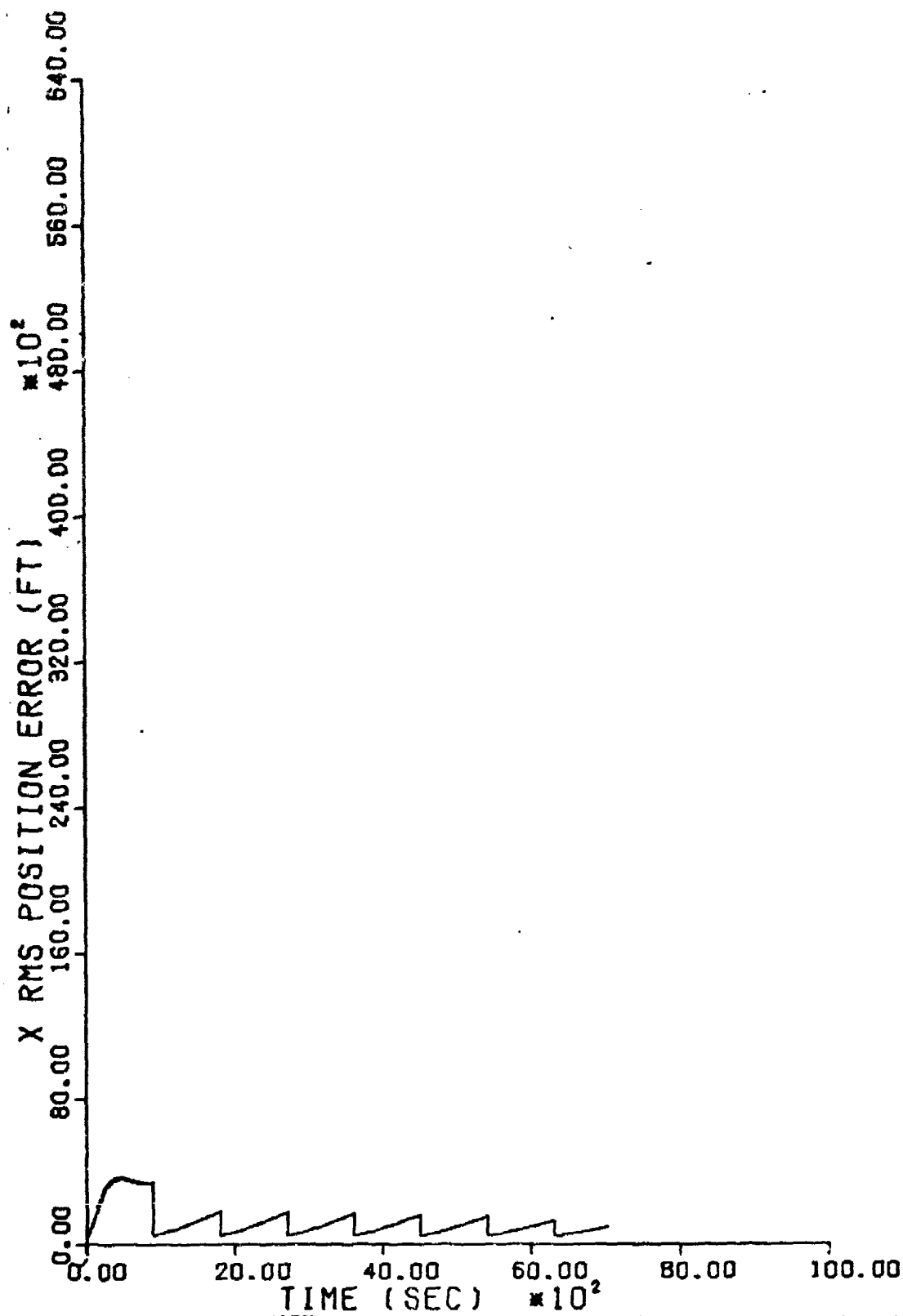


Figure 15. Optimal Filter X RMS Position Error

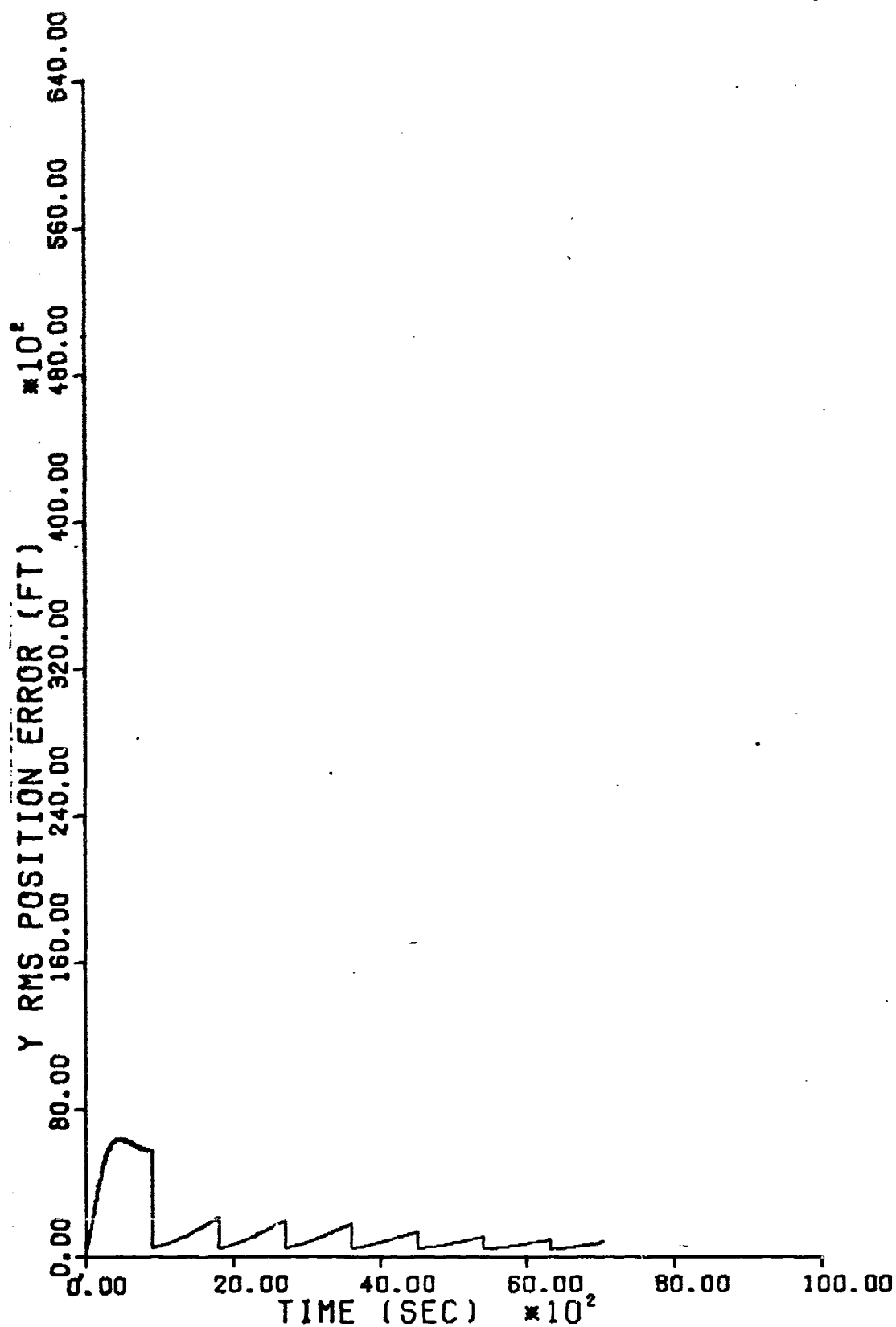


Figure 16. Optimal Filter Y RMS Position Error

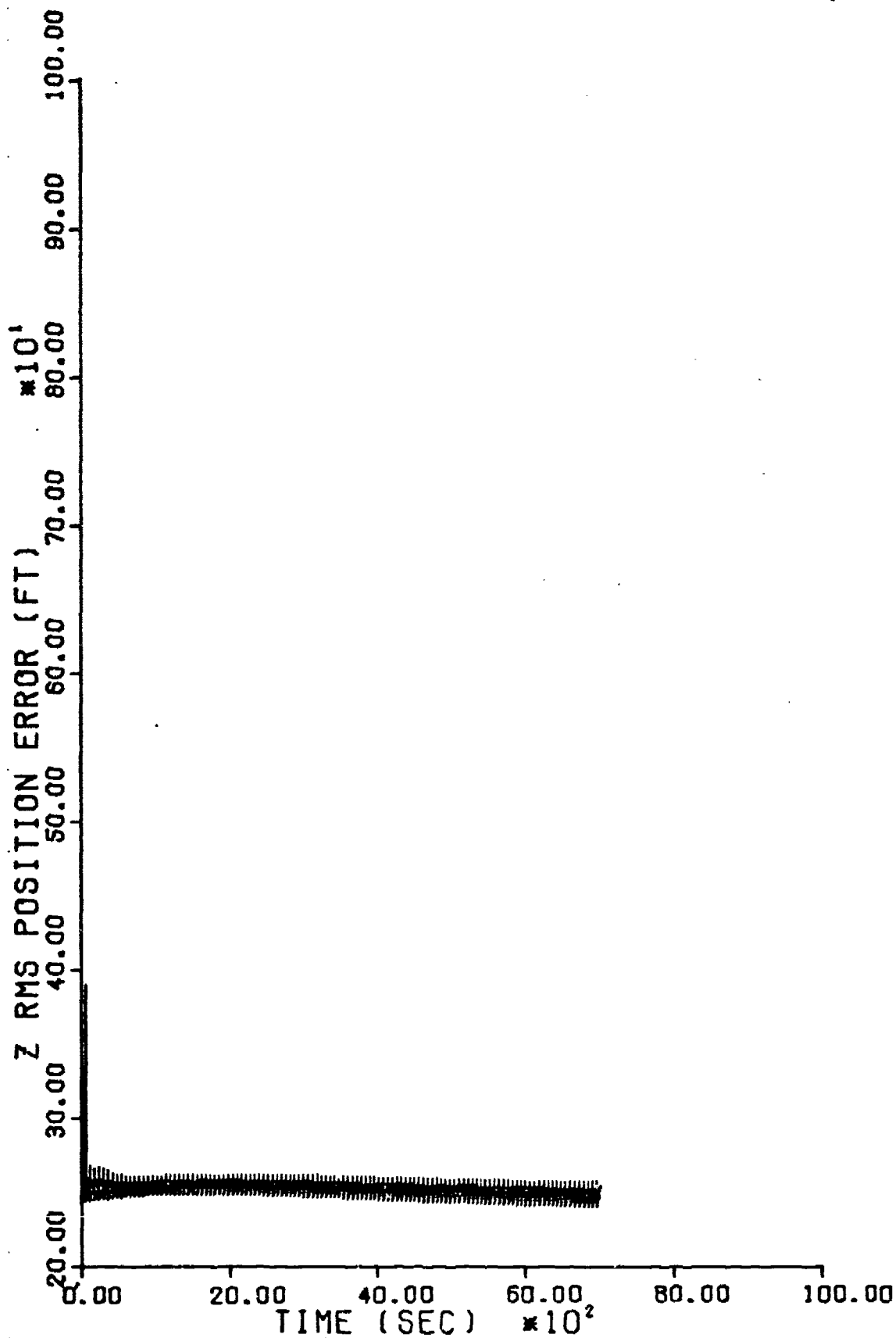


Figure 17. Optimal Filter Z RMS Position Error

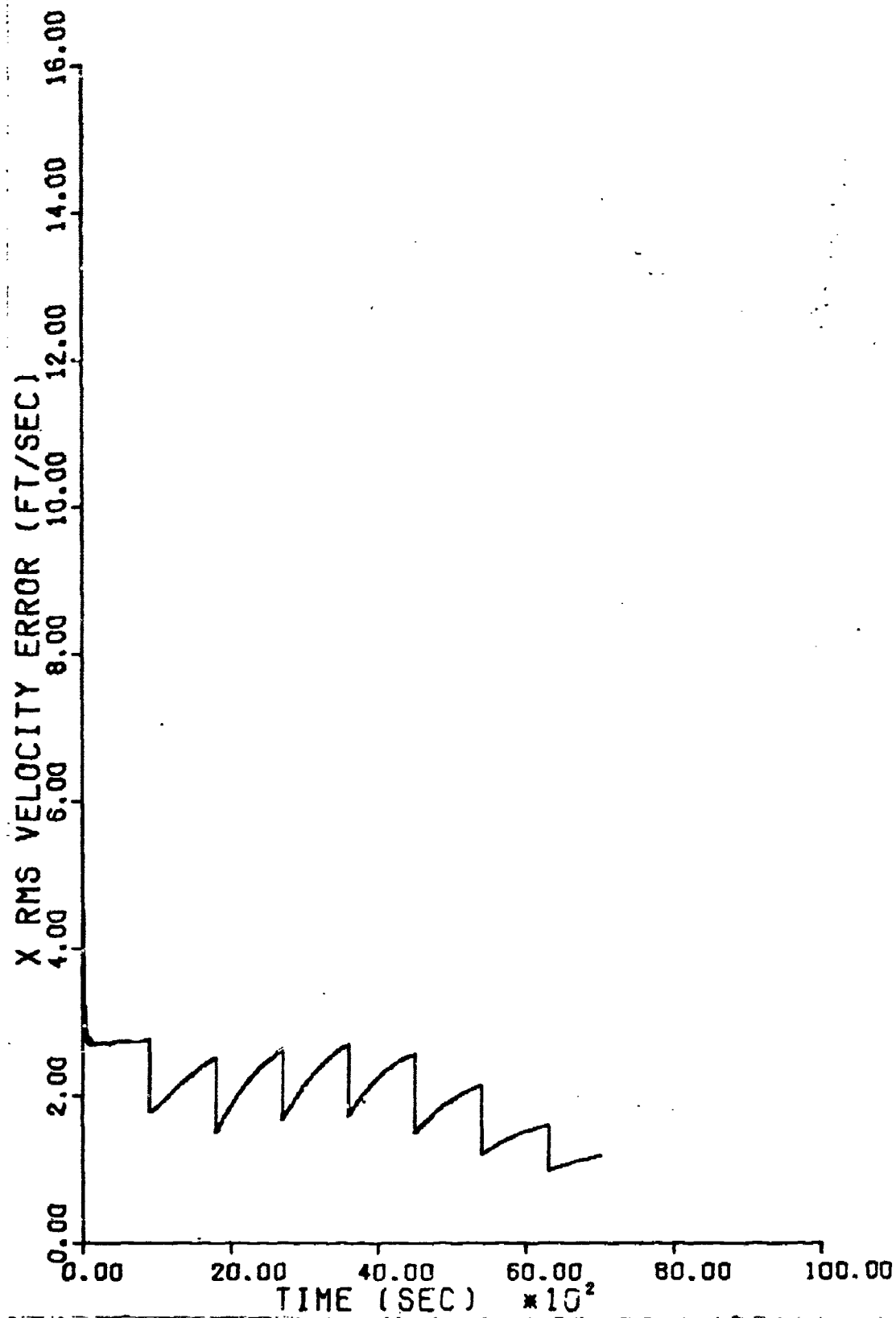


Figure 18. Optimal Filter X RMS Velocity Error



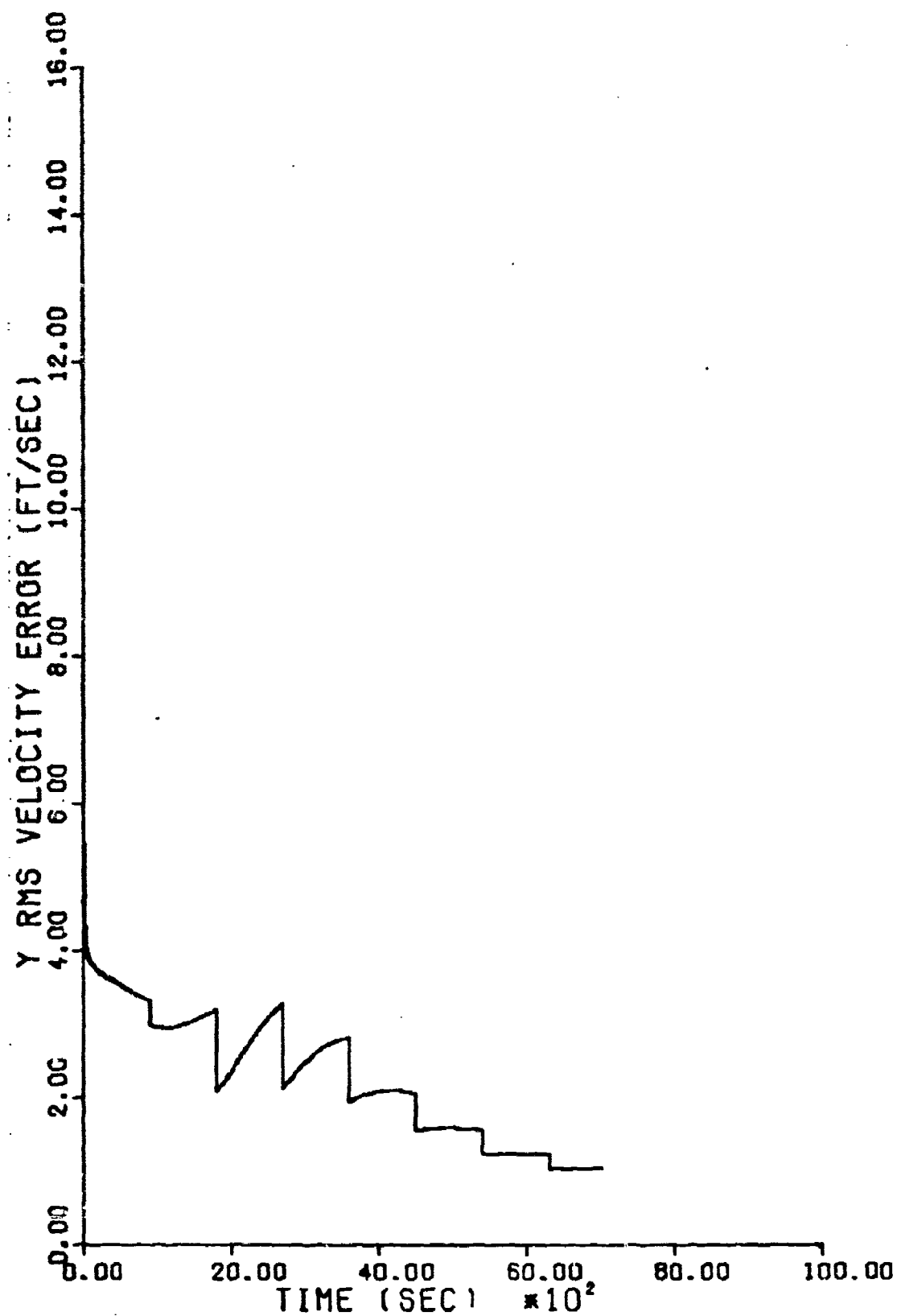


Figure 19. Optimal Filter Y RMS Velocity Error

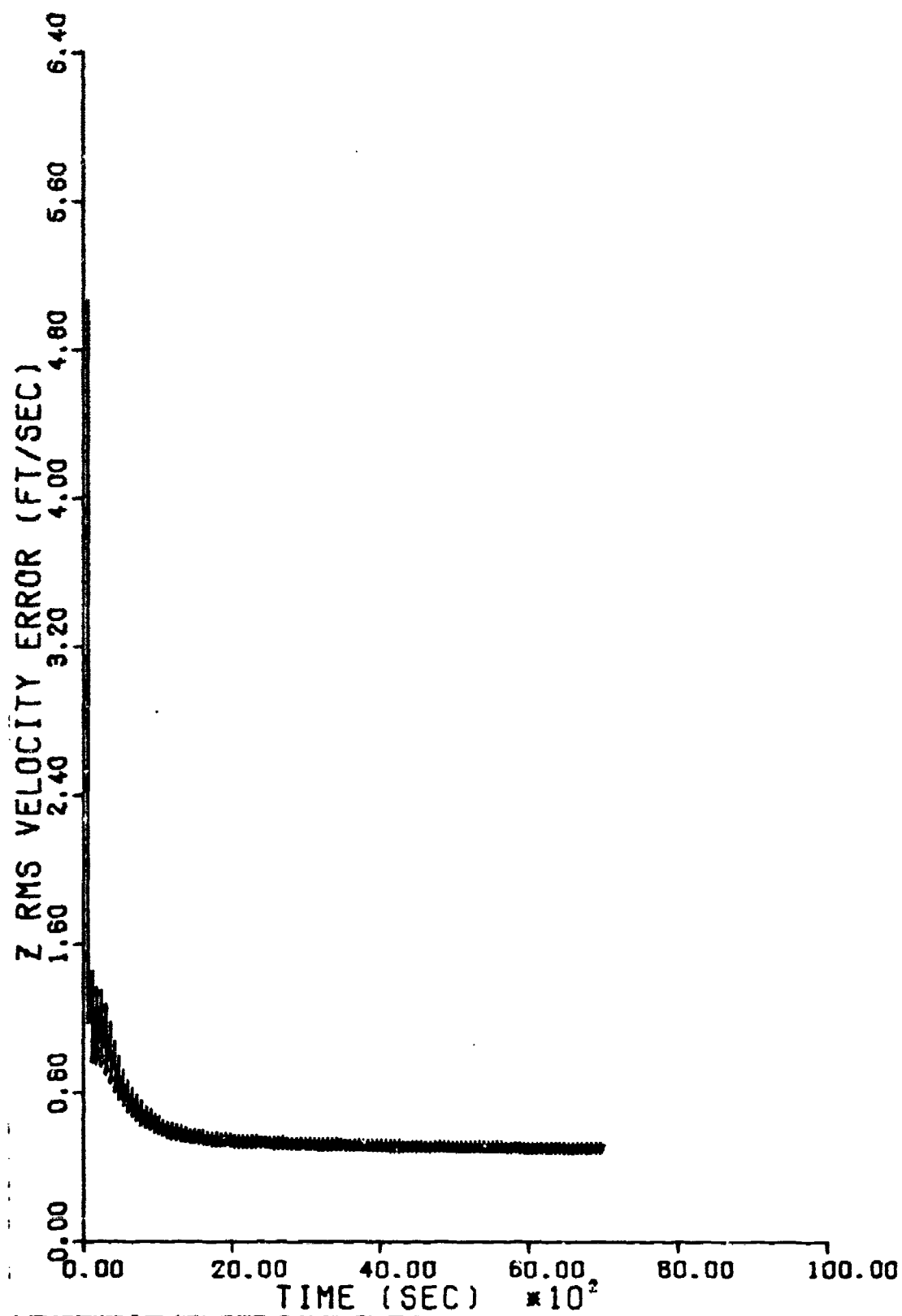


Figure 20. Optimal Filter Z RMS Velocity Error

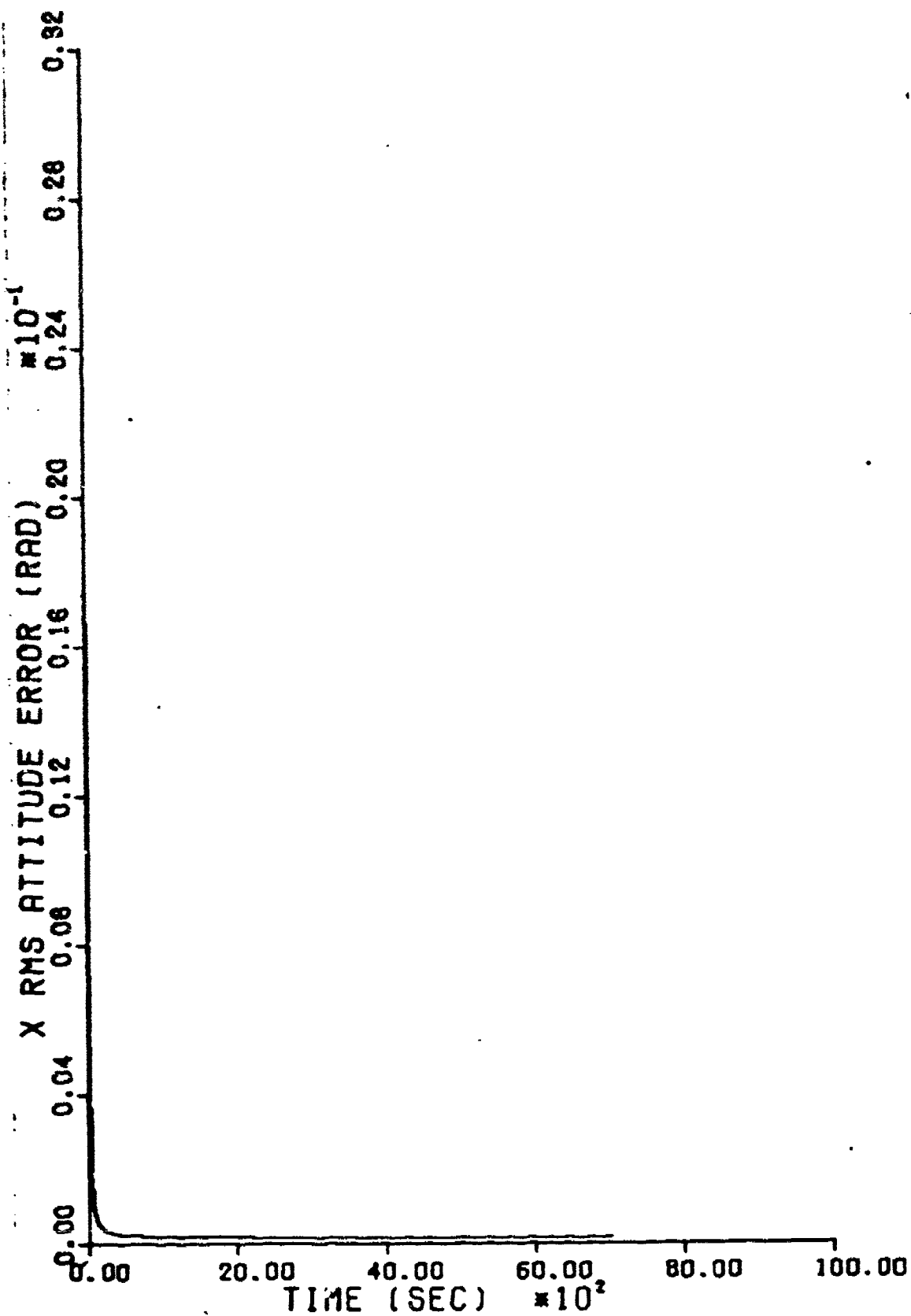


Figure 21. Optimal Filter X RMS Tilt Error

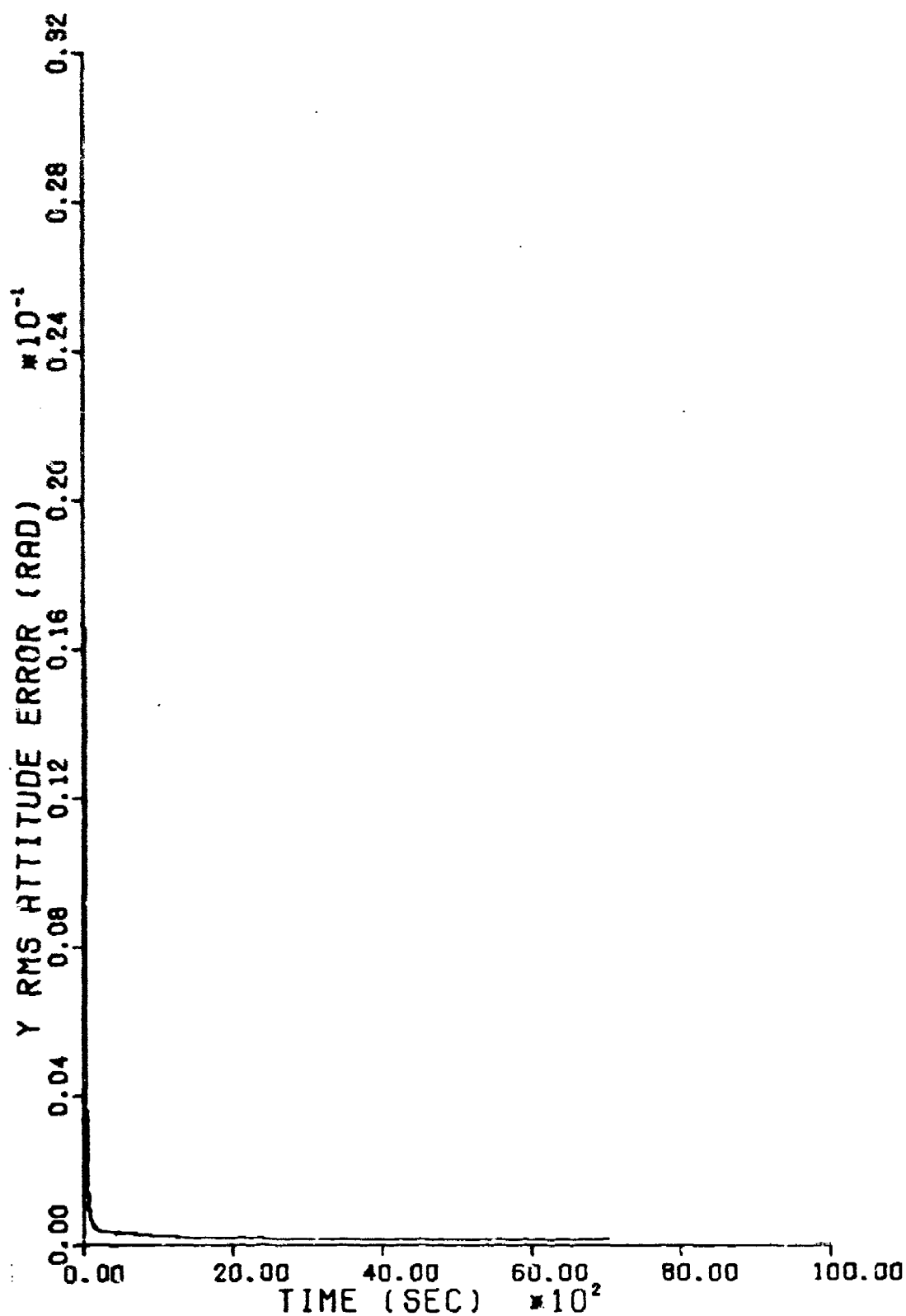


Figure 22. Optimal Filter Y RMS Tilt Error

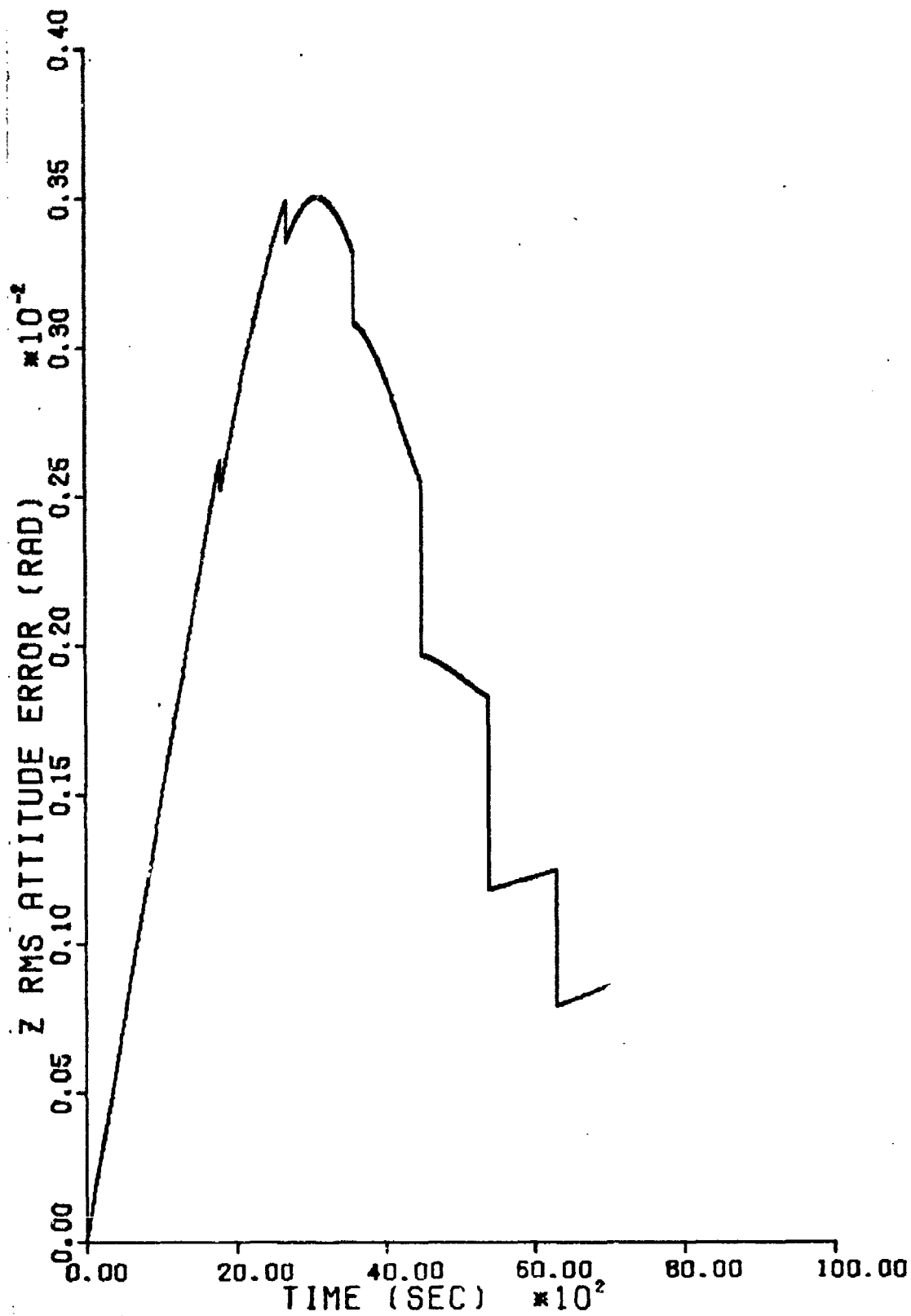


Figure 23. Optimal Filter Z RMS Tilt Error

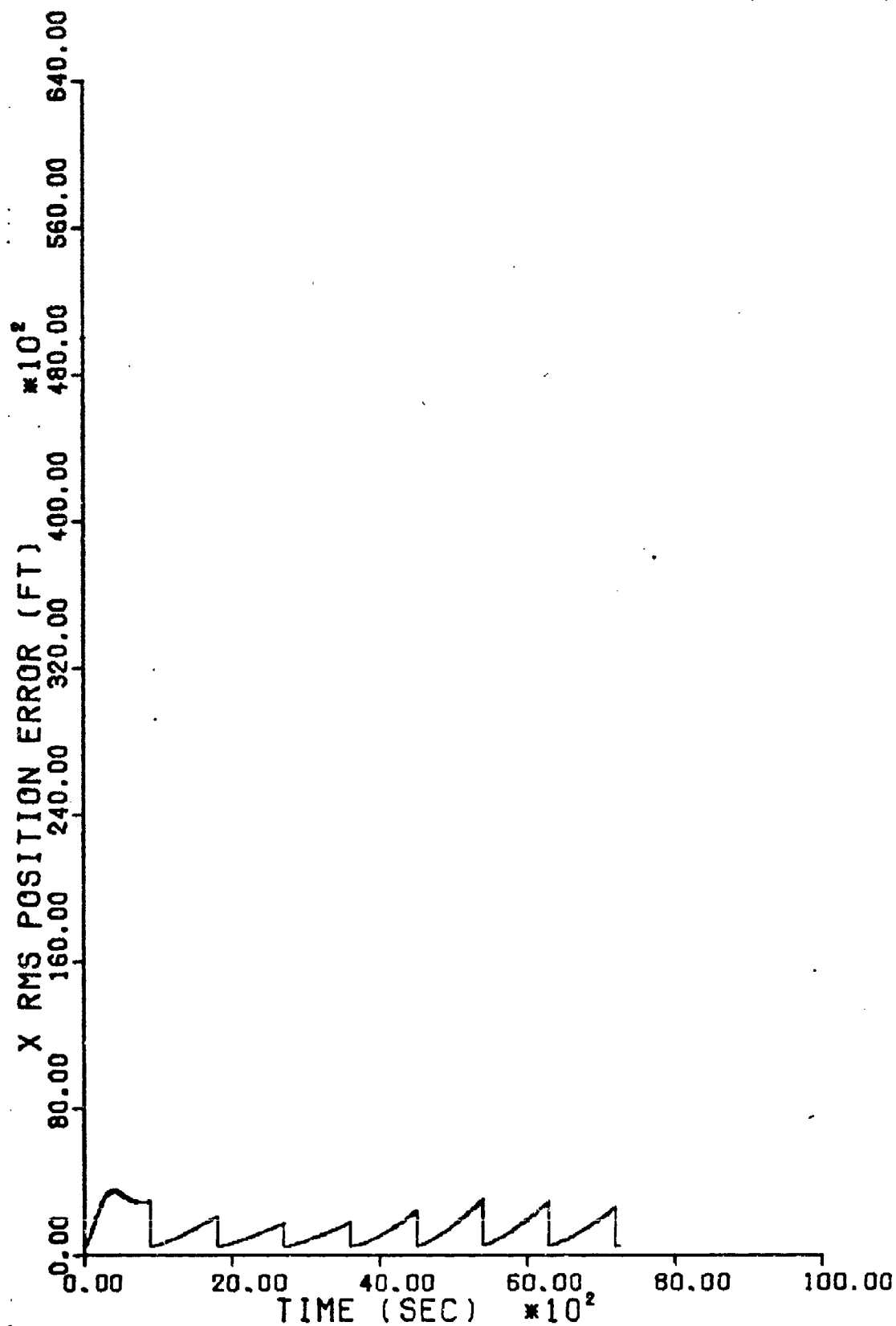


Figure 24. (13+4) Filter X RMS Position Error

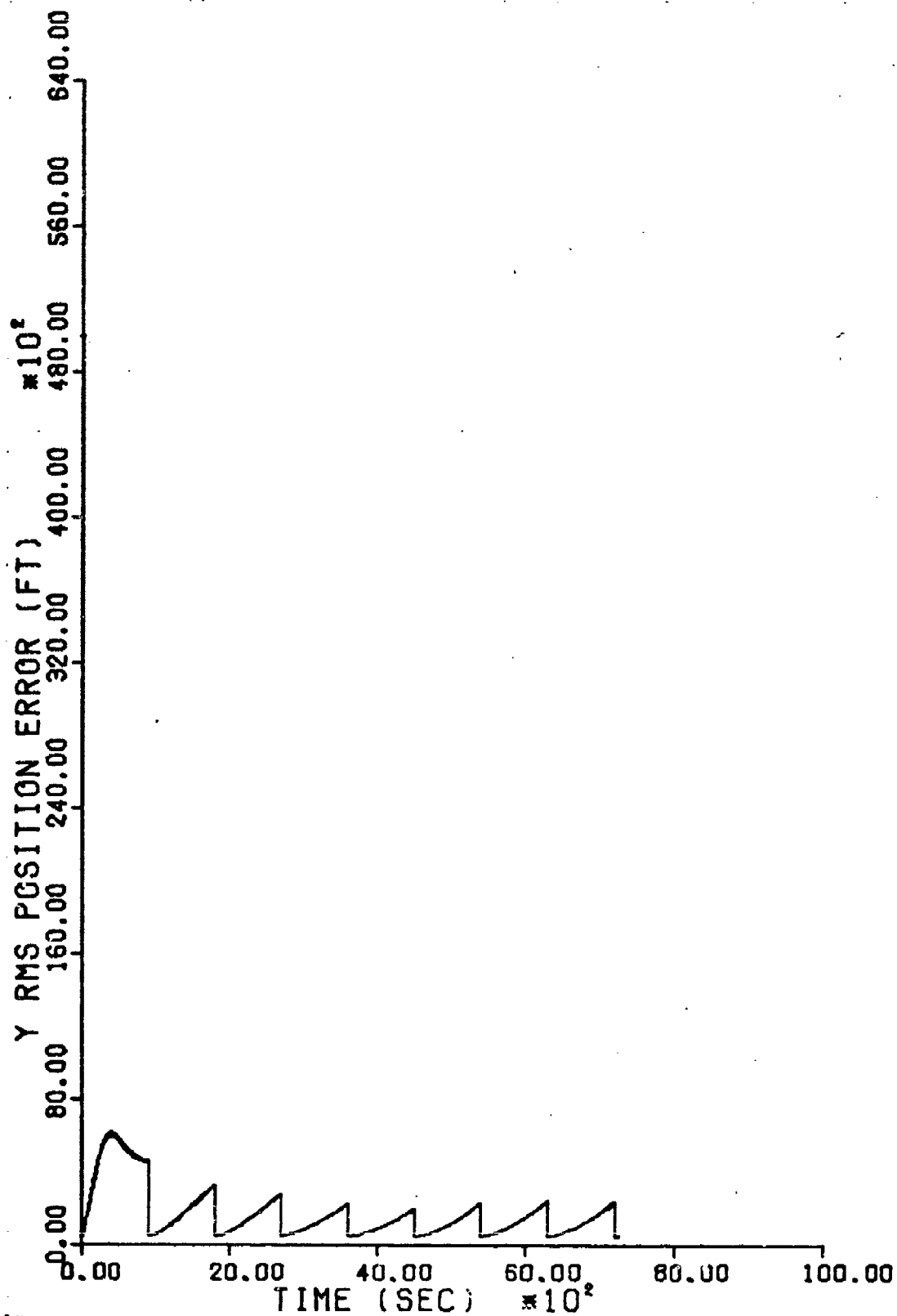


Figure 25. (13+4) Filter Y RMS Position Error

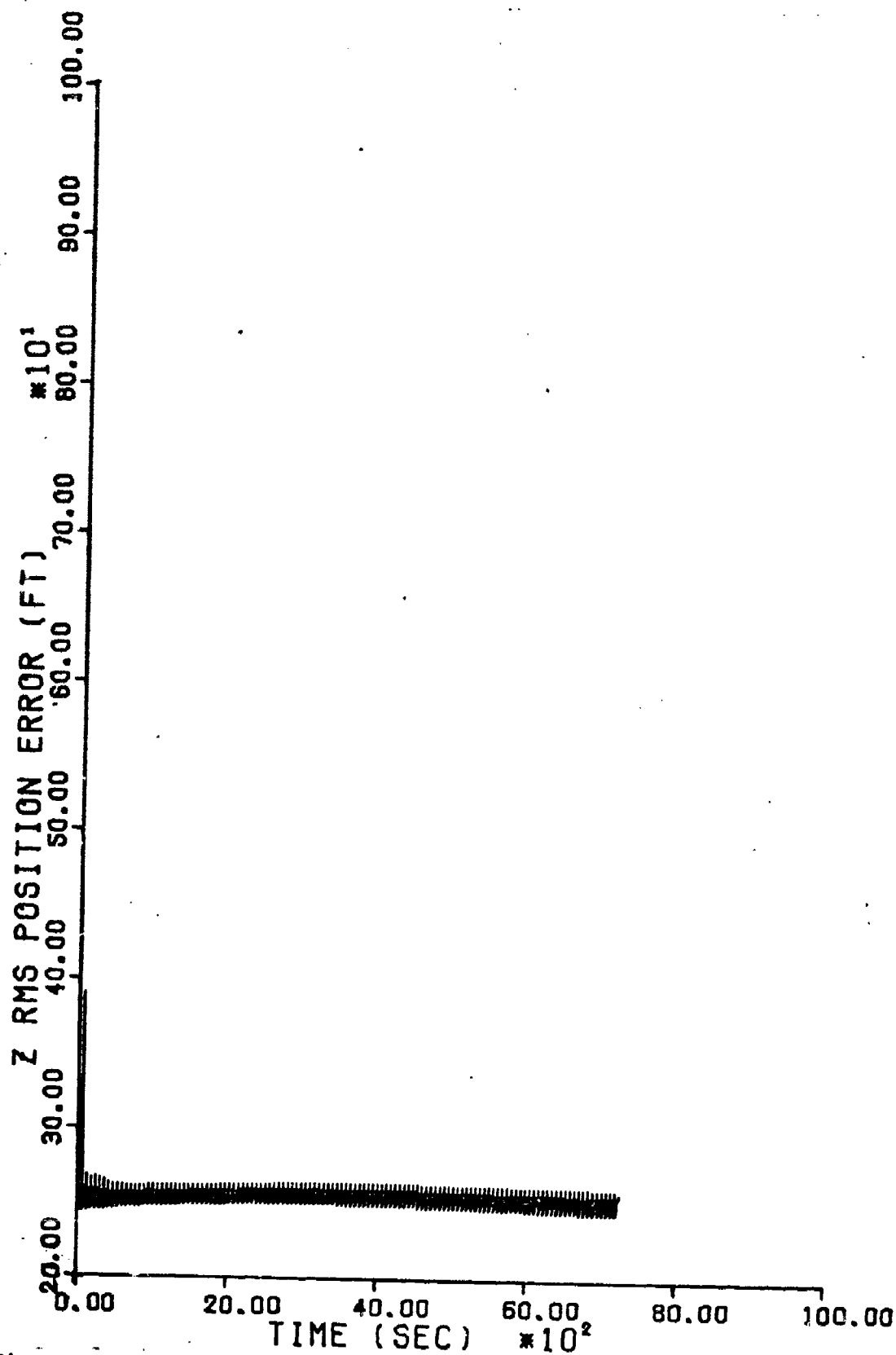


Figure 26. (13+4) Filter Z RMS Position Error



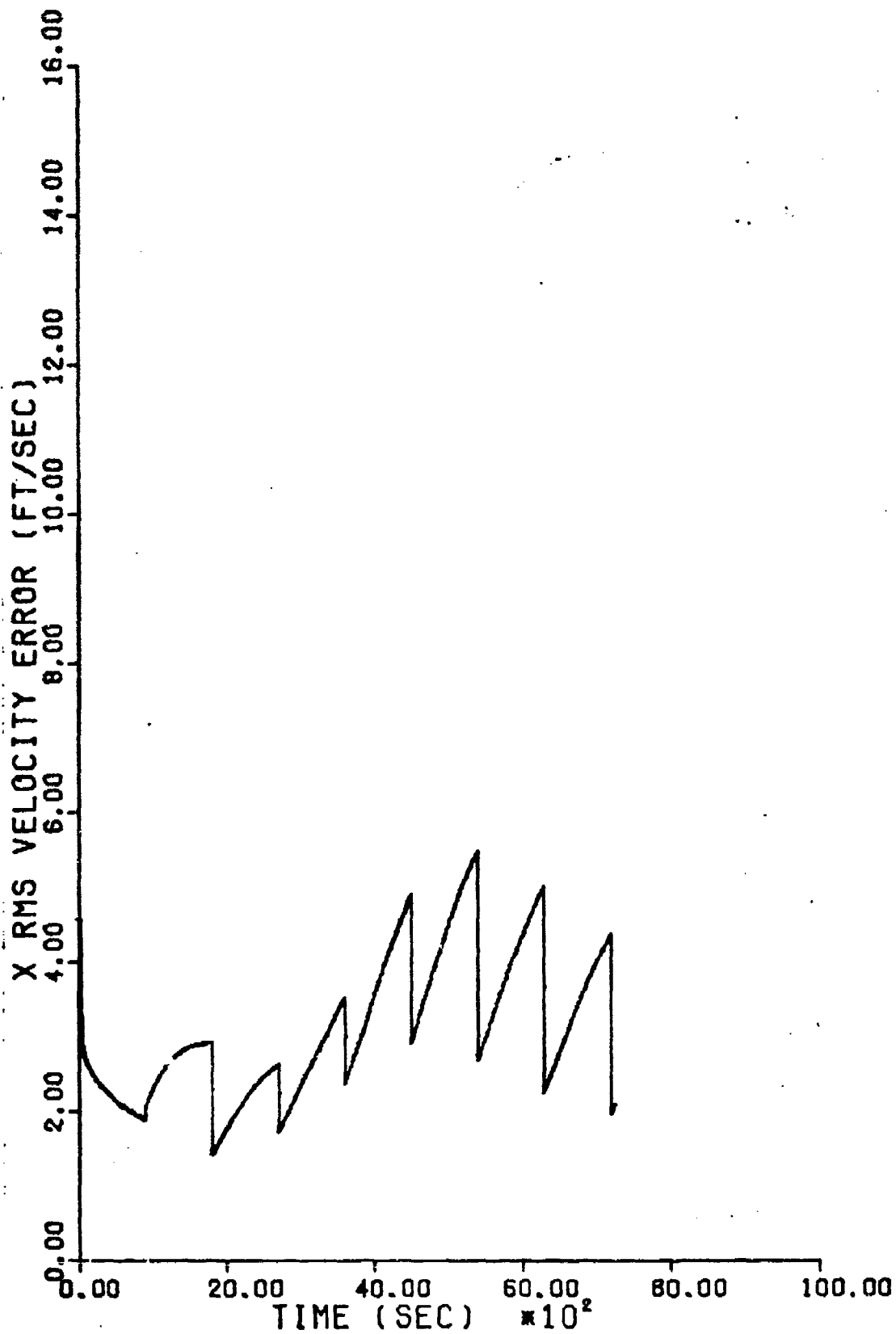


Figure 27. (13+4) Filter X RMS Velocity Error

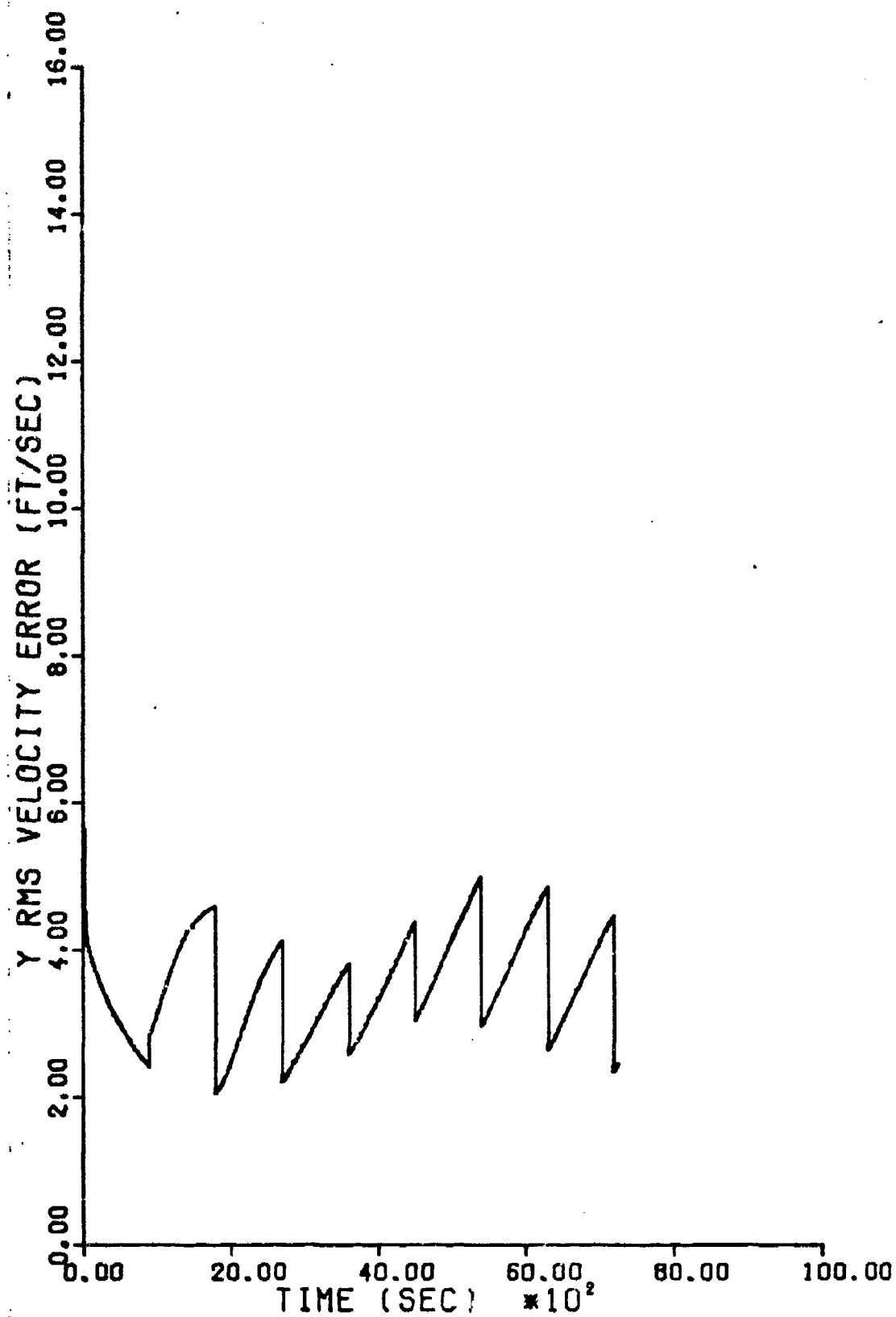


Figure 28. (13+4) Filter Y RMS Velocity Error

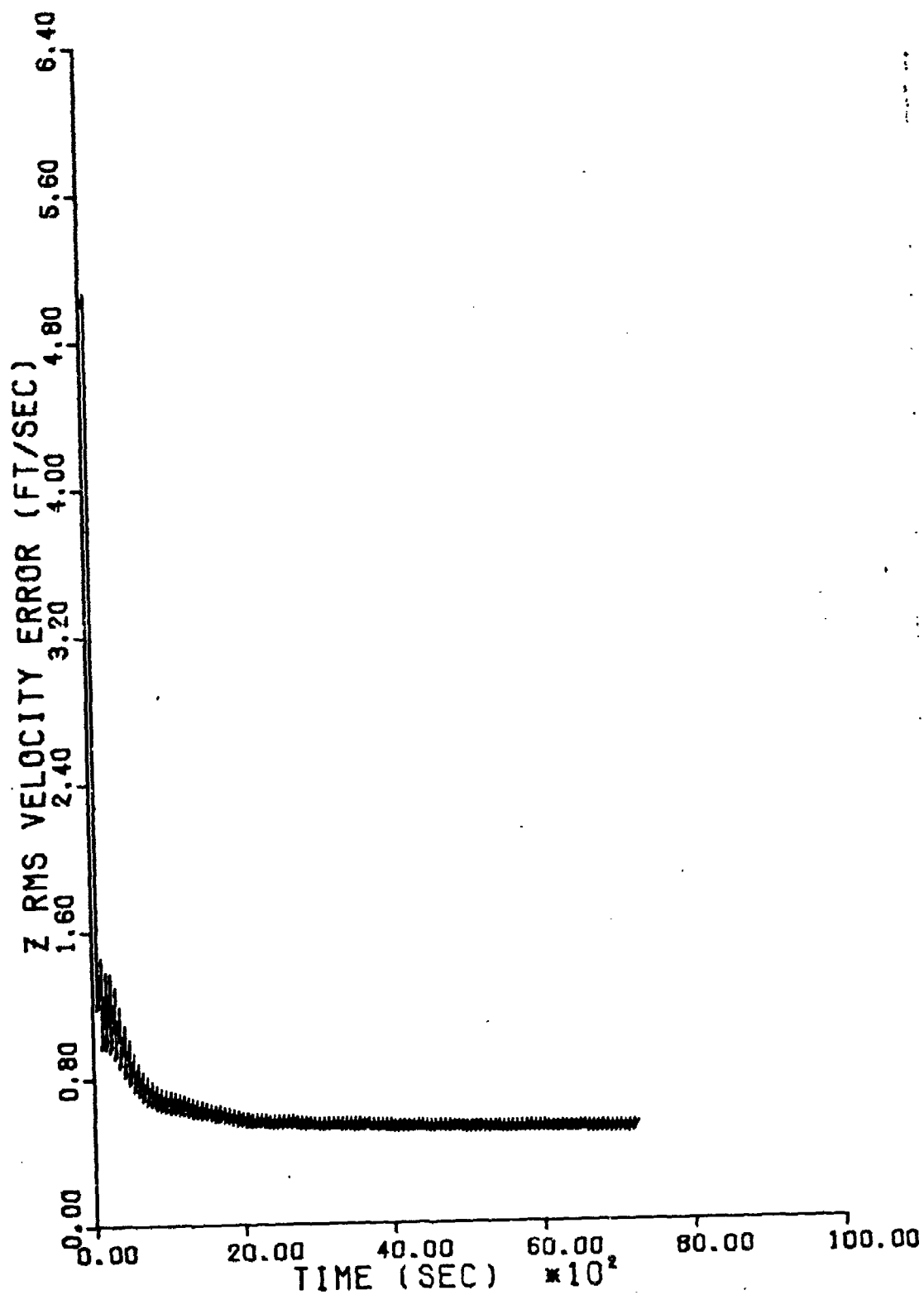


Figure 29. (13+4) Filter Z RMS Velocity Error

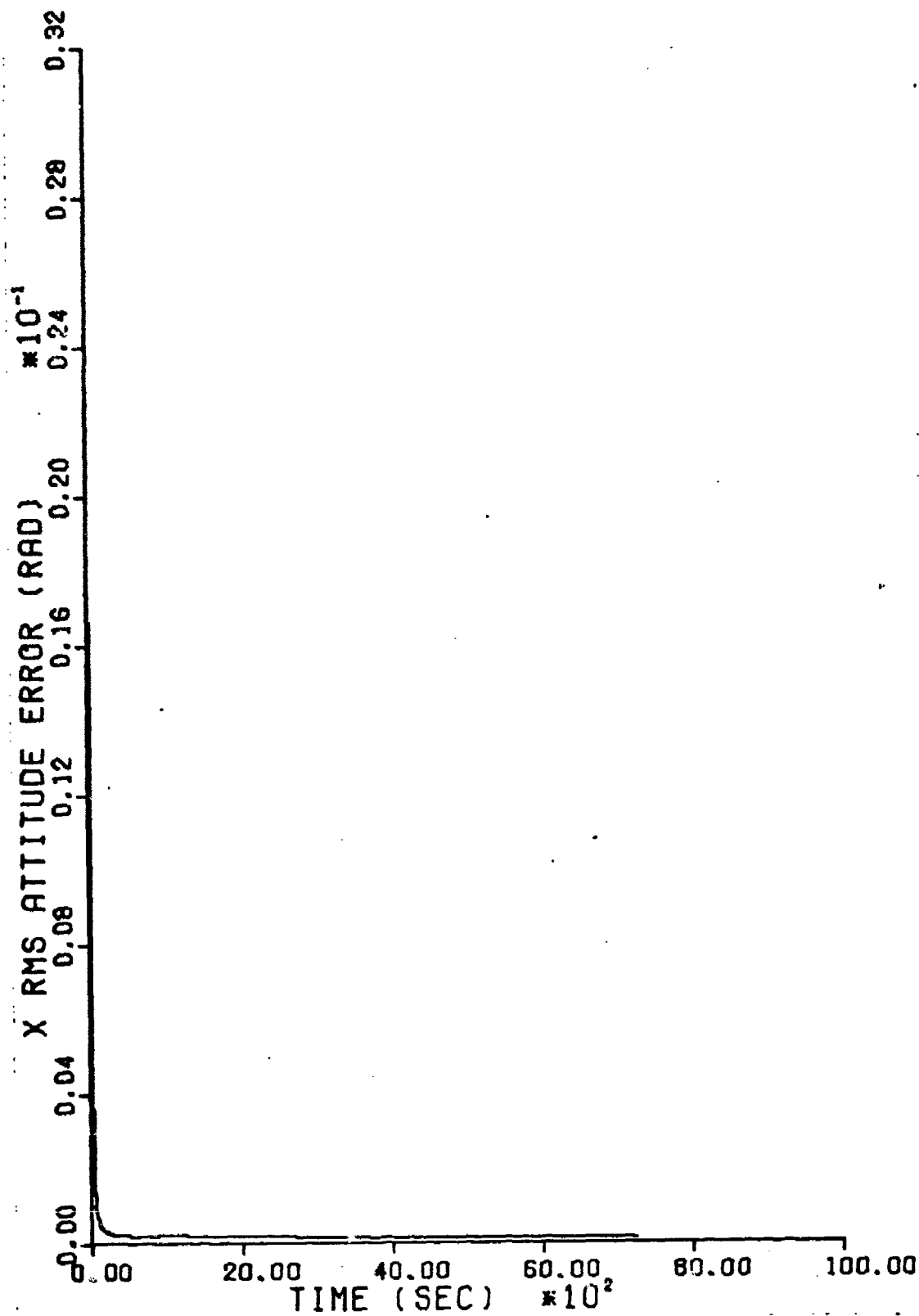


Figure 30. (13+4) Filter X RMS Tilt Error

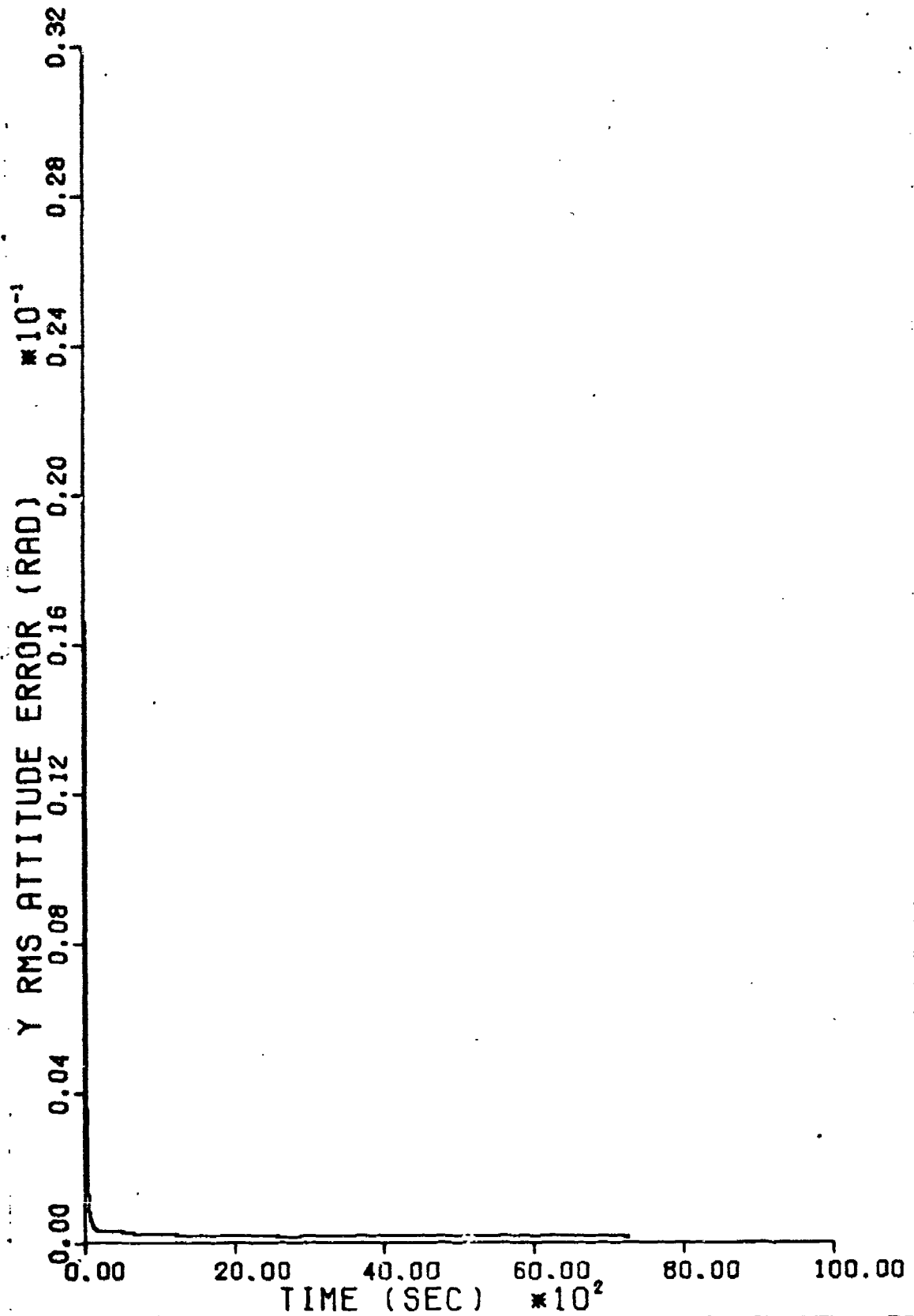


Figure 31. (13+4) Filter Y RMS Tilt Error

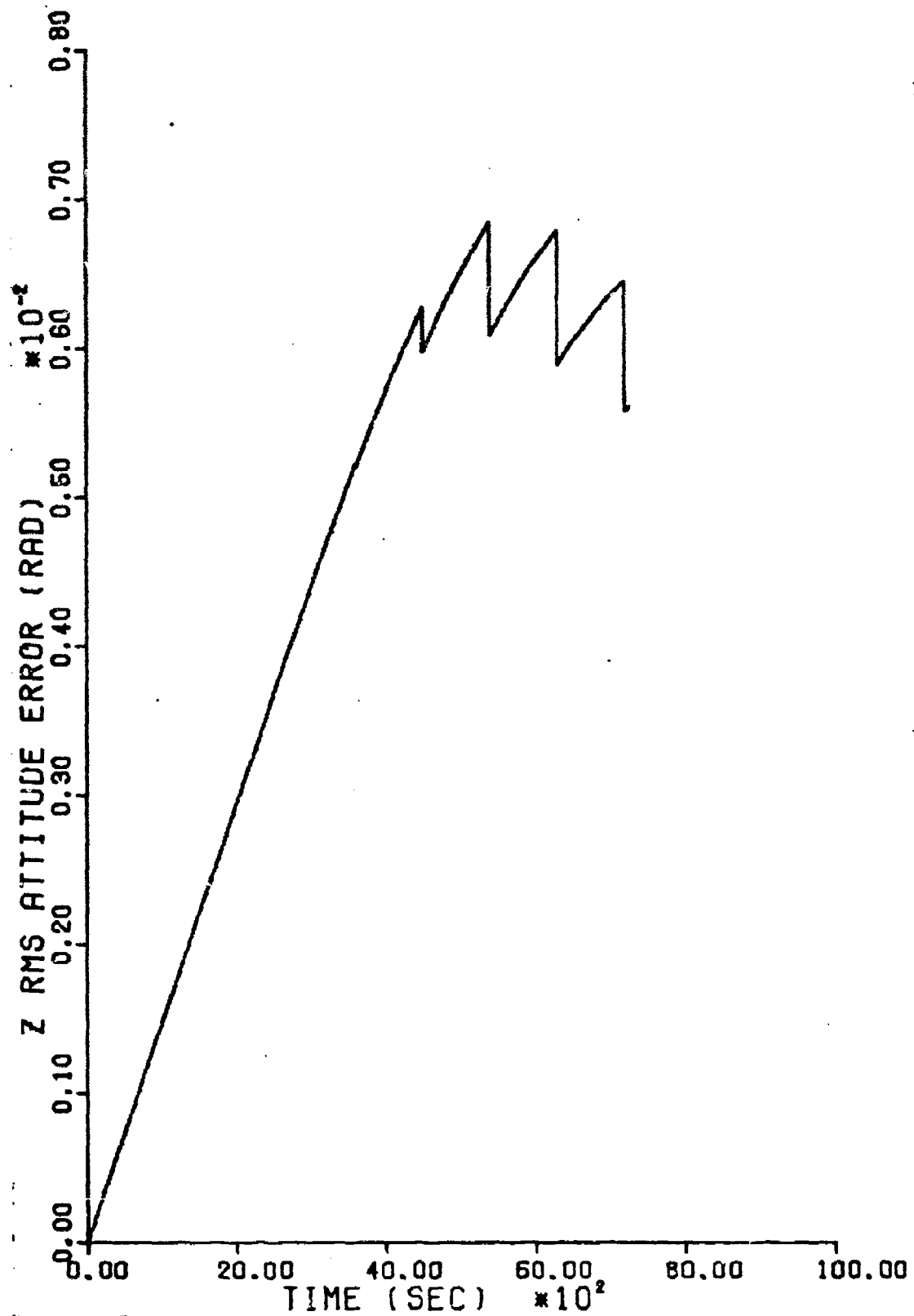


Figure 32. (13+4) Filter Z RMS Tilt Error

Table V

RMS Errors of INS Plant States

Decoupled 17-state filter and optimal 54-state filter performance at 3600 seconds compared against initial values. Values labeled H are high values and those labeled L are low values at the time specified.

Variable	Initial Condition (units)	Optimal Filter (t = 3600 sec)	Decoupled 17- State Filter (t = 3600 sec)
$\delta x$	50,000 ft	H - 1677.6 L - 513.7	H - 1804.3 L - 515.9
$\delta y$	50,000 ft	H - 1809.2 L - 513.9	H - 2259.9 L - 519.8
$\delta z$	1,000 ft	H - 259.2 L - 259.1	H - 262.2 L - 262.2
$\delta v_x$	10 ft/sec	H - 2.69 L - 1.81	H - 3.51 L - 2.52
$\delta v_y$	10 ft/sec	H - 2.81 L - 1.97	H - 3.81 L - 2.67
$\delta v_z$	5 ft/sec	H - 0.548 L - 0.546	H - 0.565 L - 0.563
$\delta \phi_x$	17.5 millirad	H - 0.155 L - 0.153	H - 0.163 L - 0.160
$\delta \phi_y$	17.5 millirad	H - 0.171 L - 0.168	H - 0.193 L - 0.192
$\delta \phi_z$	0.0 millirad	H - 3.32 L - 3.07	H - 5.22 L - 5.27

Table VI

RMS Errors of INS Plant States

Decoupled 17-state filter and optimal 54-state filter performance at 6300 seconds compared against initial values. Values labeled H are high values and those labeled L are low values at the time specified.

Variable	Initial Condition (units)	Optimal Filter (t = 6300 sec)	Decoupled 17- State Filter (t = 6300 sec)
$\delta x$	50,000 ft	H - 1299.6 L - 487.8	H - 2915.4 L - 598.0
$\delta y$	50,000 ft	H - 952.2 L - 455.0	H - 2452.7 L - 536.7
$\delta z$	1,000 ft	H - 256.2 L - 256.1	H - 260.2 L - 260.1
$\delta v_x$	10 ft/sec	H - 1.59 L - 1.00	H - 5.00 L - 2.40
$\delta v_y$	10 ft/sec	H - 1.24 L - 1.04	H - 4.85 L - 2.75
$\delta v_z$	5 ft/sec	H - 0.531 L - 0.531	H - 0.540 L - 0.540
$\delta \phi_x$	17.5 millirad	H - 0.149 L - 0.149	H - 0.169 L - 0.165
$\delta \phi_y$	17.5 millirad	H - 0.150 L - 0.150	H - 0.188 L - 0.186
$\delta \phi_z$	0.0 millirad	H - 1.248 L - 0.796	H - 6.79 L - 5.93



approximately one hour and that although all the RMS values continue to decrease from 3600 to 6300 seconds for the optimal filter this is not true for all the values with the decoupled 17-state filter. The effectiveness of both the optimal and decoupled 17-state filter is approximately the same in controlling x, y, and z position error at 3600 seconds, however, the effectiveness of the level channel of the decoupled filter has decreased considerably by 6300 seconds. For example, the difference in x position error at 3600 seconds is only 0.65% whereas it is 22.6% at 6300 seconds. Also, the optimal filter has reduced the level velocity errors to approximately 10% of their initial values as compared to only about 26% for the decoupled 17-state filter at 6300 seconds. Both filters reduce the x and y axis tilt errors. Although the z axis error increases above the initial value in both filters, the optimal filter is much more effective in controlling the increase than the decoupled 17-state filter.

The effectiveness of the optimal and decoupled 17-state filters in controlling Doppler errors (not shown) exhibits similar characteristics to the z axis tilt (heading) error mentioned above. Although both filters allow the Doppler errors to increase above the initial values, the optimal filter is more effective in controlling this increase than the sub-optimal filter at 6300 seconds the increases in  $\delta K_1$  and  $\delta \delta_1$ , are 65% and 26%

respectively for the optimal filter as compared to 90.8% and 96% for the decoupled 17-state filter.

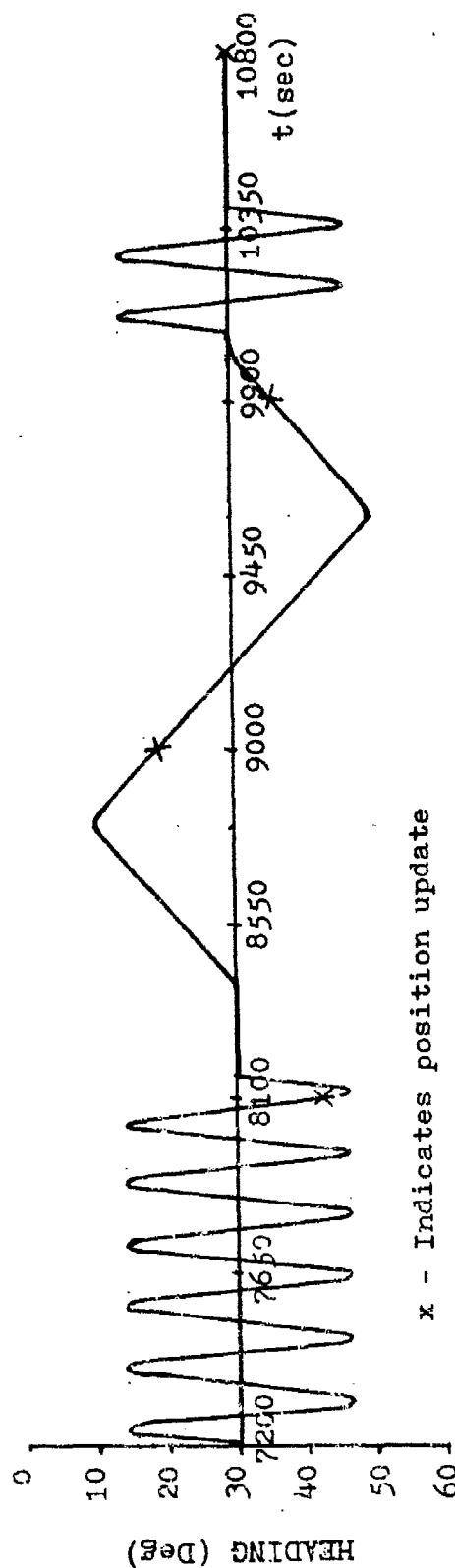
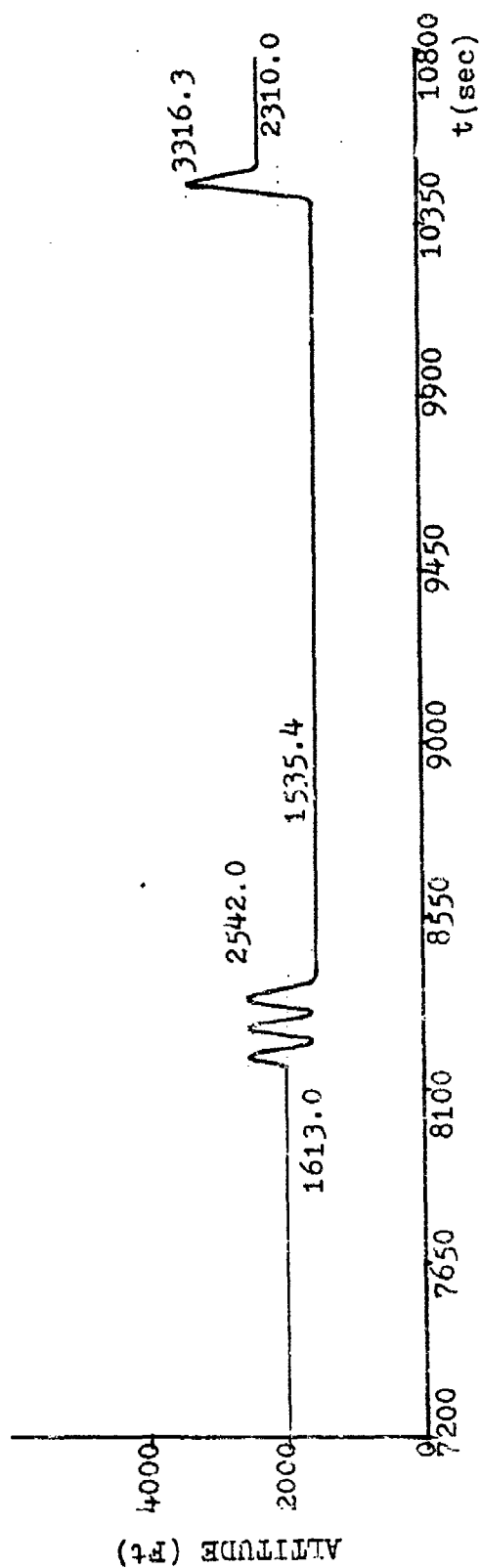
Both filter implementations essentially maintain the initial altimeter error although the optimal filter provides a 4% reduction compared to 2% for the sub-optimal filter.

#### Flight Profile with Dynamic Maneuvers

The dynamic flight profile used for the evaluation consists of twenty separate flight path segments simulating a sinusoidal heading change, rapid but shallow climbs and dives, heading changes intermixed with acceleration and deceleration, another short period of sinusoidal heading change followed by a climb and dive, and finally a short period of straight and level flight. The short period of straight and level flight was included to obtain a measure of the residual effects of maneuvers on filter performance. The undisturbed values of altitude, heading, and aircraft velocity are the same as used in the baseline data (i.e. altitude = 2000 ft, heading =  $30^{\circ}$ , velocity = 710 ft/sec). The dynamic flight profile has a total duration of 3600 seconds and a breakdown of the actual dynamics is given in Figure 33 and Table VII.

The dynamic aircraft flight profile was simulated using the PROFGEN computer program described in Reference 7. The rate of change of aircraft heading and pitch rate were chosen as 0.5 degrees per second. Tangential accelerations required by the profile generator program were computed

8



x - Indicates position update

Figure 33. Dynamic Flight Profile

Table VII

Dynamic Flight Profile Data

Segment	Time Duration (Seconds)	Maneuver	Value
1	960	Sinusoidal Heading Change	$0.5^{\circ}/\text{sec}$ $T = 160 \text{ sec}$
2	20	Pitch Up	$+ 2.5^{\circ}$
3-7	200	Pitch Oscillations	$\pm 5.0^{\circ}$
8	20	Pitch Up (Level off)	$+ 2.5^{\circ}$
9	40	Left Turn	$20^{\circ}$
10	360	Acceleration	710 to 760 ft/sec $(4.3 \times 10^{-3})g$
11	80	Right Turn	$40^{\circ}$
12	720	Straight and Level	0.
13	80	Left Turn	$40^{\circ}$
14	360	Deceleration	760 to 710 ft/sec $(4.3 \times 10^{-3})g$
15	40	Right Turn	$20^{\circ}$
16	320	Sinusoidal Heading Change	$0.5^{\circ}/\text{sec}$ $T = 160 \text{ sec}$
17	60	Pitch Up	$+ 2.5^{\circ}$
18	40	Dive	$- 5.0^{\circ}$
19	10	Pitch Up (Level off)	$+ 2.5^{\circ}$
20	290	Straight and Level	0.

8  
using coordinated turn criteria for horizontal turns and a maximum of 0.2 g additional load factor for vertical maneuvers. .

Plots of the same nine plant error state (RMS values) shown previously are given in Figures 34 through 42 for the decoupled 17-state filter during the additional one hour of straight and level flight. As stated previously, these plots are the basis for the dynamic flight profile performance evaluation. Note the horizontal portion of the curve which represents the initial condition value as if it were constant for the first two hours of flight. The data for the additional hour of flight is displayed between 7200 seconds and 10800 seconds. This data can be considered as simply a continuation of the error plots shown in Figures 24 through 32. Note, however, the vertical scale has been reduced to depict the error plots in greater detail. Also note that the minimum value on the ordinate axis is not always zero.

Although the curves seem to indicate a sudden increase in the error for all nine error states at  $t=7200$  seconds, this is not the case. The initial conditions put into the P matrix for the additional hour of flight were values obtained just after the update at 7200 seconds and, in fact, represent a "low" point on the error curves. Therefore, it is reasonable to expect the error to grow prior to the next update as shown by the curves.

It is of interest to note from Figures 34 through 42 that the greatest reduction of errors occurs at position

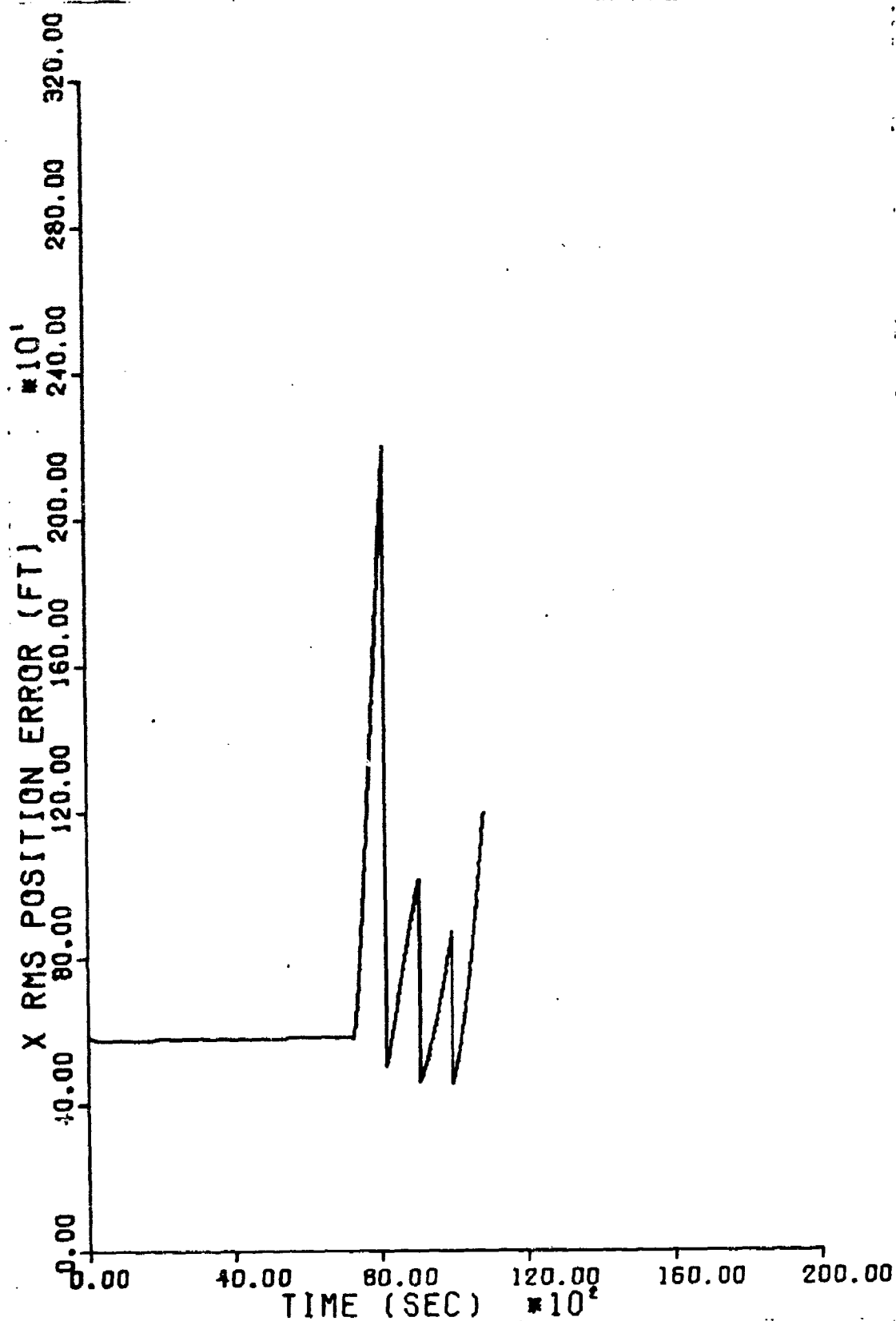


Figure 34. Decoupled Filter Baseline X RMS Position Error

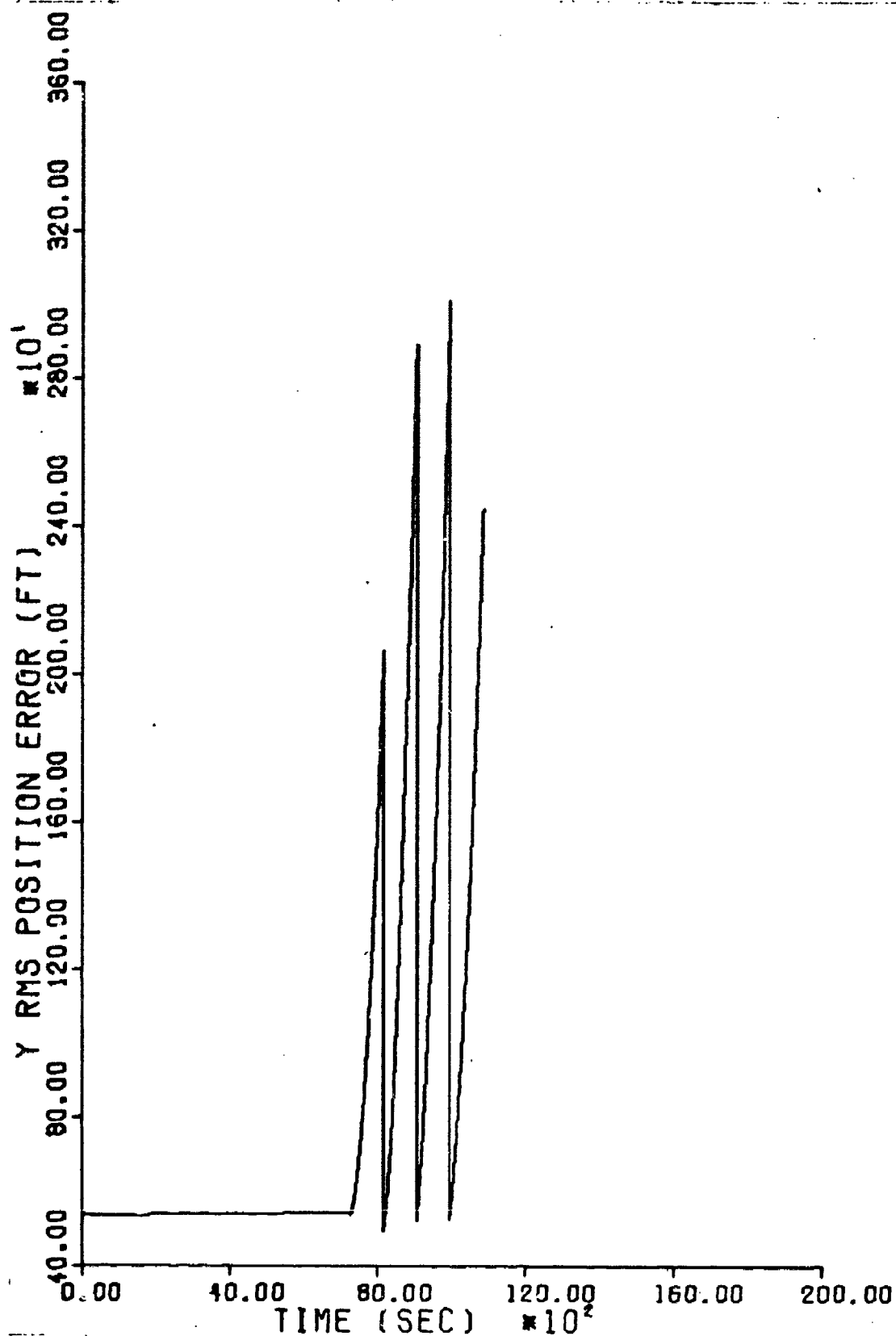


Figure 35. Decoupled Filter Baseline Y RMS Position Error

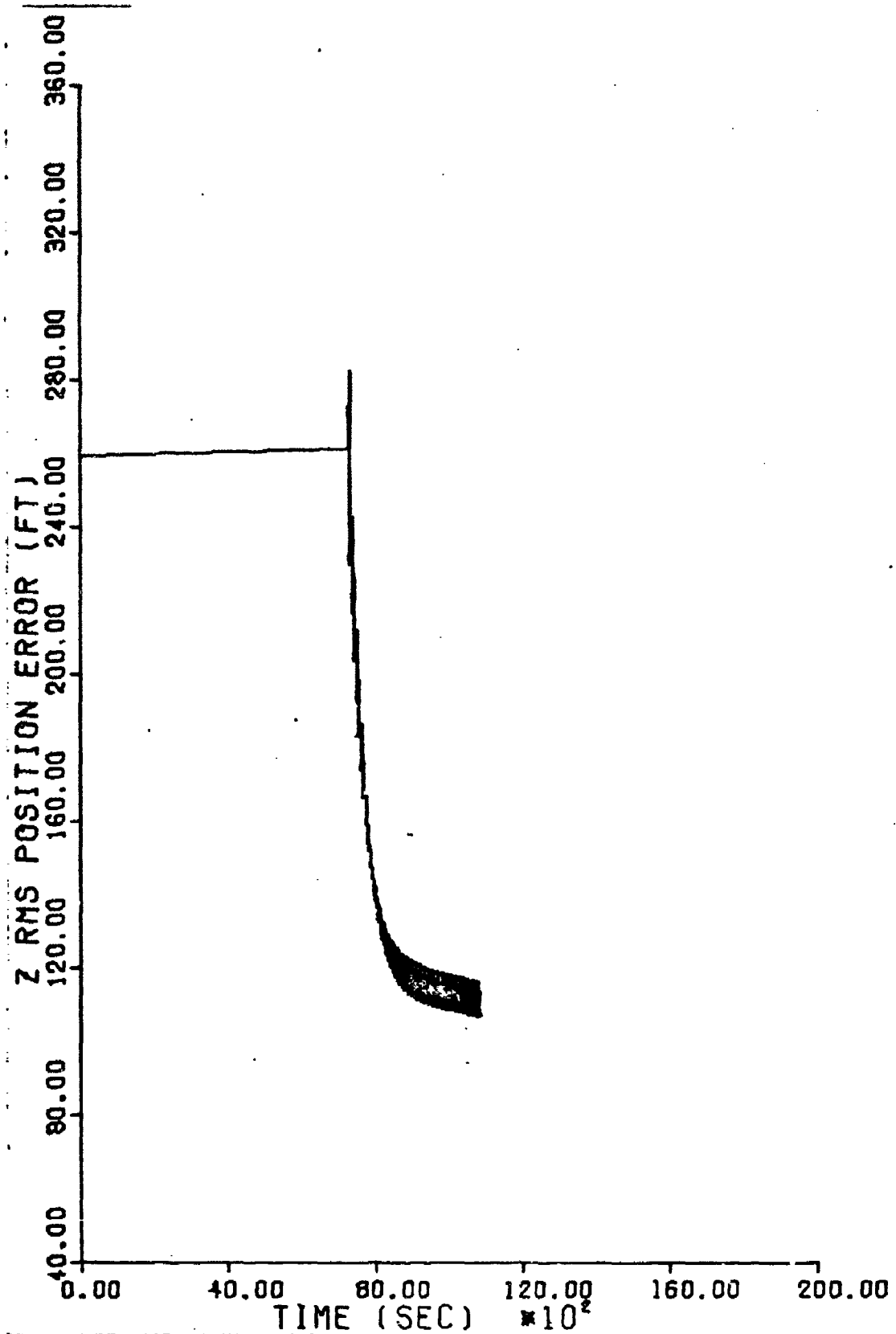


Figure 36. Decoupled Filter Baseline Z RMS Position Error



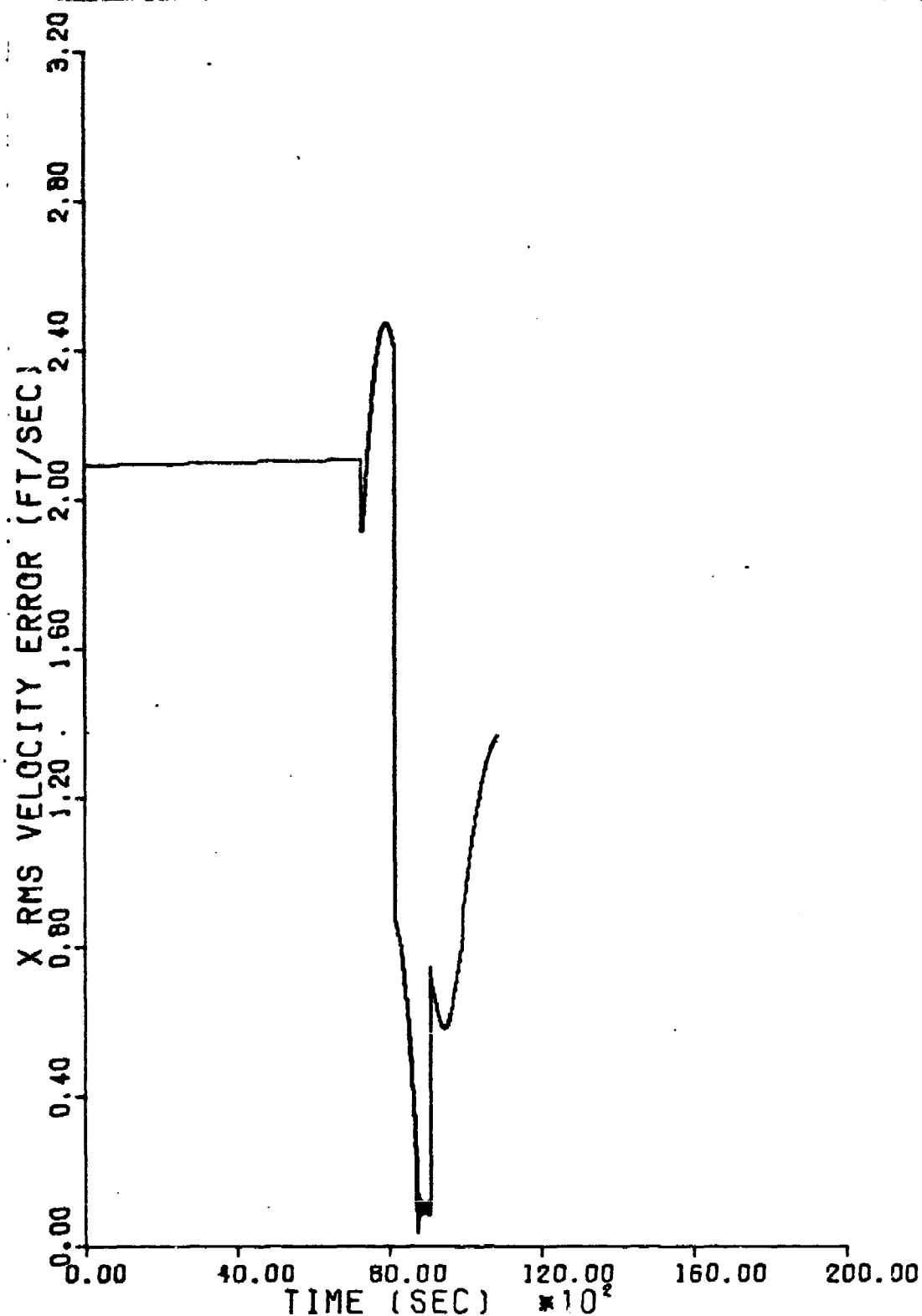


Figure 37. Decoupled Filter Baseline X RMS Velocity Error

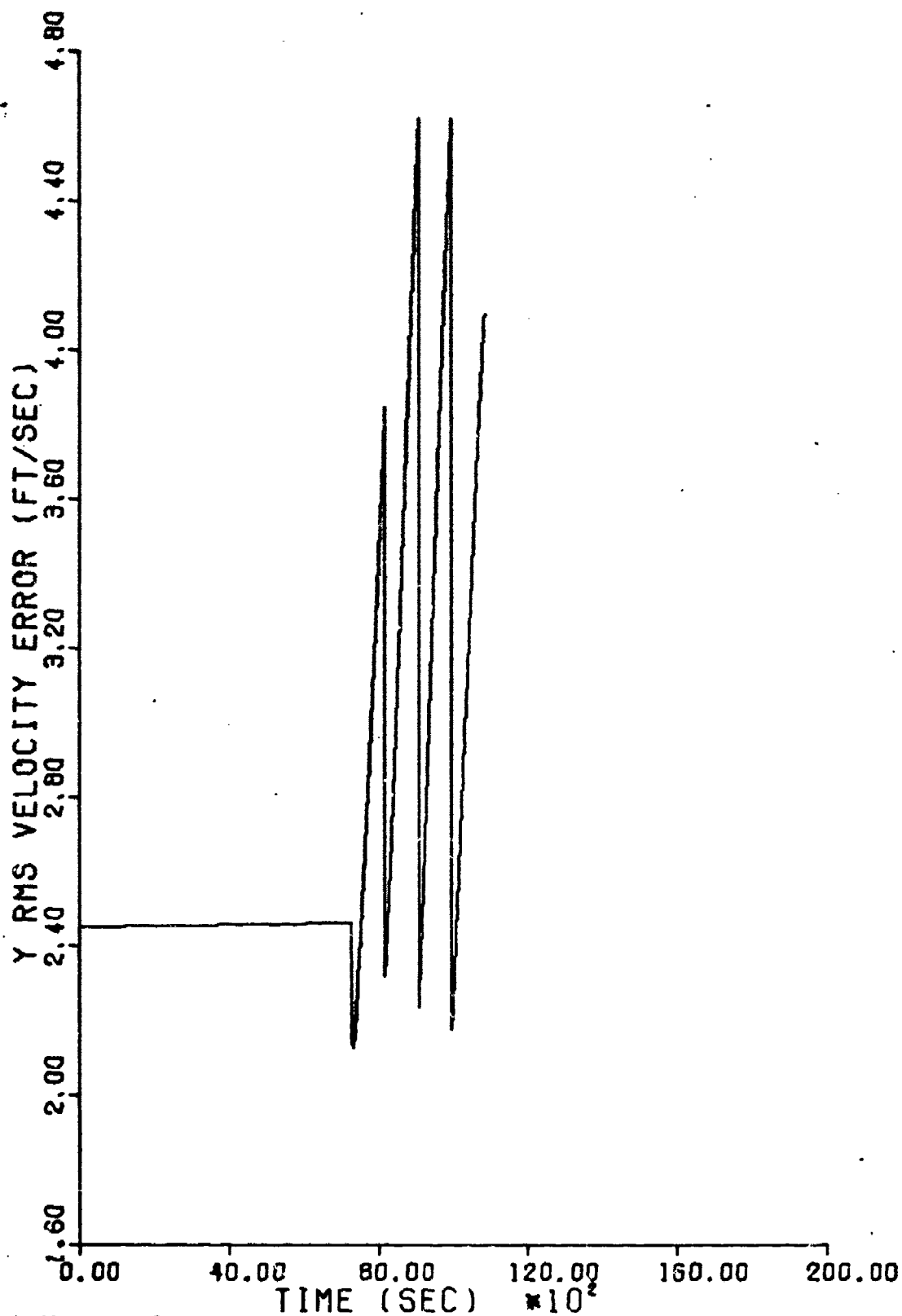


Figure 38. Decoupled Filter Baseline Y RMS Velocity Error

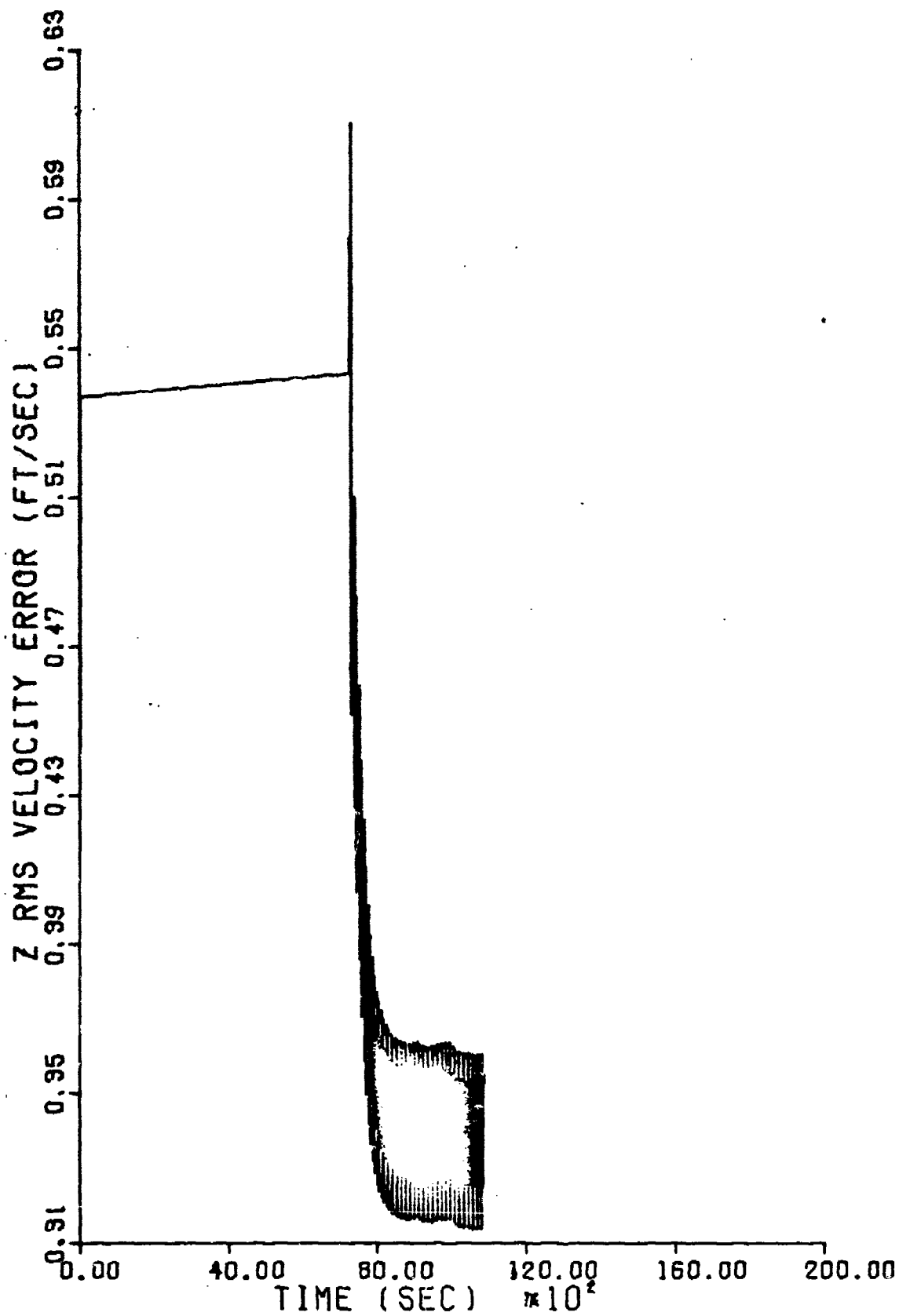


Figure 39. Decoupled Filter Baseline Z RMS Velocity Error

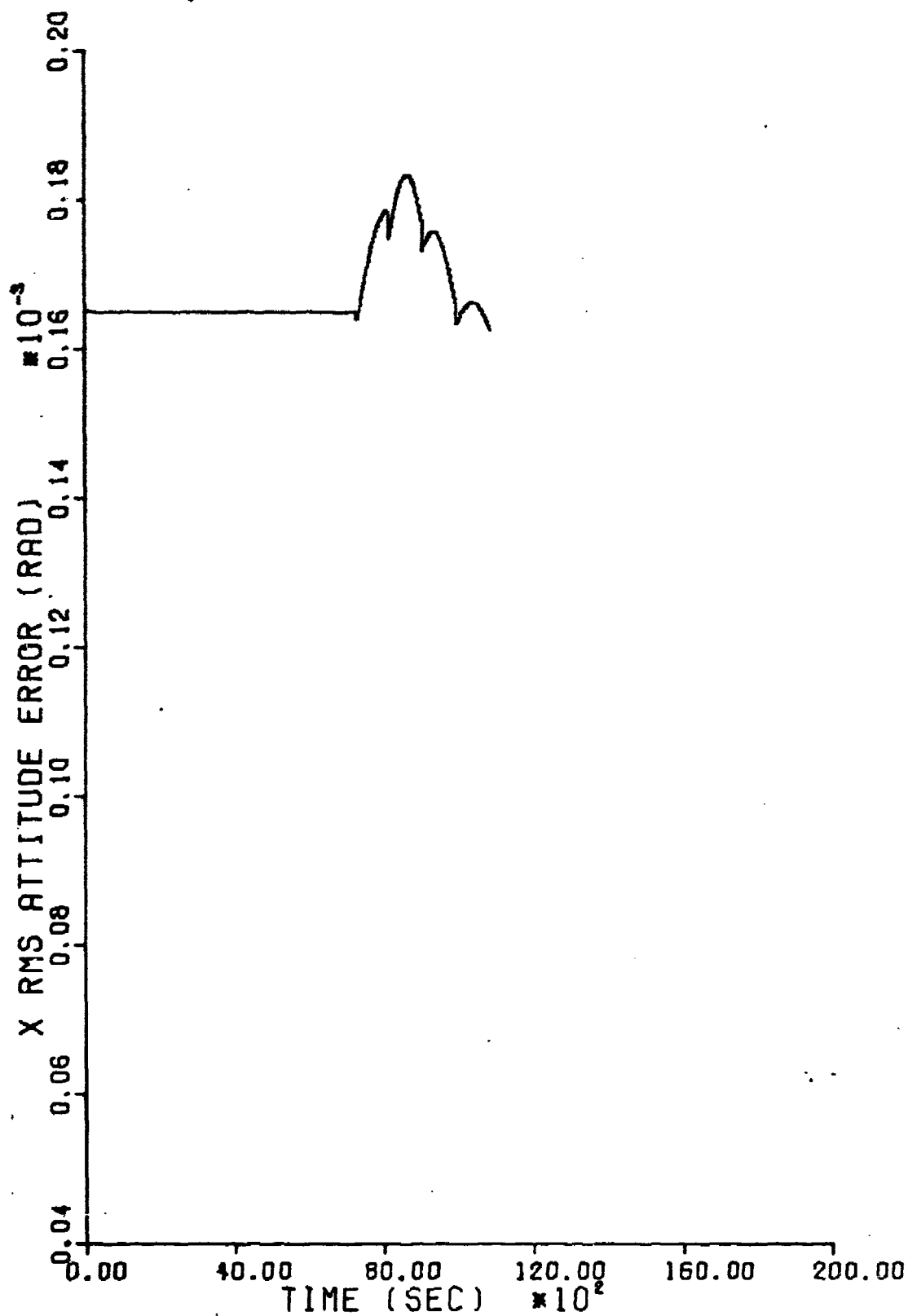


Figure 40. Decoupled Filter Baseline X RMS Tilt Error

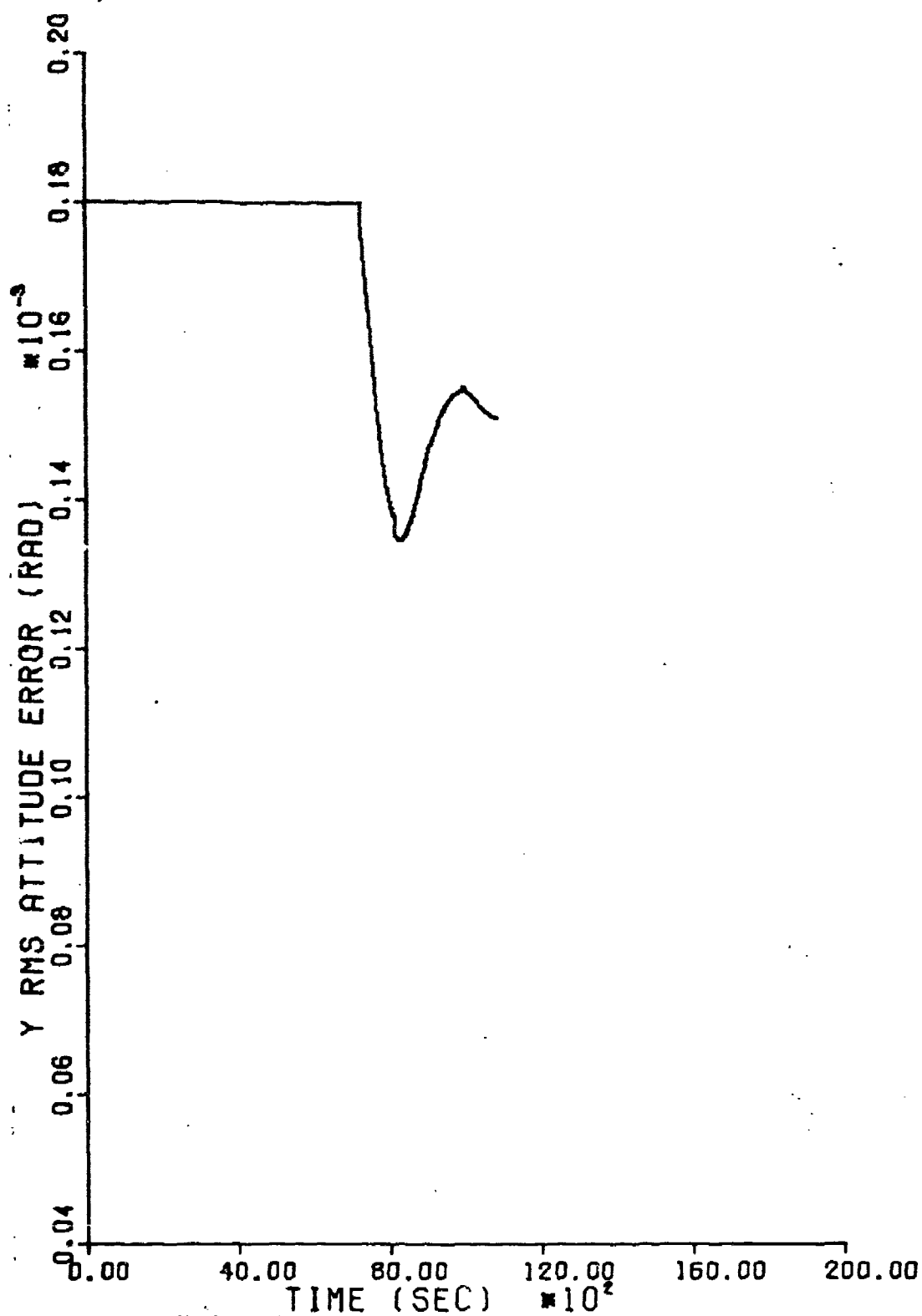


Figure 41. Decoupled Filter Baseline Y RMS Tilt Error

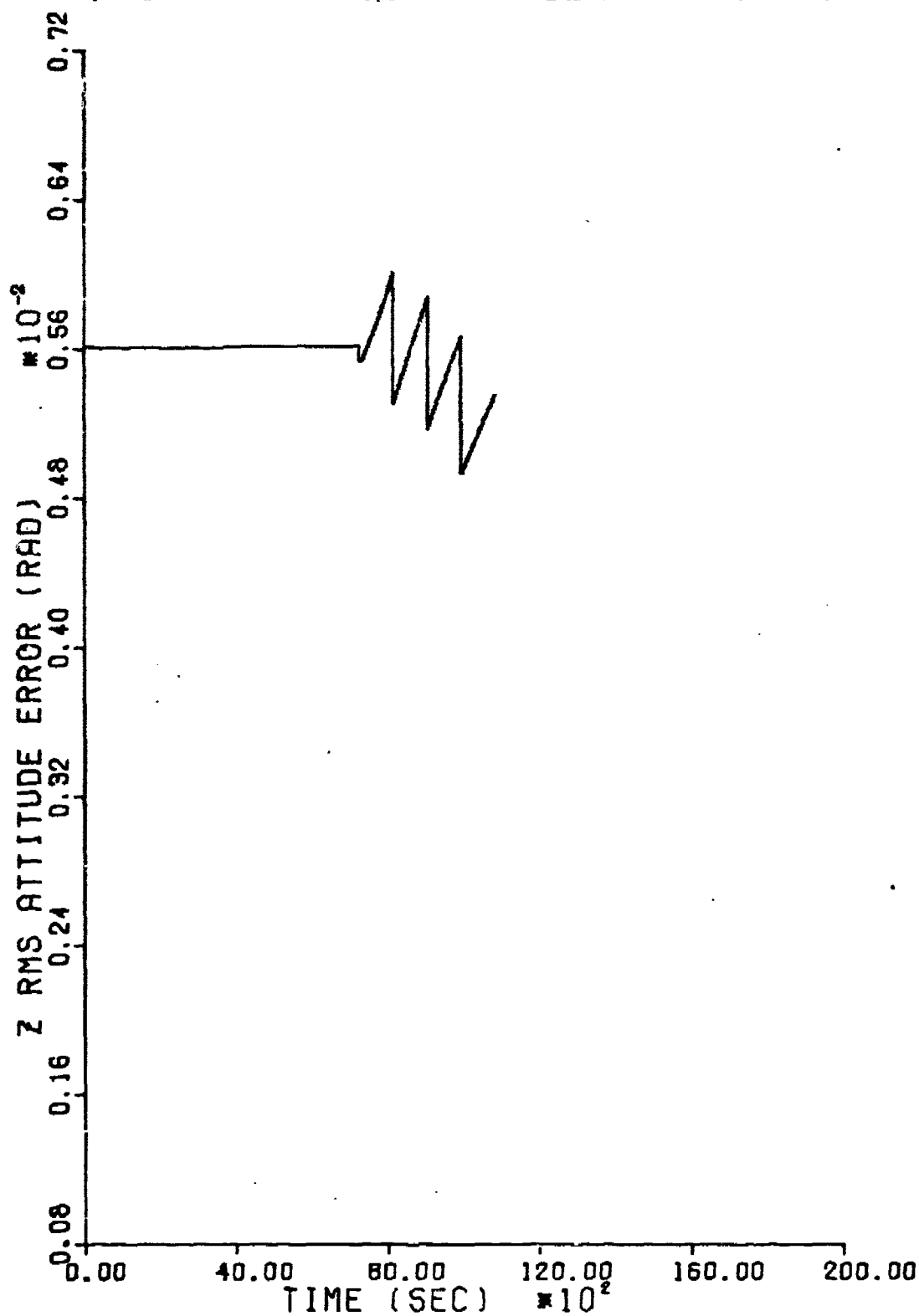


Figure 42. Decoupled Filter Baseline Z RMS Tilt Error

update time for all variables except z RMS position and velocity errors. It seems therefore, that although velocity updates occur every six seconds and altimeter updates every 60 seconds, the position update rate or availability has the primary effect on reducing errors to acceptable values.

Table VIII compares the x, y, and z position, velocity, and tilt errors during the additional hour of straight and level flight with the initial values. By comparison with the data of Table VI, it can be seen that, with the exception of Y RMS position and velocity error, all errors have been further reduced. The increase in Y RMS position and velocity error can be seen by comparing average values for both variables. The average values of Y position and velocity error from Table VI are 1494.7 feet and 3.24 feet per second respectively. The average values obtained from Table VIII are 1780.95 feet and 3.445 feet per second respectively. Thus the increase in Y RMS position error is 286.25 feet and the increase in Y RMS velocity error is 0.205 feet per second. This apparent increase can be shown to be due to a maximum value in the periodic oscillation of the errors about a steady state average value at a frequency which corresponds to the Schuler period of 84 minutes. In fact, X RMS position and velocity errors also exhibit this oscillation, but have reached a minimum value at time = 10,020 seconds. This periodic oscillation is readily shown on the x and y position and velocity error curves in Figures 24, 25, 27, and 28.

Table VIII

Straight and Level RMS Errors of INS Plant States

Decoupled 17-state filter performance compared against initial values. Values labeled H are high values and those labeled L are low values at the time specified. Initial values input the P matrix are L values.

Variable (units)	Initial Condition (t=7200 sec)	Decoupled 17-State Filter	
		(t=8640 sec)	(t=10,020 sec)
$\delta x$ ft	H - 2616.3	H - 778.2	H - 870.3
	L - 574.6	L - 743.1	L - 475.4
$\delta y$ ft	H - 2404.7	H - 1376.8	H - 2987.2
	L - 537.0	L - 1214.1	L - 574.7
$\delta z$ ft	H - 259.4	H - 117.0	H - 109.0
	L - 259.4	L - 116.1	L - 108.9
$\delta v_x$ ft/sec	H - 4.36	H - 0.498	H - 0.947
	L - 2.09	L - 0.382	L - 0.838
$\delta v_y$ ft/sec	H - 4.46	H - 3.41	H - 4.60
	L - 2.45	L - 3.25	L - 2.29
$\delta v_z$ ft/sec	H - 0.537	H - 0.359	H - 0.359
	L - 0.537	L - 0.359	L - 0.358
$\delta \phi_x$ millirad	H - 0.168	H - 0.183	H - 0.166
	L - 0.165	L - 0.183	L - 0.164
$\delta \phi_y$ millirad	H - 0.182	H - 0.138	H - 0.155
	L - 0.180	L - 0.137	L - 0.154
$\delta \phi_z$ millirad	H - 6.45	H - 5.61	H - 5.67
	L - 5.61	L - 5.57	L - 4.96



Plots of the x, y, and z position, velocity, and tilt errors for the decoupled 17-state filter in maneuvering flight are shown in Figures 43 through 51. Note the increase in the x position and velocity and y tilt errors. Also note the decrease in the y position and velocity and the x tilt errors. The z axis errors remain unchanged except for a decrease in the z tilt (heading) error. As during straight and level flight, the position updates have the greatest effect in reducing the magnitude of the errors. The sinusoidal heading change during the initial portion of the maneuvering flight profile has the greatest effect on x and y velocity errors. However, after three position updates, the sinusoidal heading change later in the profile seems to have negligible effect. Slow turns and path accelerations increased the x position and velocity errors, and although these errors decreased during the 720 second period of straight and level flight midway through the profile, the average values are approximately  $1\frac{1}{2}$  times those reached during straight and level flight for the entire hour. Although y velocity error decreases slightly, the magnitude of this change is small compared to the increase in x velocity error. Table IX compares the x, y, and z position, velocity, and tilt errors during the additional hour of maneuvering flight with the initial values. The changes in magnitude of the errors can be seen by comparing Tables VIII and IX. This comparison is shown in Table X. The values given in Table X are "average" values and are obtained by adding the RMS error value of a

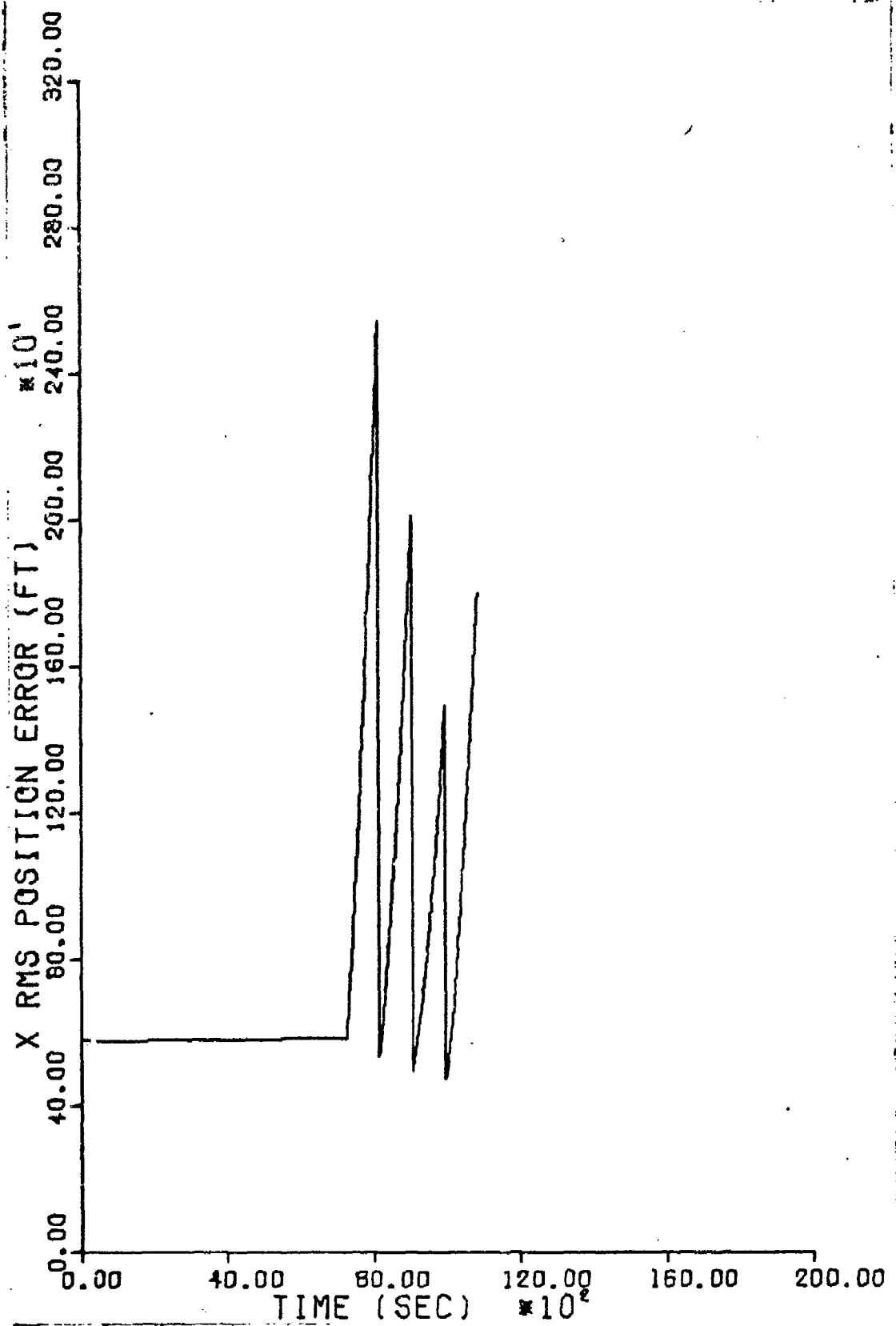


Figure 43. Decoupled Filter Maneuvering X RMS Position Error

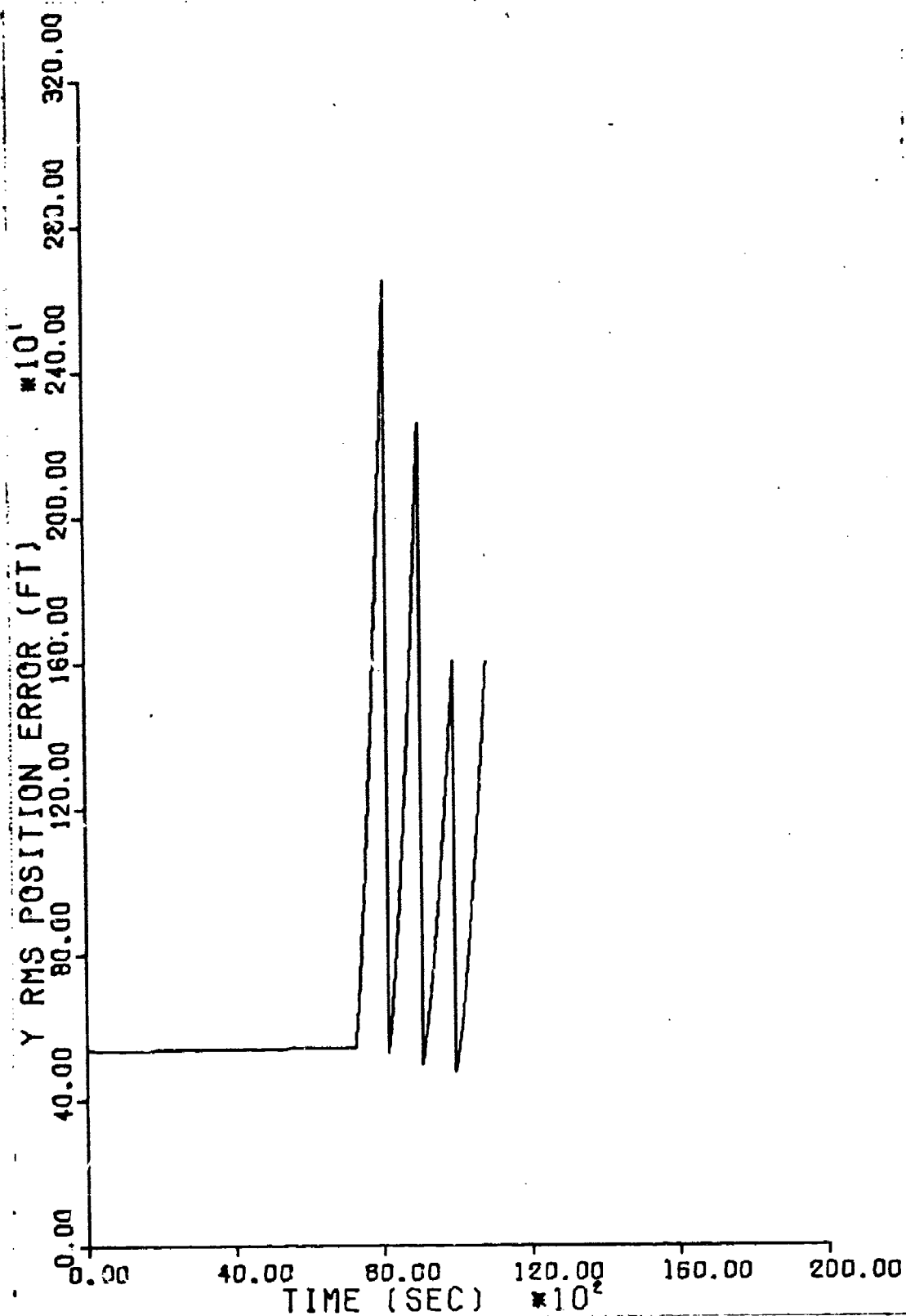


Figure 44. Decoupled Filter Maneuvering Y RMS Position Error

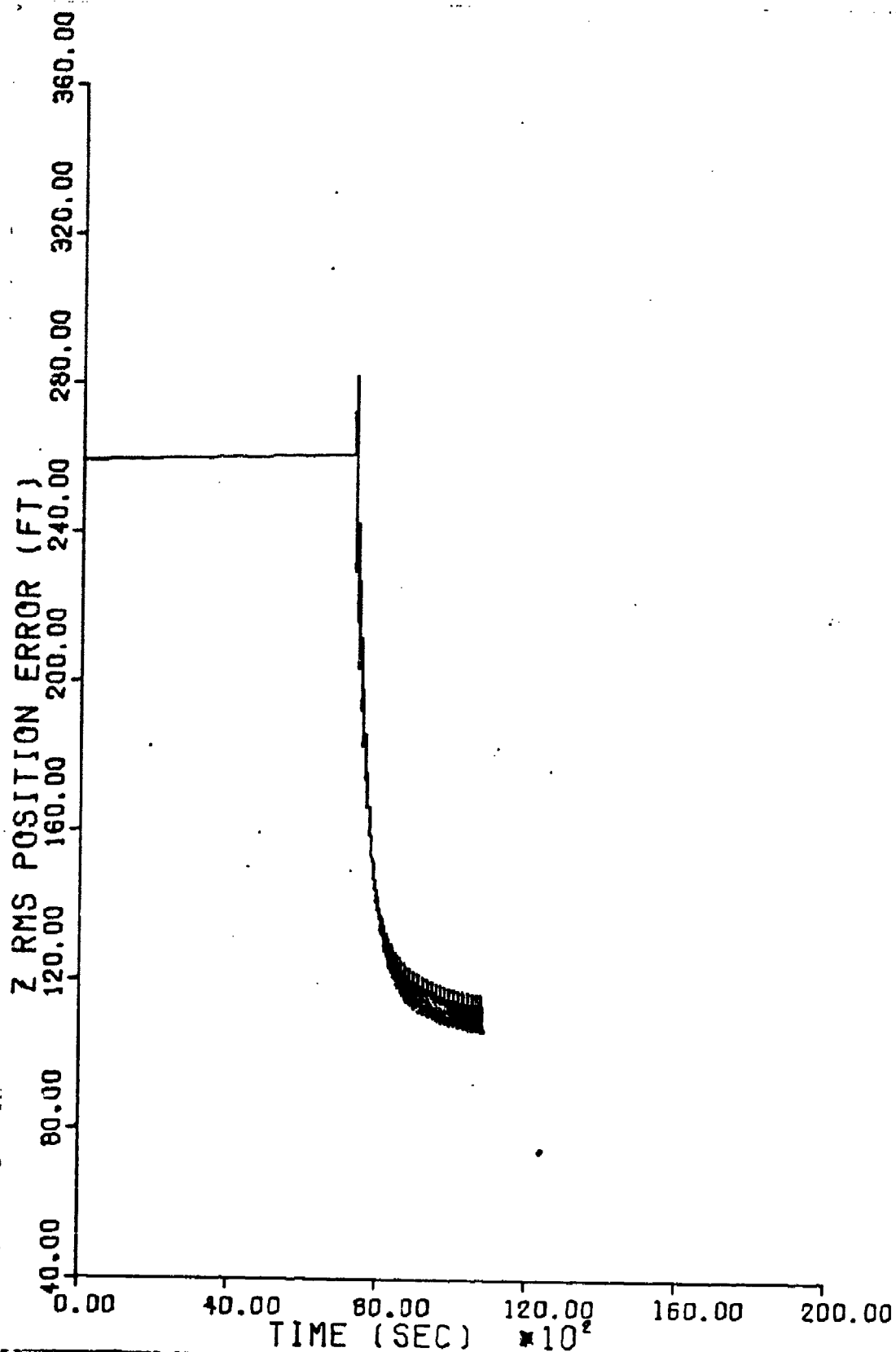


Figure 45. Decoupled Filter Maneuvering Z RMS Position Error

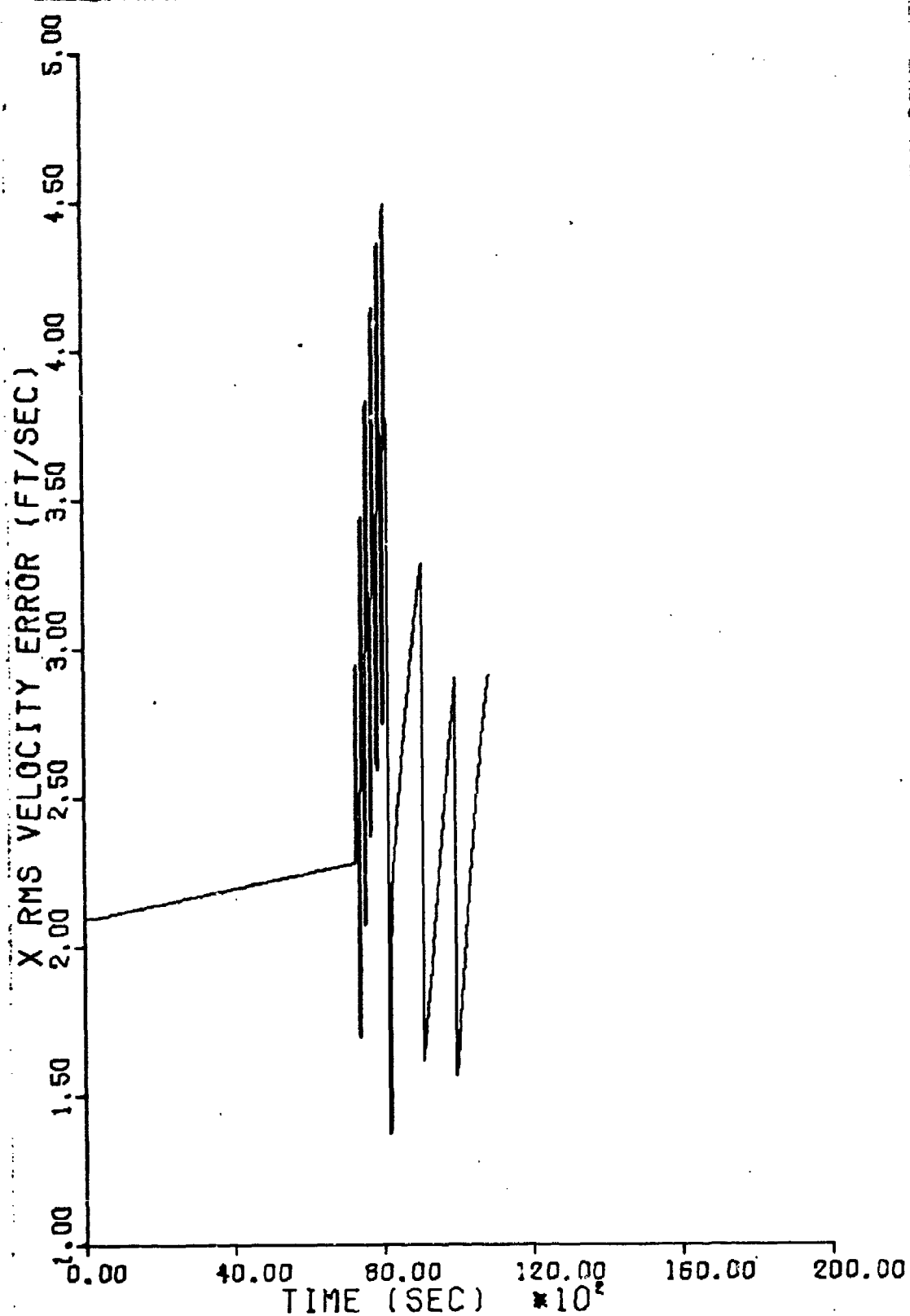


Figure 46. Decoupled Filter Maneuvering X RMS Velocity Error

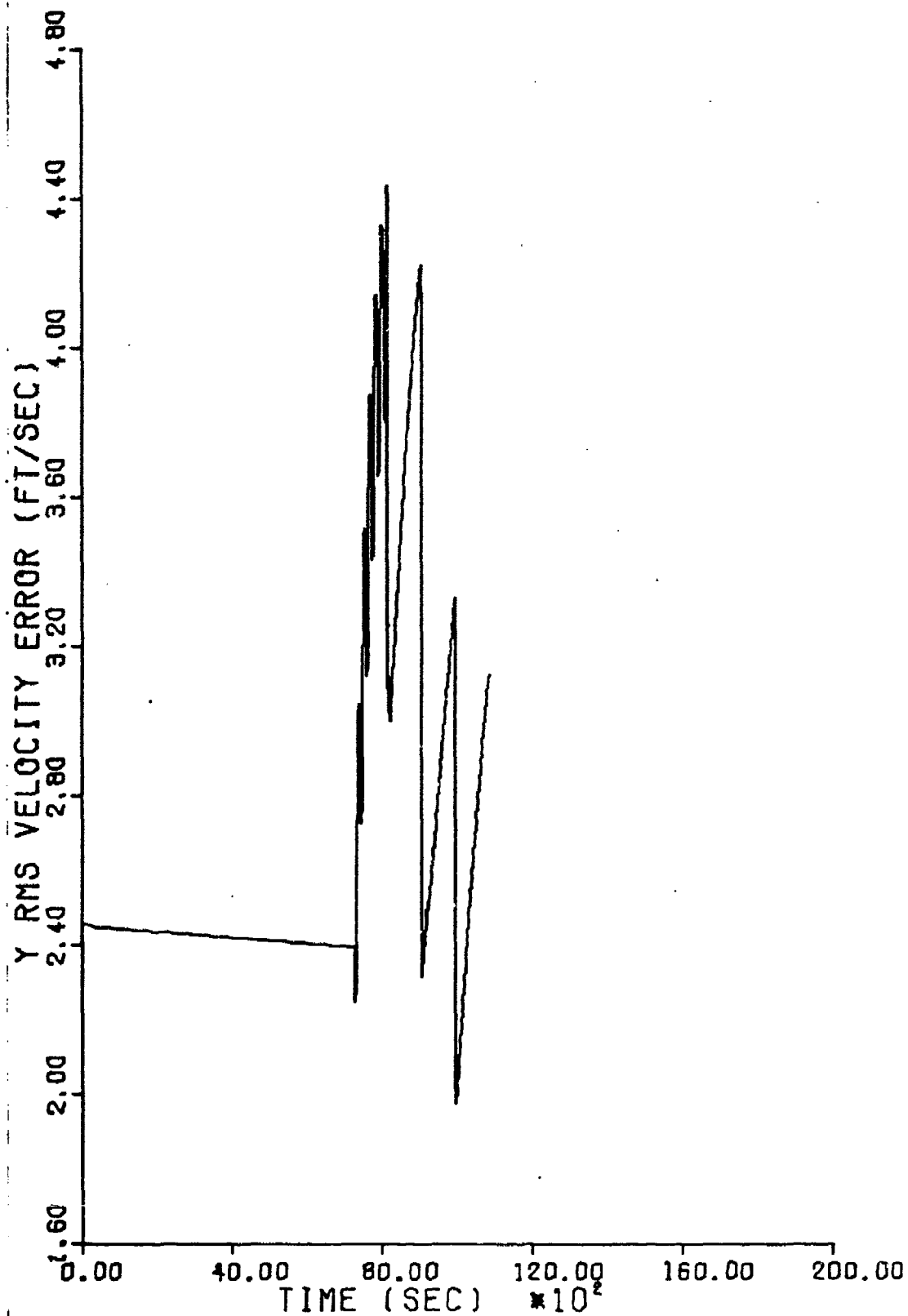


Figure 47. Decoupled Filter Maneuvering Y RMS Velocity Error

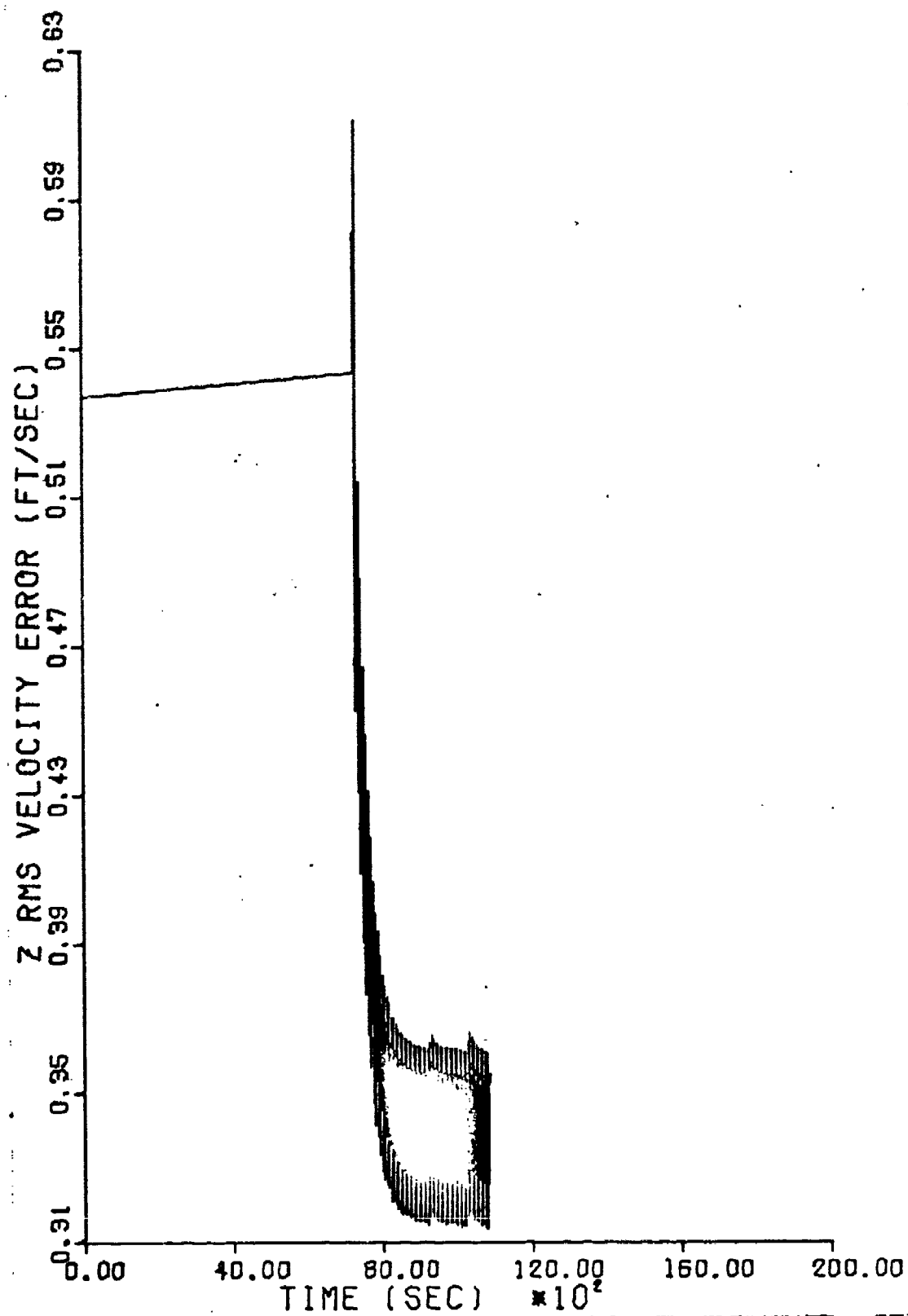


Figure 48. Decoupled Filter Maneuvering Z RMS Velocity Error

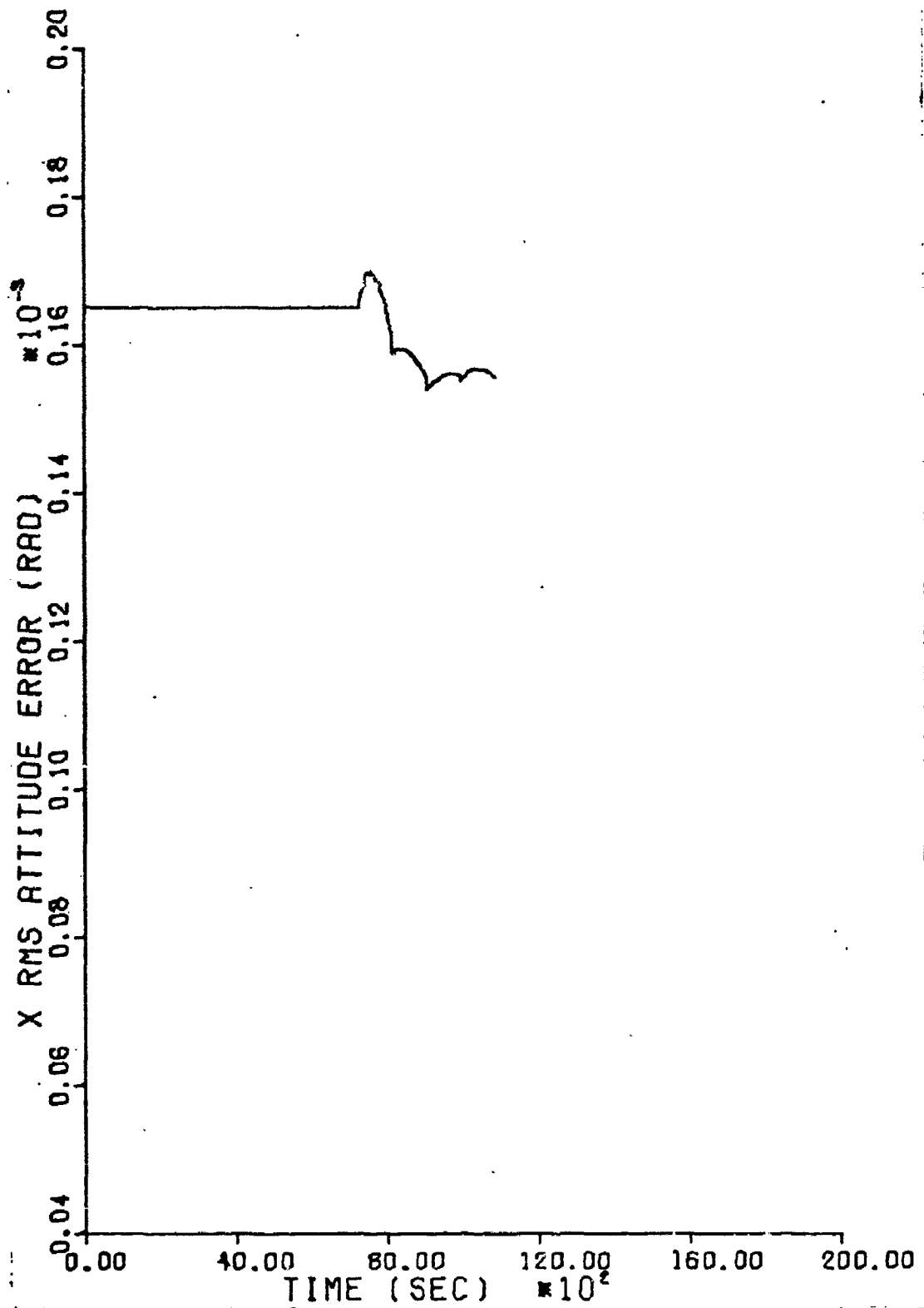


Figure 49. Decoupled Filter Maneuvering X RMS Tilt Error



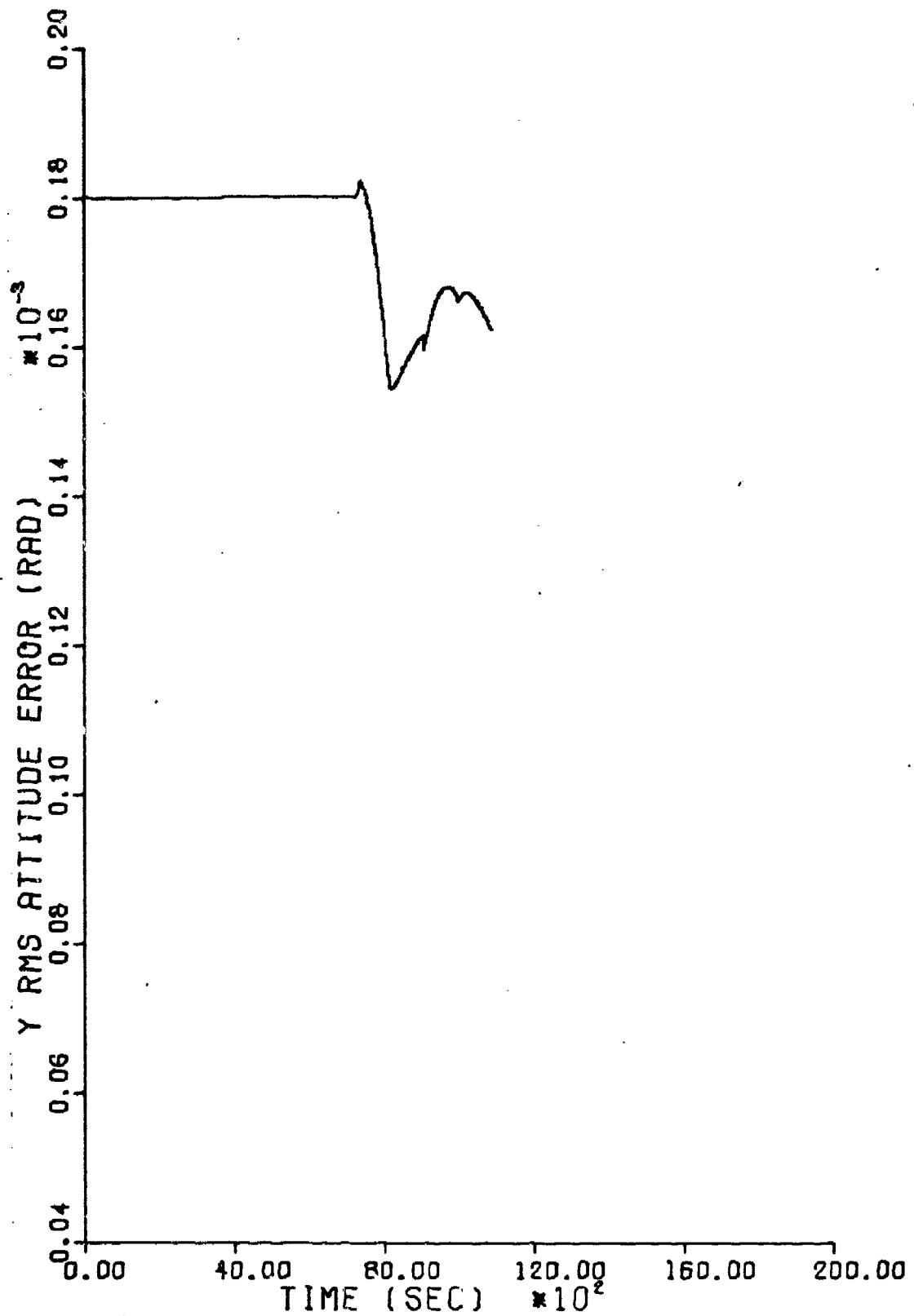


Figure 50. Decoupled Filter Maneuvering Y RMS Tilt Error

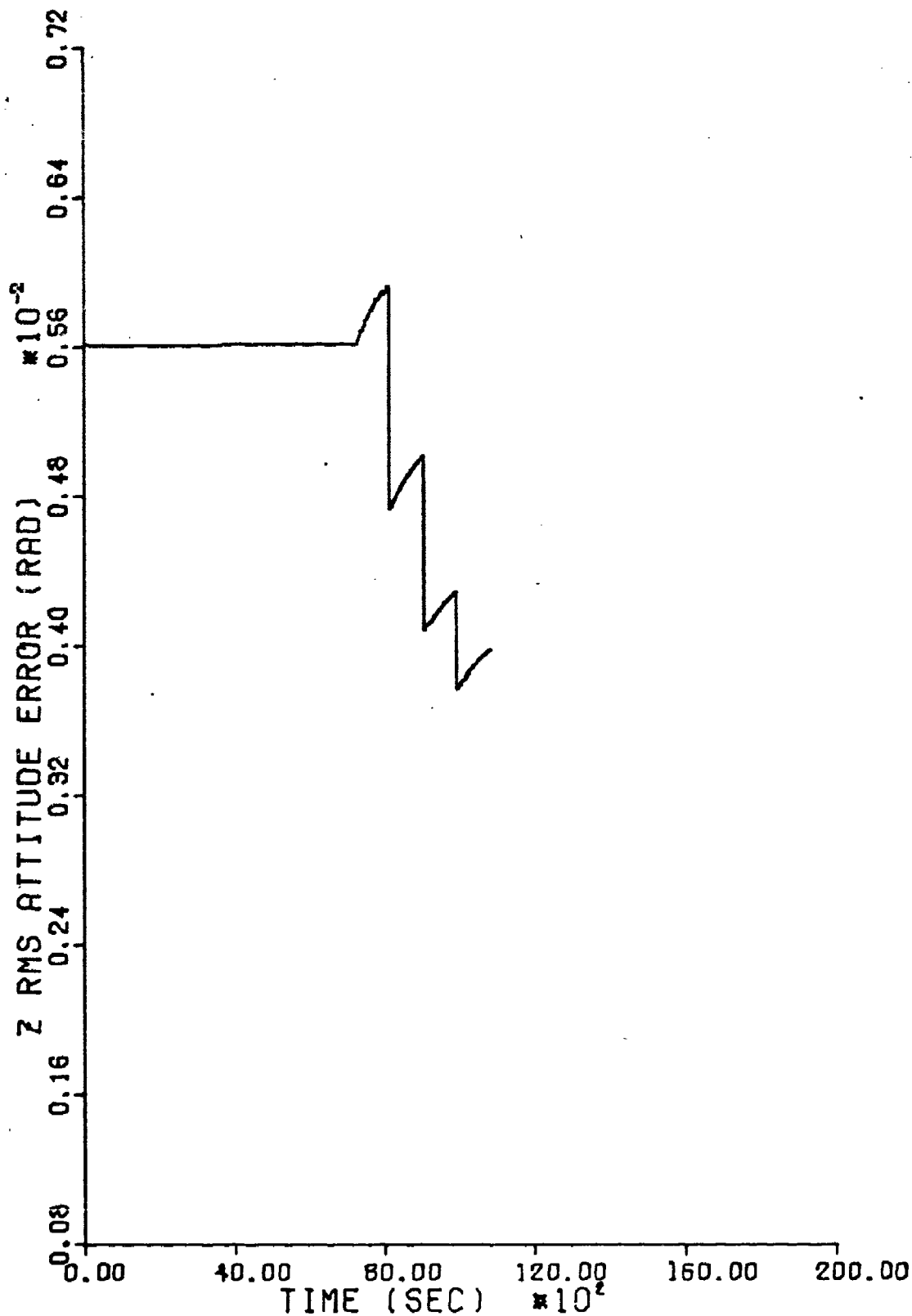


Figure 51. Decoupled Filter Maneuvering Z RMS Tilt Error

Table IX

Maneuvering RMS Errors of INS Plant States

Decoupled 17-state filter performance compared against initial values. Values labeled H are high values and those labeled L are low values at the time specified. Initial values input in the P matrix are L values.

Variable (units)	Initial Condition (t=7200 sec)	Decoupled 17-State Filter	
		(t=8640 sec)	(t=10,020 sec)
$\delta x$ ft	H - 2616.3	H - 1181.4	H - 1482.4
	L - 574.6	L - 1078.7	L - 505.2
$\delta y$ ft	H - 2404.7	H - 1245.9	H - 1593.8
	L - 537.0	L - 1127.0	L - 503.6
$\delta z$ ft	H - 259.4	H - 95.0	H - 103.1
	L - 259.4	L - 93.7	L - 103.1
$\delta v_x$ ft/sec	H - 4.36	H - 2.77	H - 2.89
	L - 2.09	L - 2.69	L - 1.65
$\delta v_y$ ft/sec	H - 4.46	H - 3.69	H - 3.33
	L - 2.45	L - 3.60	L - 2.05
$\delta v_z$ ft/sec	H - 0.537	H - 0.365	H - 0.353
	L - 0.537	L - 0.364	L - 0.352
$\delta \phi_x$ millirad	H - 0.168	H - 0.159	H - 0.156
	L - 0.165	L - 0.159	L - 0.155
$\delta \phi_y$ millirad	H - 0.182	H - 0.158	H - 0.167
	L - 0.180	L - 0.158	L - 0.167
$\delta \phi_z$ millirad	H - 6.45	H - 4.90	H - 4.29
	L - 5.61	L - 4.88	L - 3.78

Table X

Comparison of Decoupled 17-State Filter Average RMS Errors

Decoupled 17-state filter performance for straight and level versus maneuvering flight profiles. Average values are obtained from Tables VIII and IX by adding the high and low values and dividing by two. Flight profiles are straight and level (S-L) and maneuvering (M).

Variable (units)	Flight Time			
	8640 sec		10,020 sec	
	Flight Profile		Flight Profile	
	S-L	M	S-L	M
$\delta x$ ft	760.65	1130.05	672.85	993.80
$\delta y$ ft	1295.45	1186.45	1780.95	1048.70
$\delta z$ ft	116.55	94.35	108.95	103.10
$\delta v_x$ ft/sec	0.44	2.73	0.89	2.27
$\delta v_y$ ft/sec	3.33	3.65	3.45	2.69
$\delta v_z$ ft/sec	0.3590	0.3645	0.3585	0.3525
$\delta \phi_x$ millirad	0.183	0.159	0.165	0.156
$\delta \phi_y$ millirad	0.138	0.158	0.155	0.167
$\delta \phi_z$ millirad	5.59	4.89	5.32	4.04

variable at the time instant before the data sample time to its value just after the data sample time and dividing by two.

### Error Budget Determination

The error budget determination was made using five separate computer runs during both straight and level and maneuvering flight. The nine basic INS plant error state errors were plotted and then superimposed to obtain the data. The system reference model was altered for each computer run by adding the appropriate models for gyro, accelerometer, Doppler, and altimeter errors progressively to the basic INS plant error model. Thus five curves appear on each figure showing the error contribution from each source added to the previous curve. The first curve depicts the error contributed by the basic INS decoupled plant model. The  $\underline{P}(0)$ , and  $\underline{Q}$  matrix elements not associated with these first ten states (see Table I) are all set to zero. Since no conclusive data was available to determine the separate measurement noise contribution from the INS, radar, altimeter, Doppler, etc., all elements of the  $\underline{R}$  matrix were assumed to correspond to variables in the basic INS plant model and their values are included at this point. The second curve gives a plot of the errors after including the gyro modeling terms and the associated values in the  $\underline{Q}$  matrix. Next the accelerometer model and associated  $\underline{Q}$  elements were added. The fourth curve includes the effect of the Doppler while the last curve adds the altimeter model and noise to complete the system reference model. The plots for straight and level

flight are shown in Figures 52 through 60 while the error budget for maneuvering flight is given in Figures 61 through 69.

As can be seen from the plots, the propagation of the initial conditions through the plant model alone contributes most of the error for the position and x velocity curves but exhibits the minimum error for z velocity. Note that z position and velocity errors as well as x, y, and z attitude (tilt) errors are a minimum for the plant model alone. The addition of the gyro and accelerometer models increases the tilt errors but decreases the x, y, and z position and velocity errors. The Doppler appears to reduce x and y position and velocity errors with little effect on z position and velocity or on tilt errors. This data is suspect in that the change from an error free Doppler to a noise corrupted Doppler model should not cause a decrease in the Doppler error contribution. As more error sources are added to the model, the volume of the error ellipsoid (i.e., the eigenvalues of the covariance matrix) must not decrease. A possible explanation of this phenomenon is that some off-diagonal terms may have increased unobserved while the individual RMS values (diagonal term square roots) decreased. This would allow the volume of the error ellipsoid to increase although the RMS values indicate it is decreasing. Addition of the altimeter has a greater effect on z position and velocity than on any of the other variables.

Tables XI through XX show the high and low values of

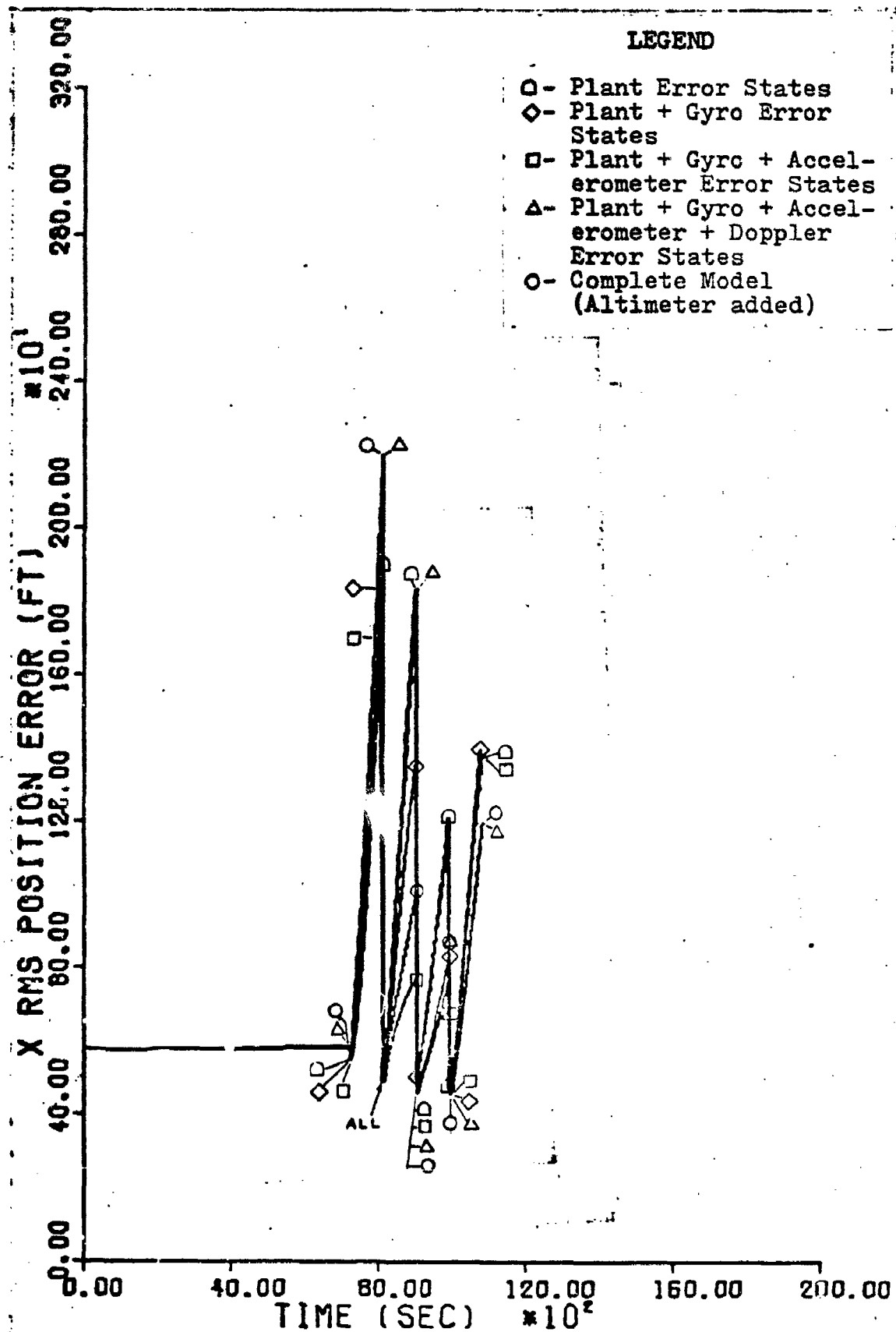


Figure 52. Straight and Level X RMS Position Error Budget

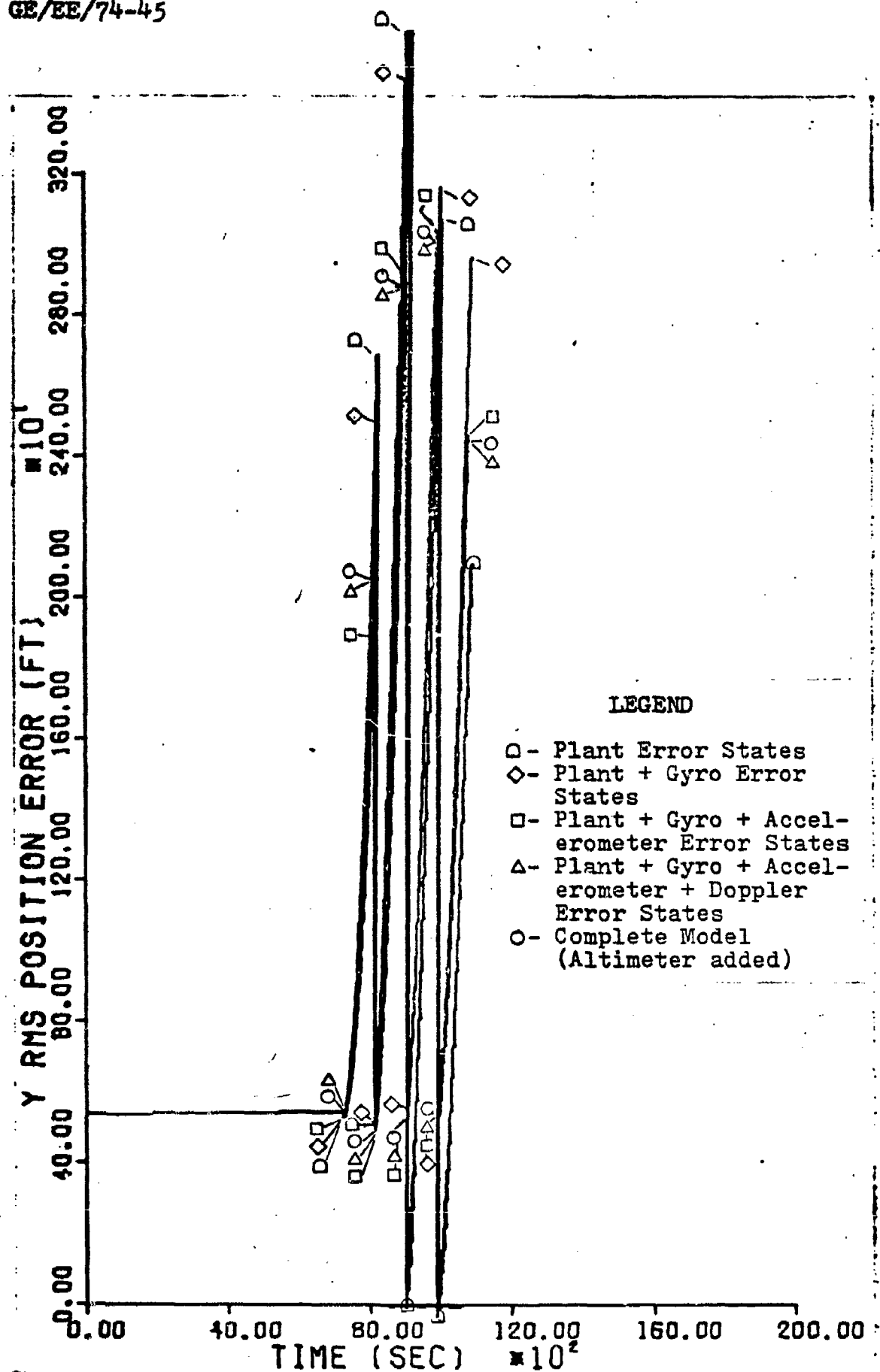


Figure 53. Straight and Level Y RMS Position Error Budget



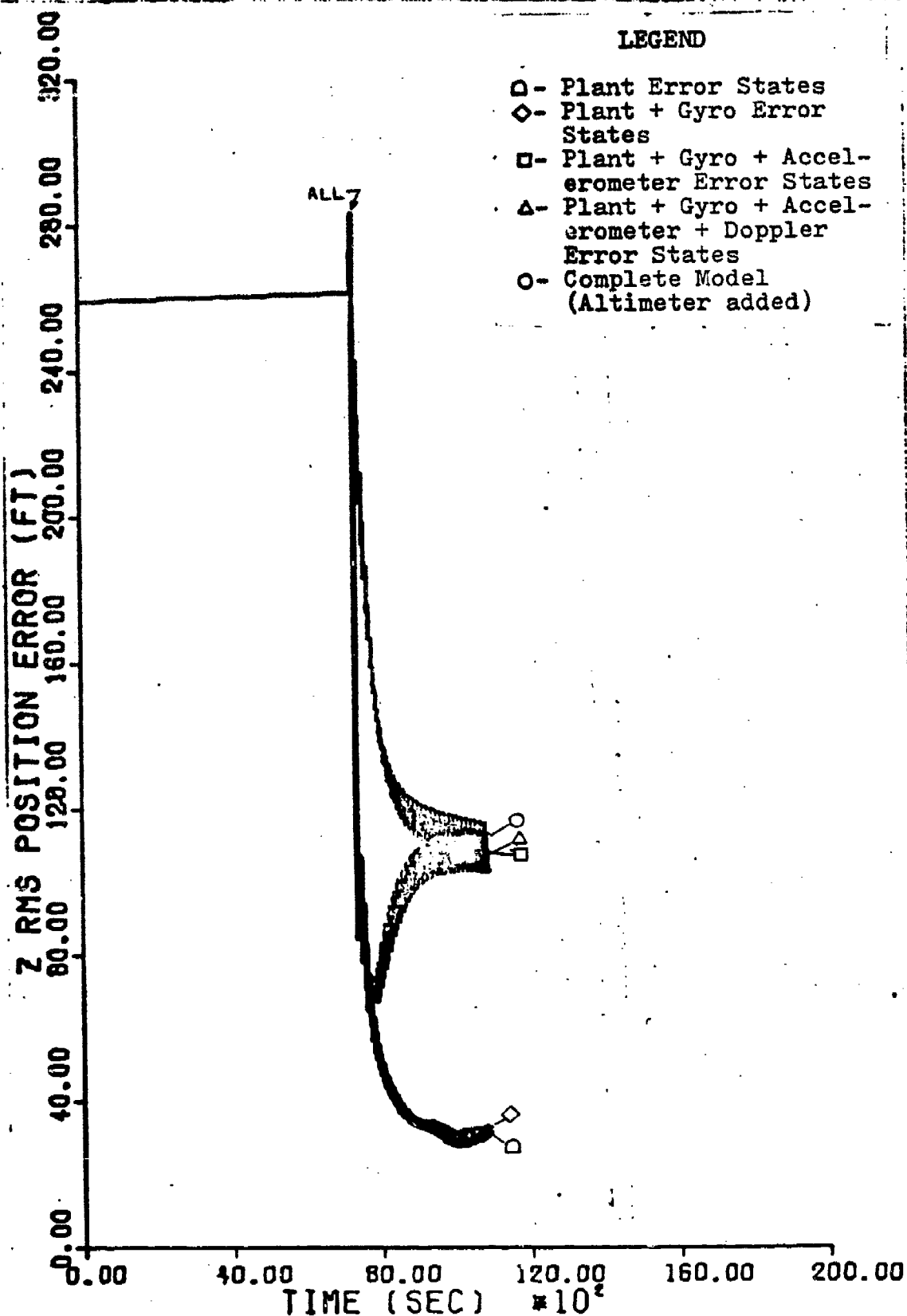


Figure 54. Straight and Level Z RMS Position Error Budget

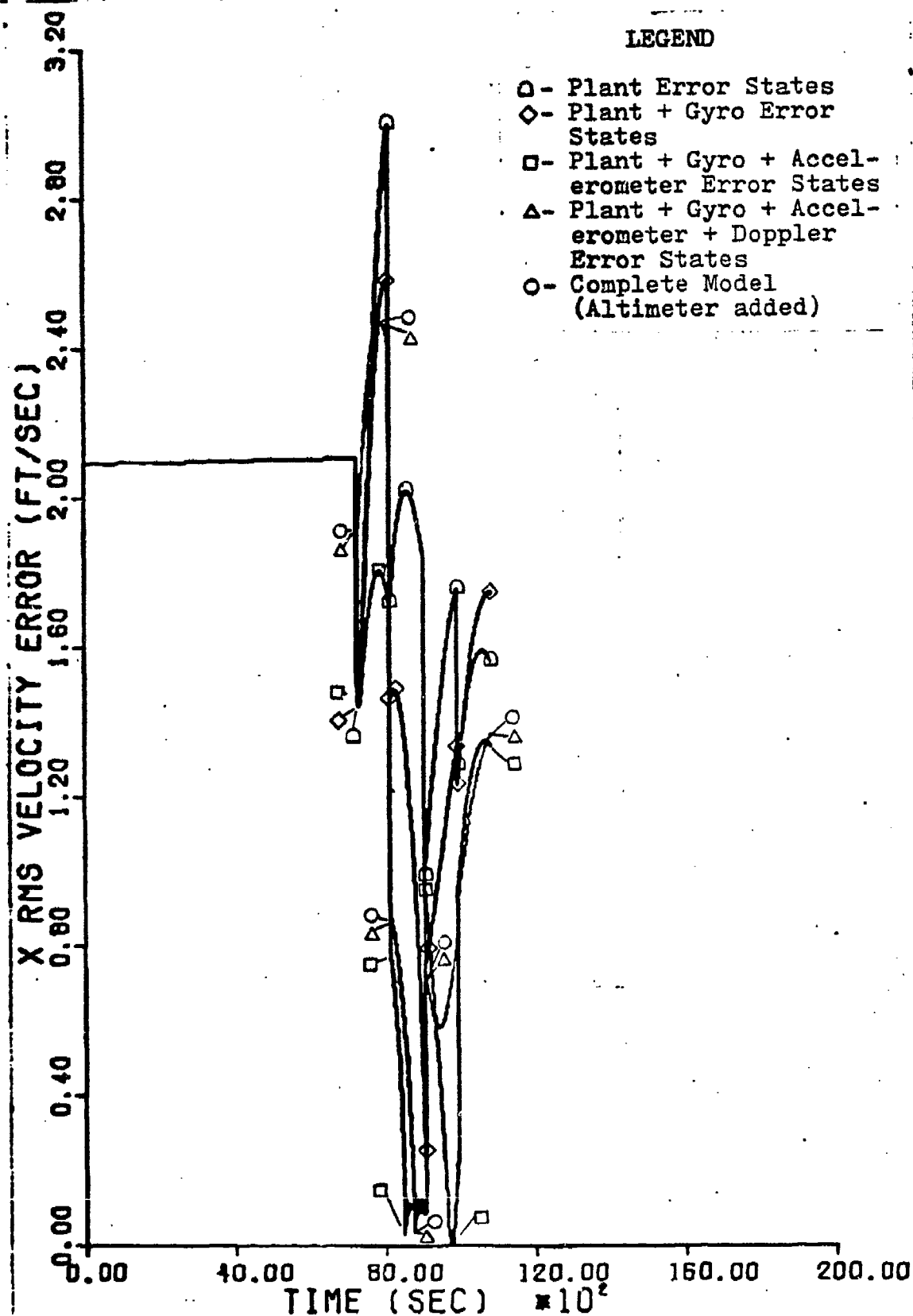


Figure 55. Straight and Level X RMS Velocity Error Budget

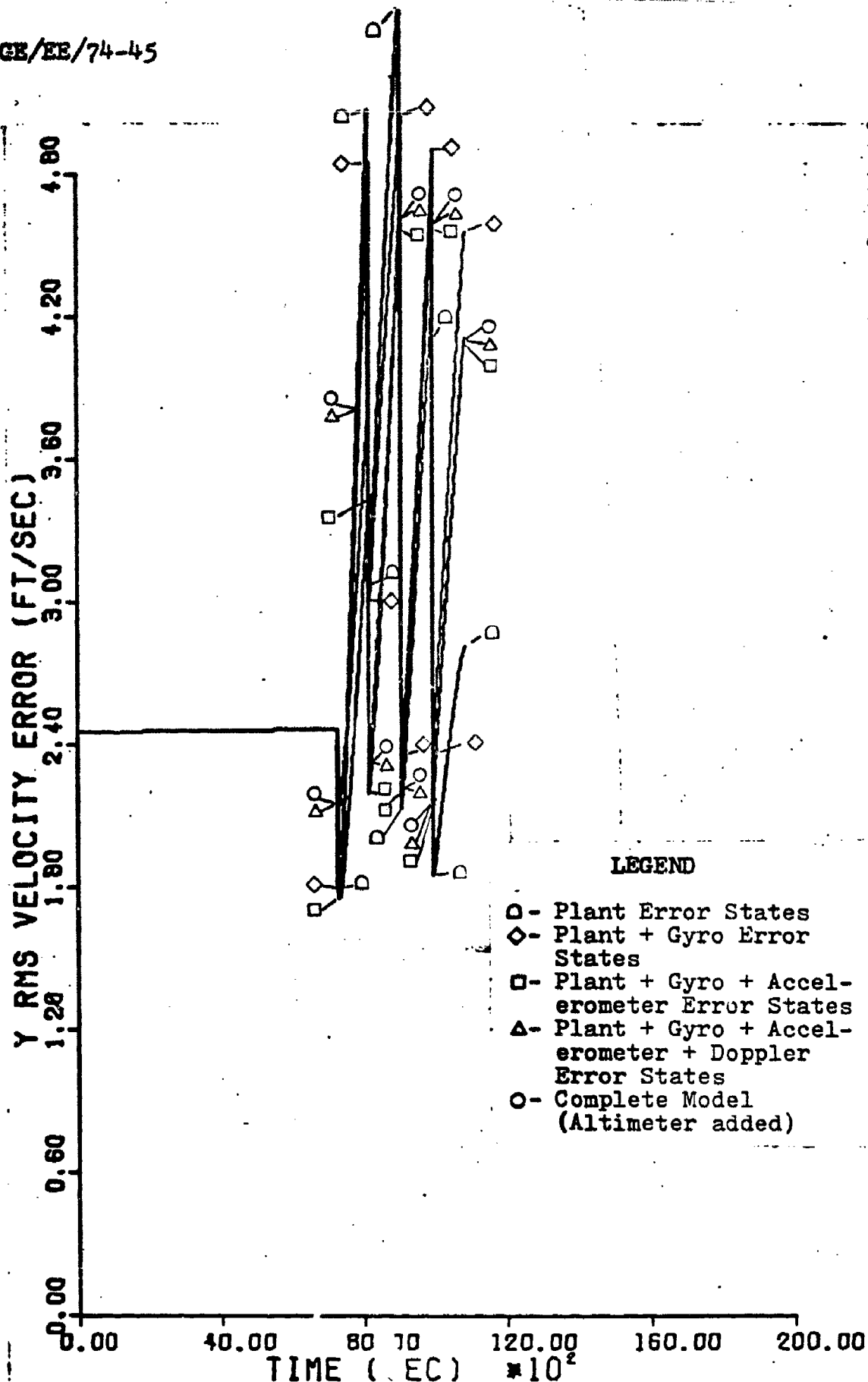


Figure 56. Straight and Level Y RMS Velocity Error Budget

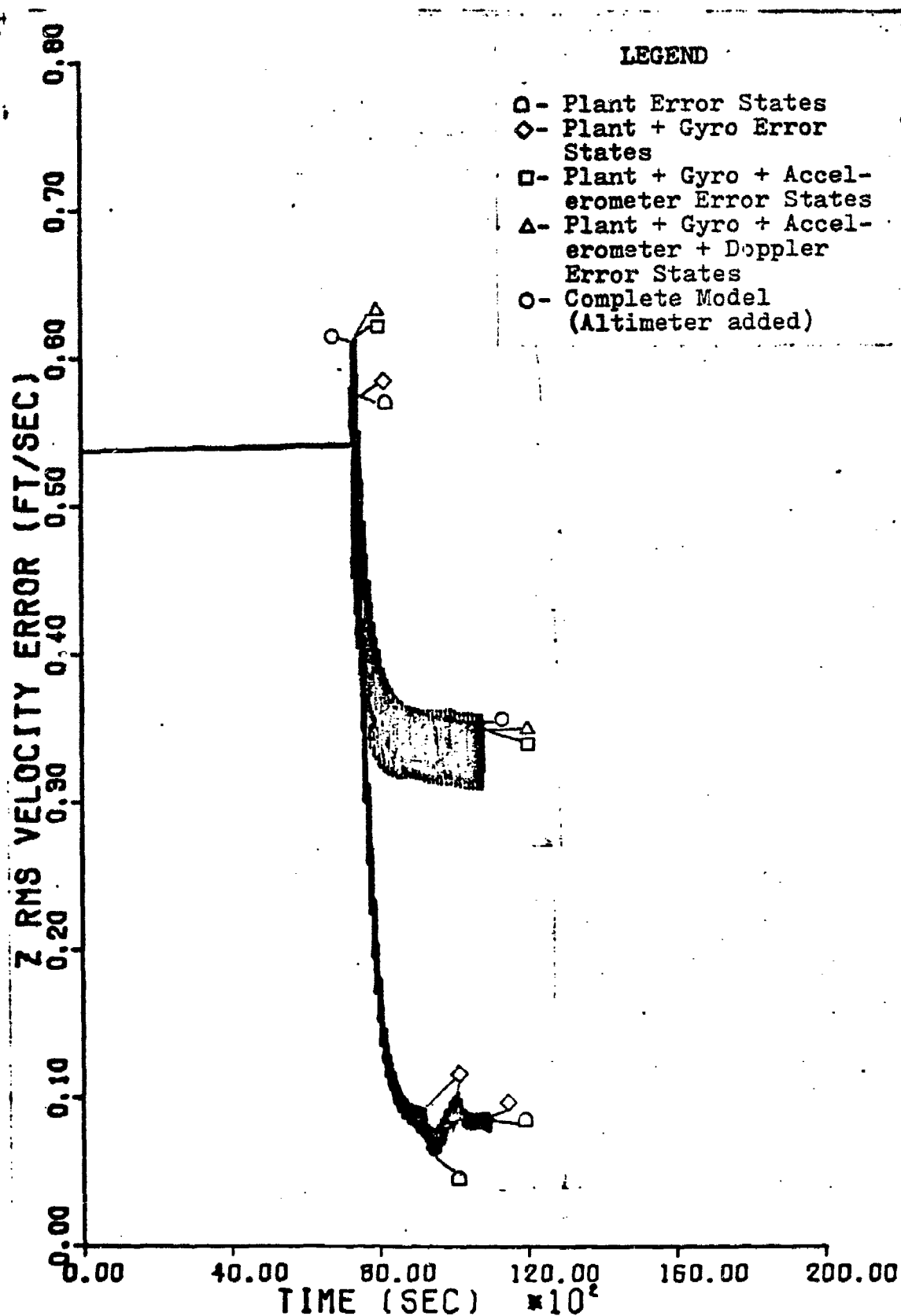


Figure 57. Straight and Level Z RMS Velocity Error Budget

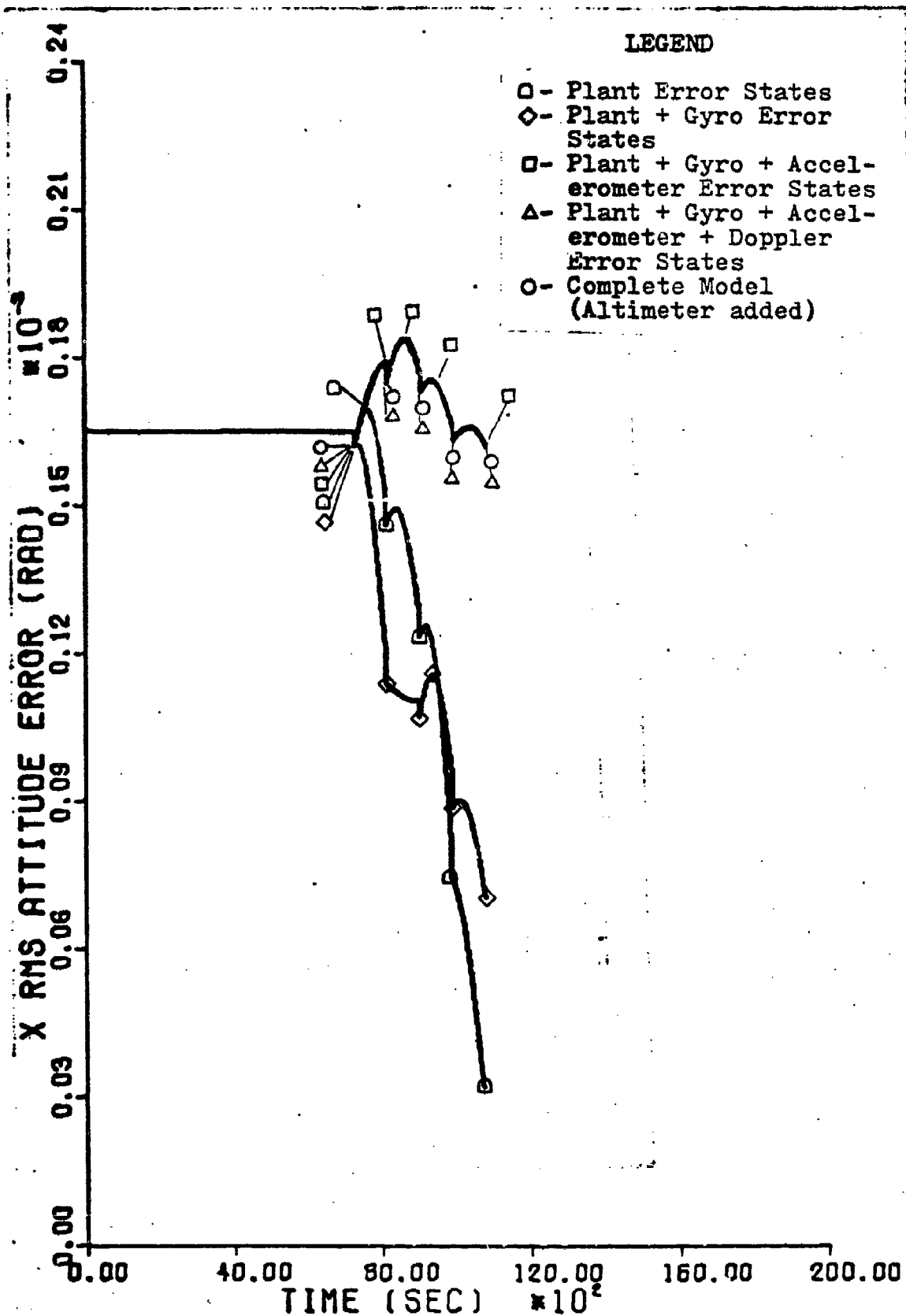


Figure 58. Straight and Level X RMS Tilt Error Budget

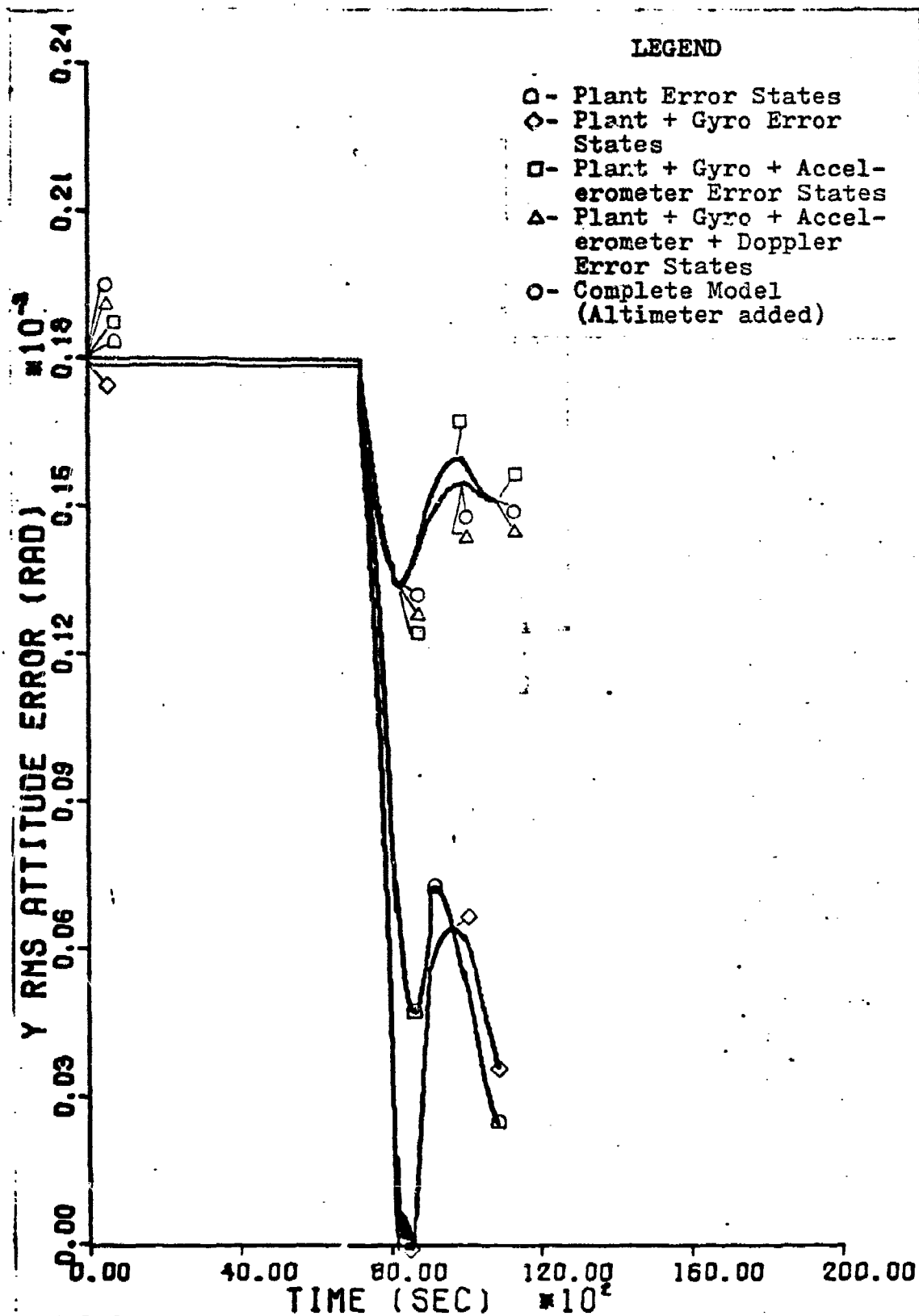


Figure 59. Straight and Level Y RMS Tilt Error Budget

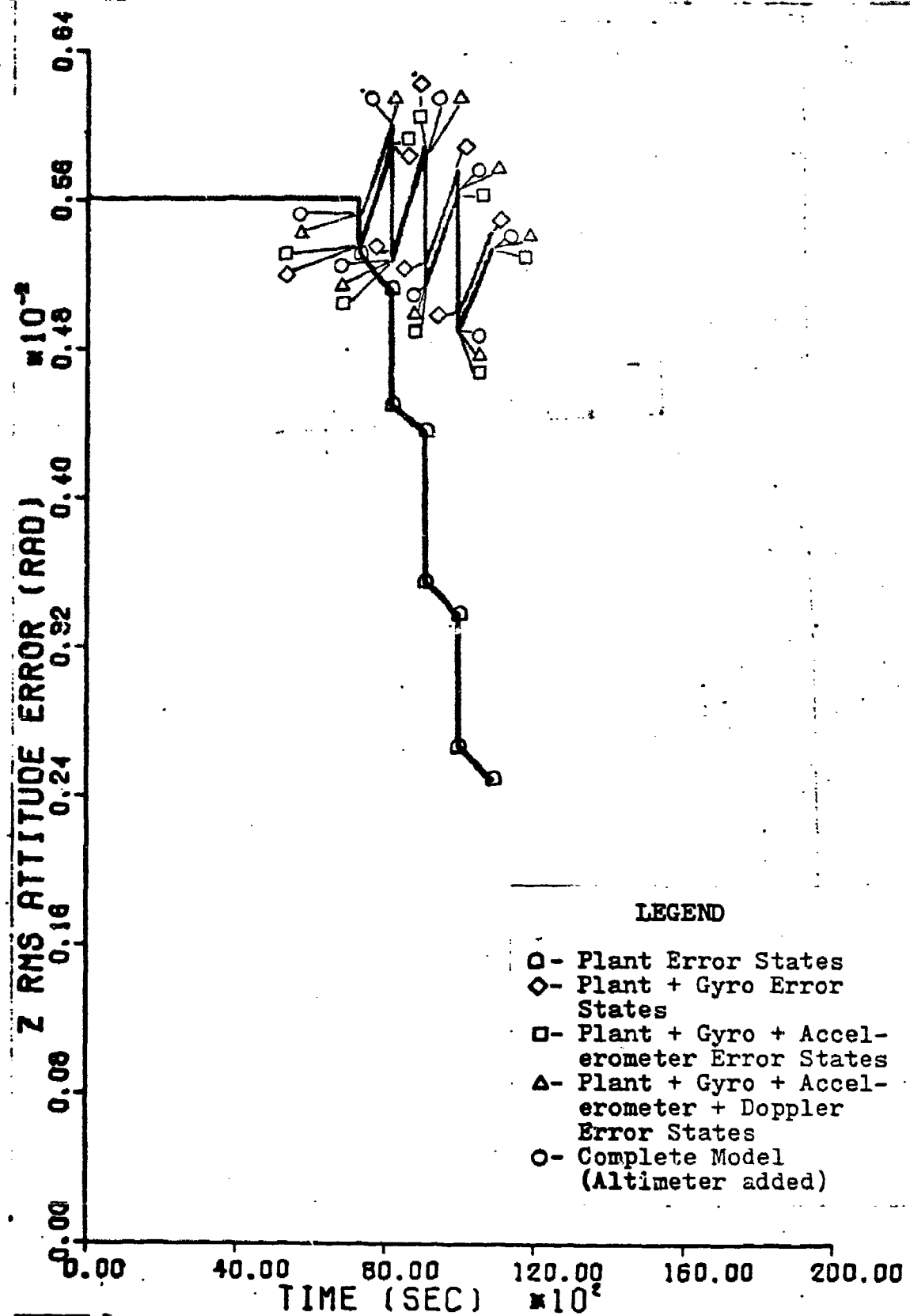


Figure 60. Straight and Level Z RMS Tilt Error Budget

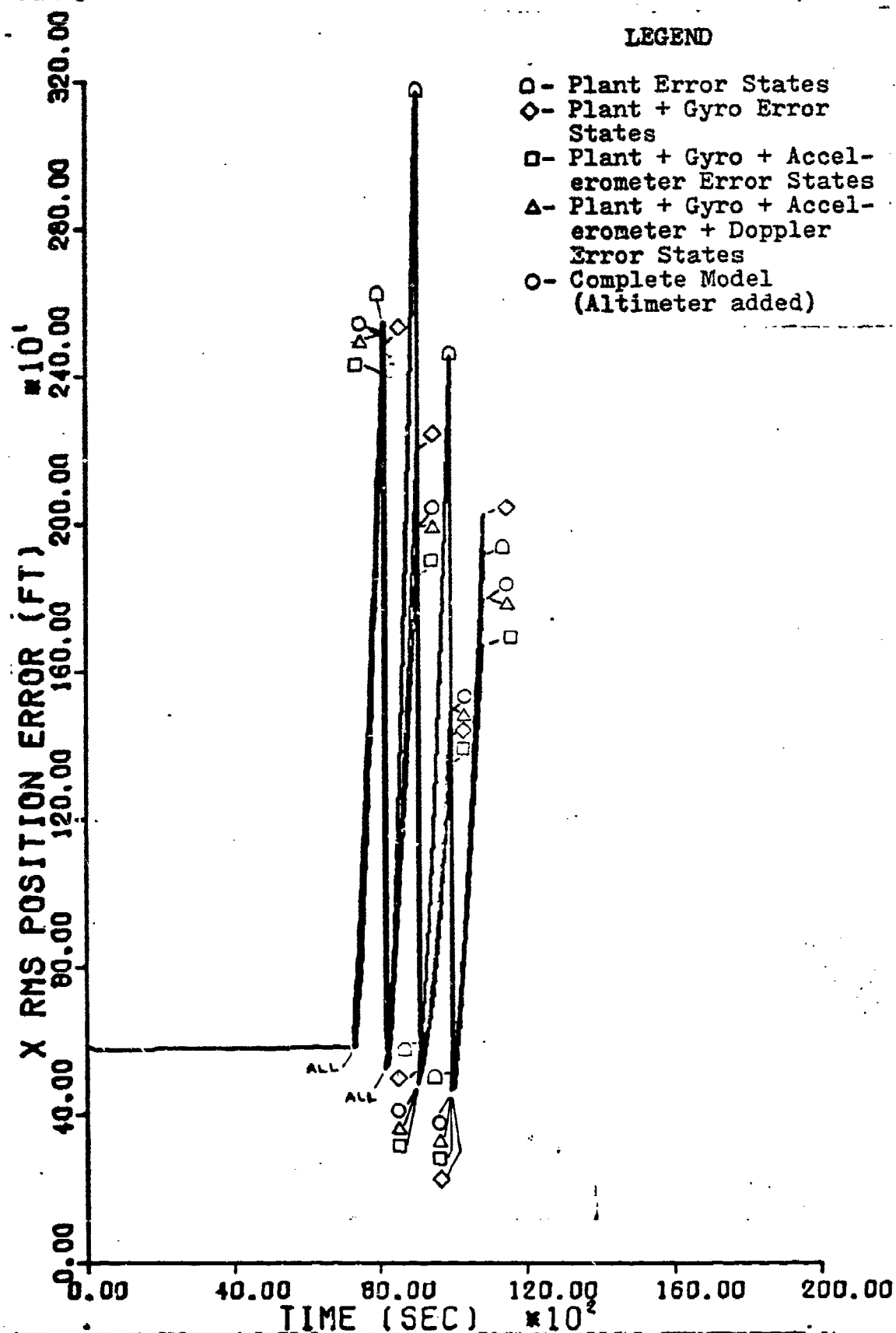


Figure 61. Maneuvering X RMS Position Error Budget



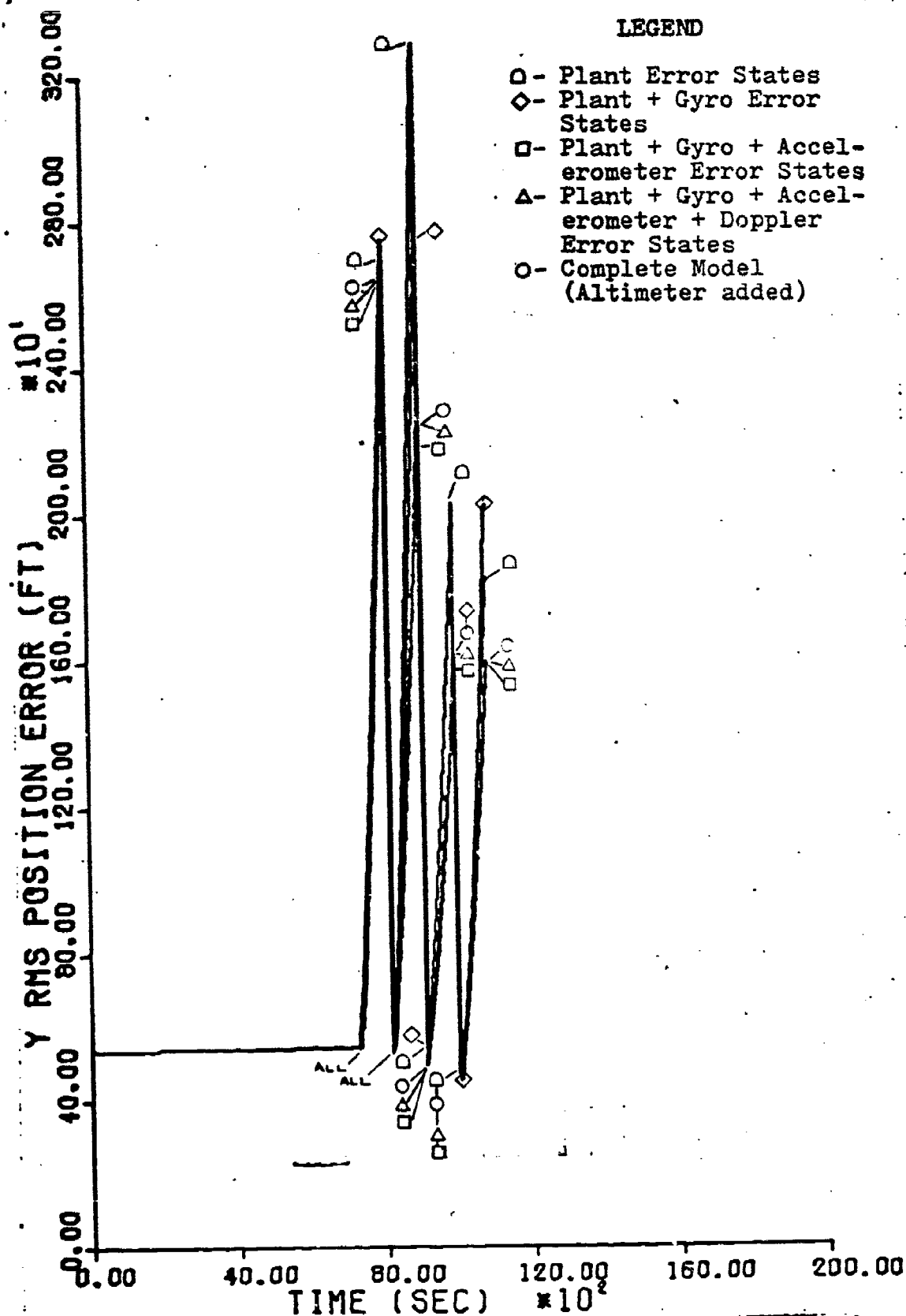


Figure 62. Maneuvering Y RMS Position Error Budget

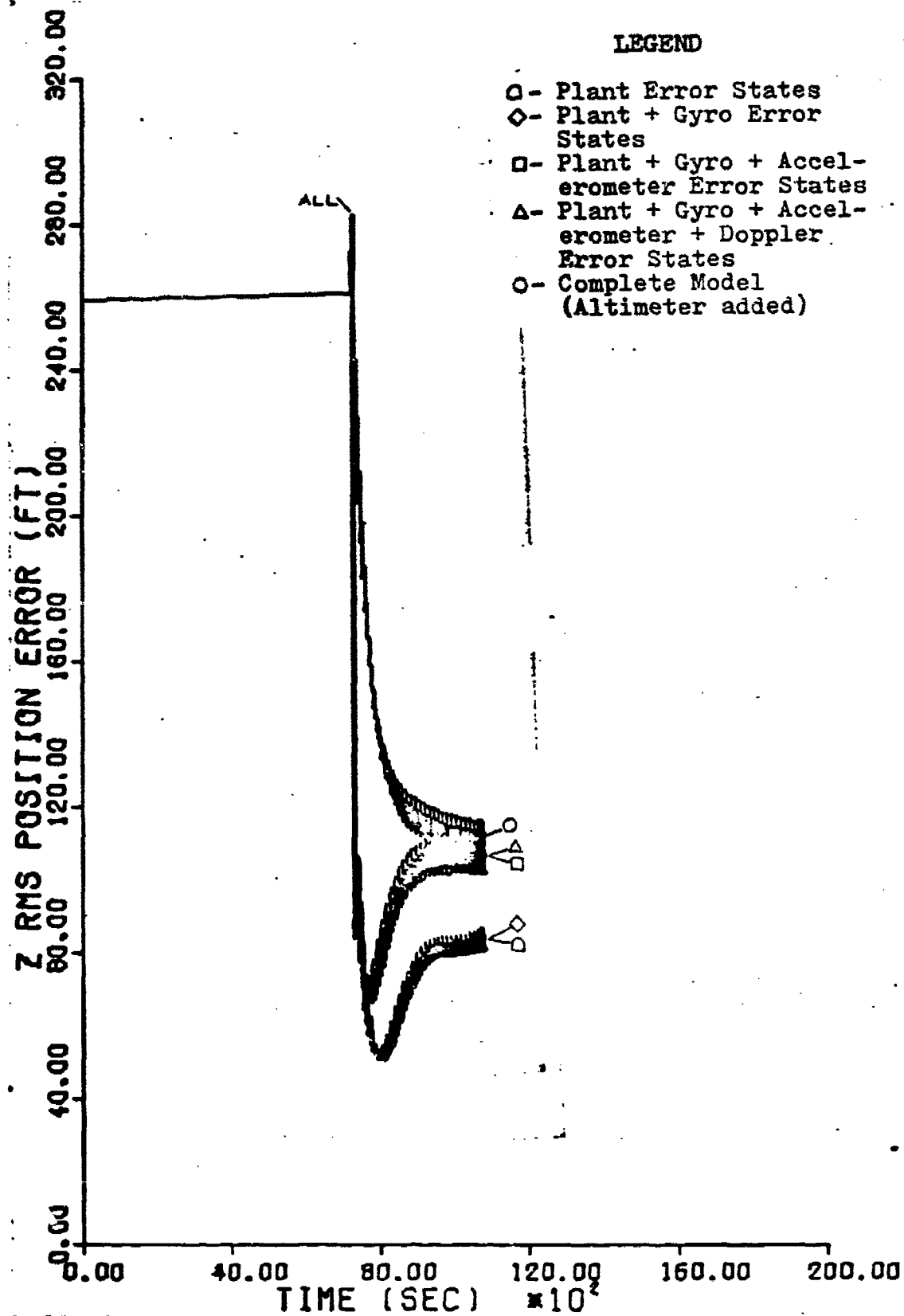


Figure 63. Maneuvering Z RMS Position Error Budget

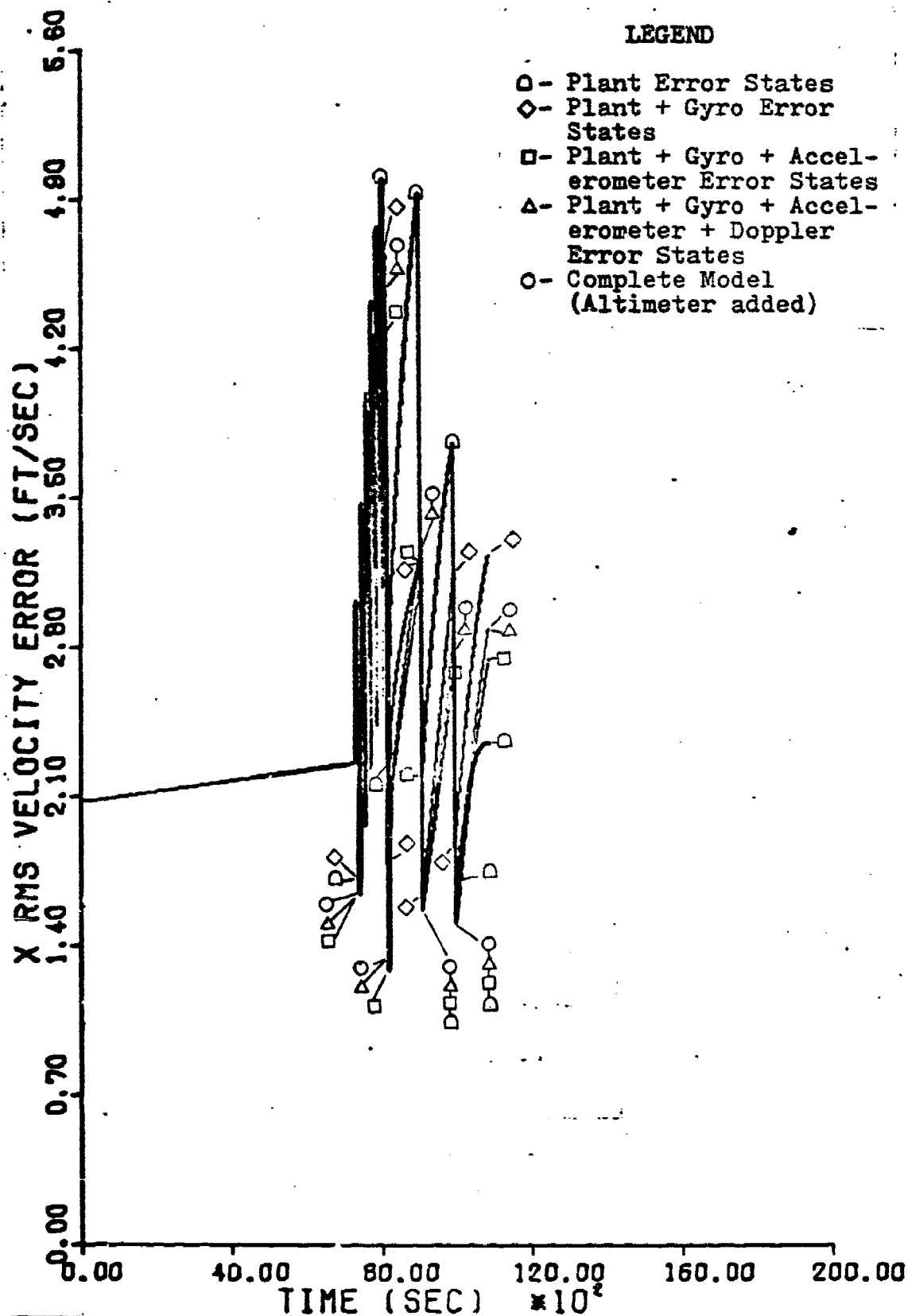


Figure 64. Maneuvering X RMS Velocity Error Budget

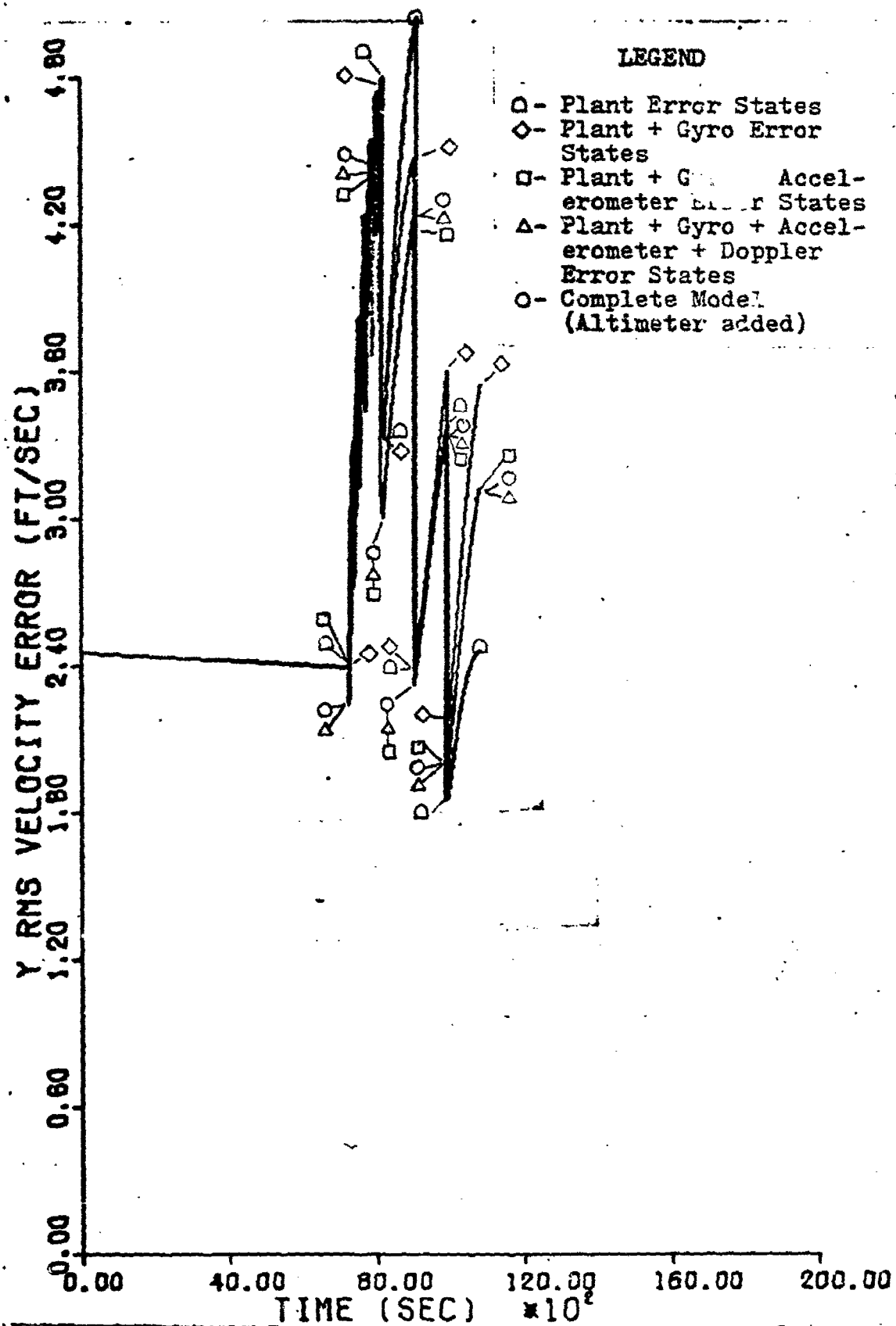


Figure 65. Maneuvering Y RMS Velocity Error Budget

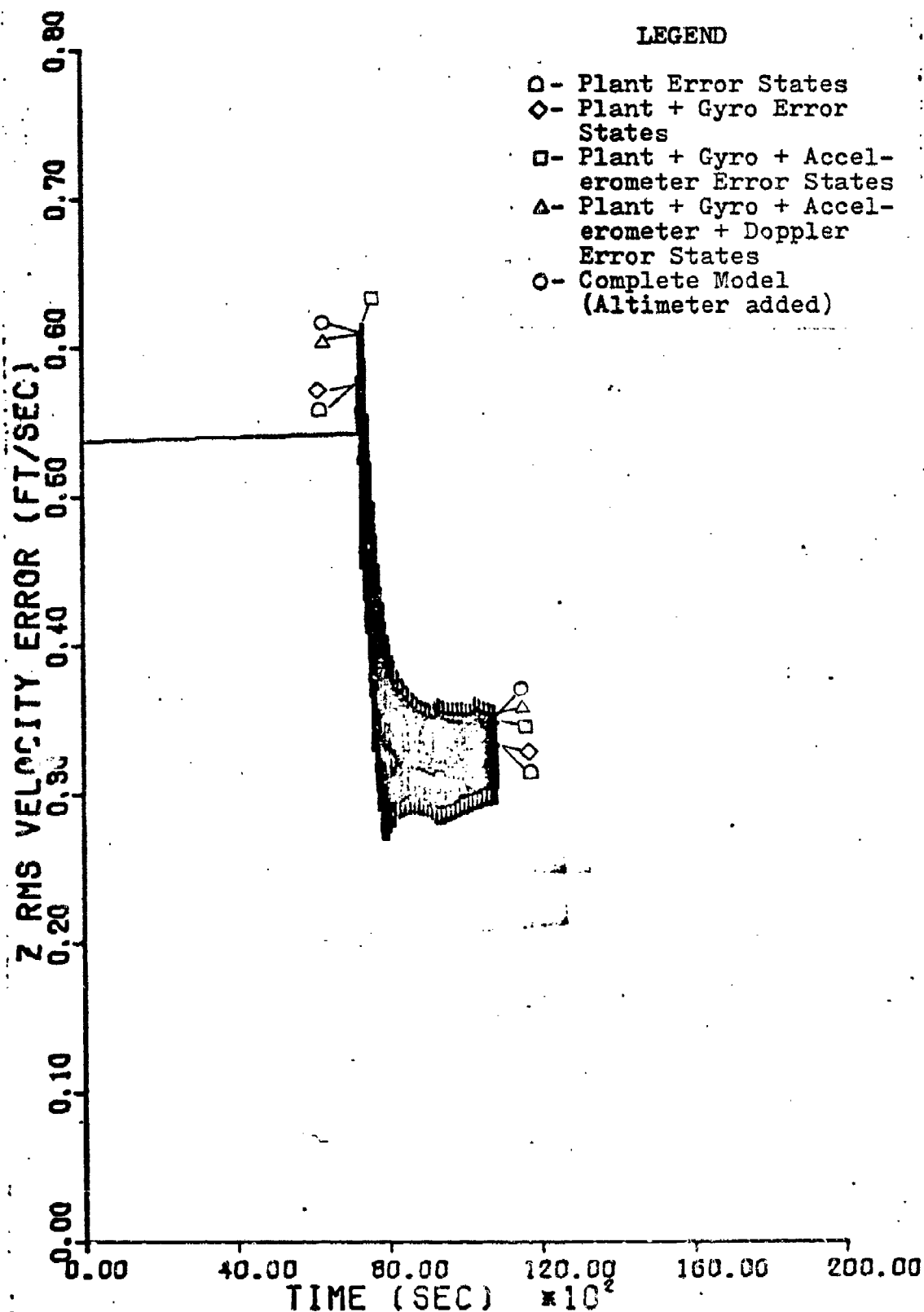


Figure 66. Maneuvering Z RMS Velocity Error Budget

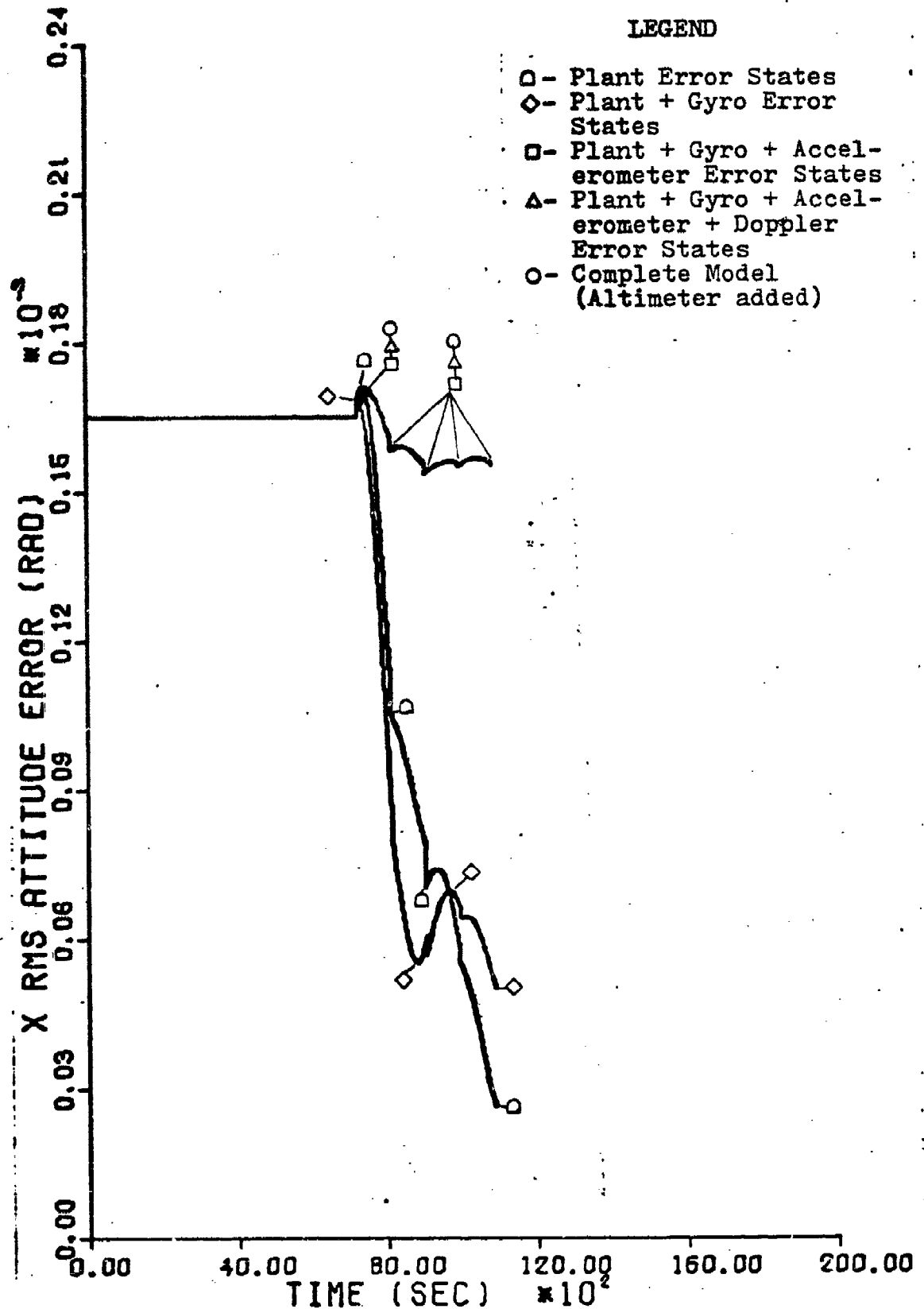


Figure 67. Maneuvering RMS Tilt Error Budget

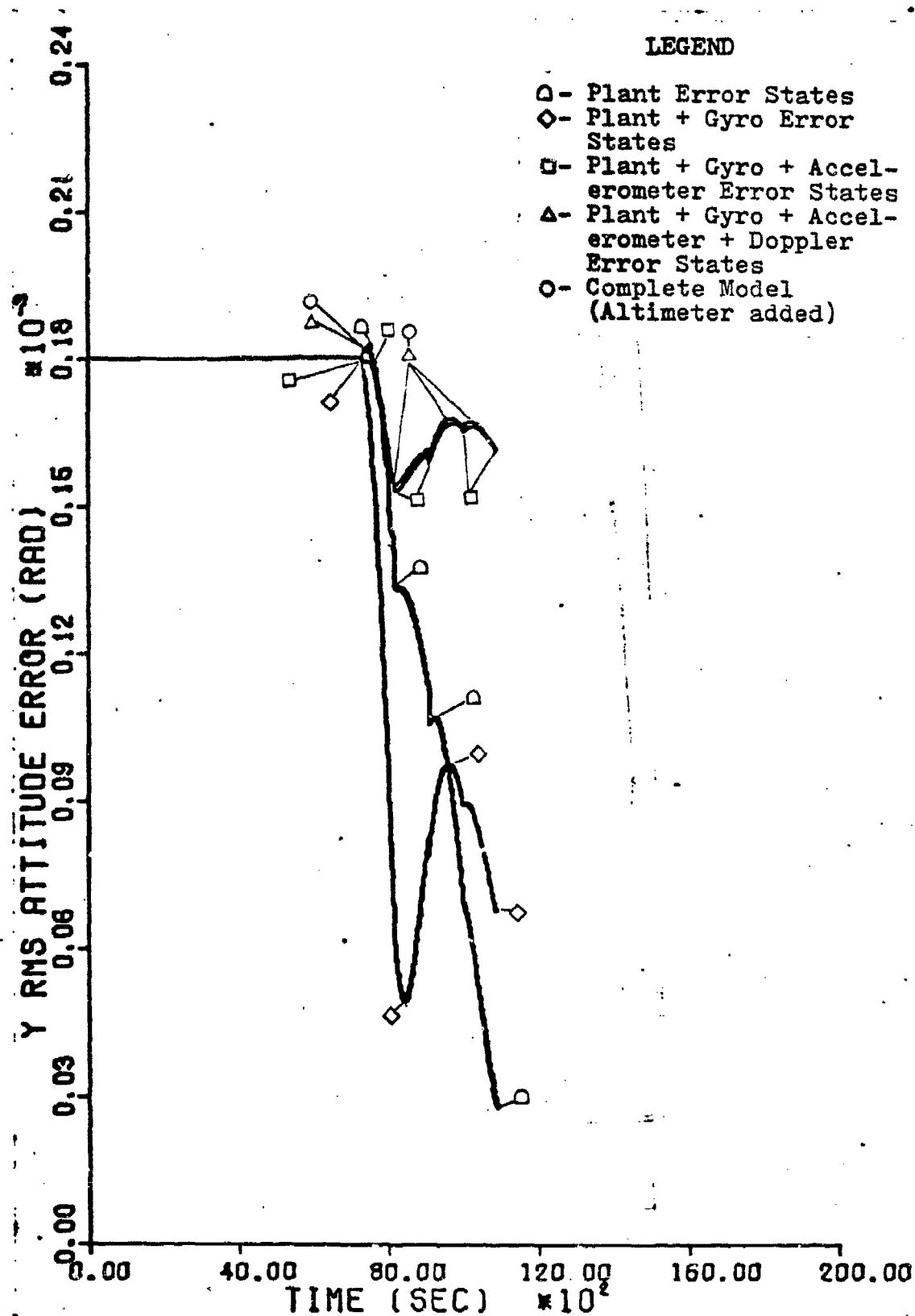


Figure 68. Maneuvering Y RMS Tilt Error Budget

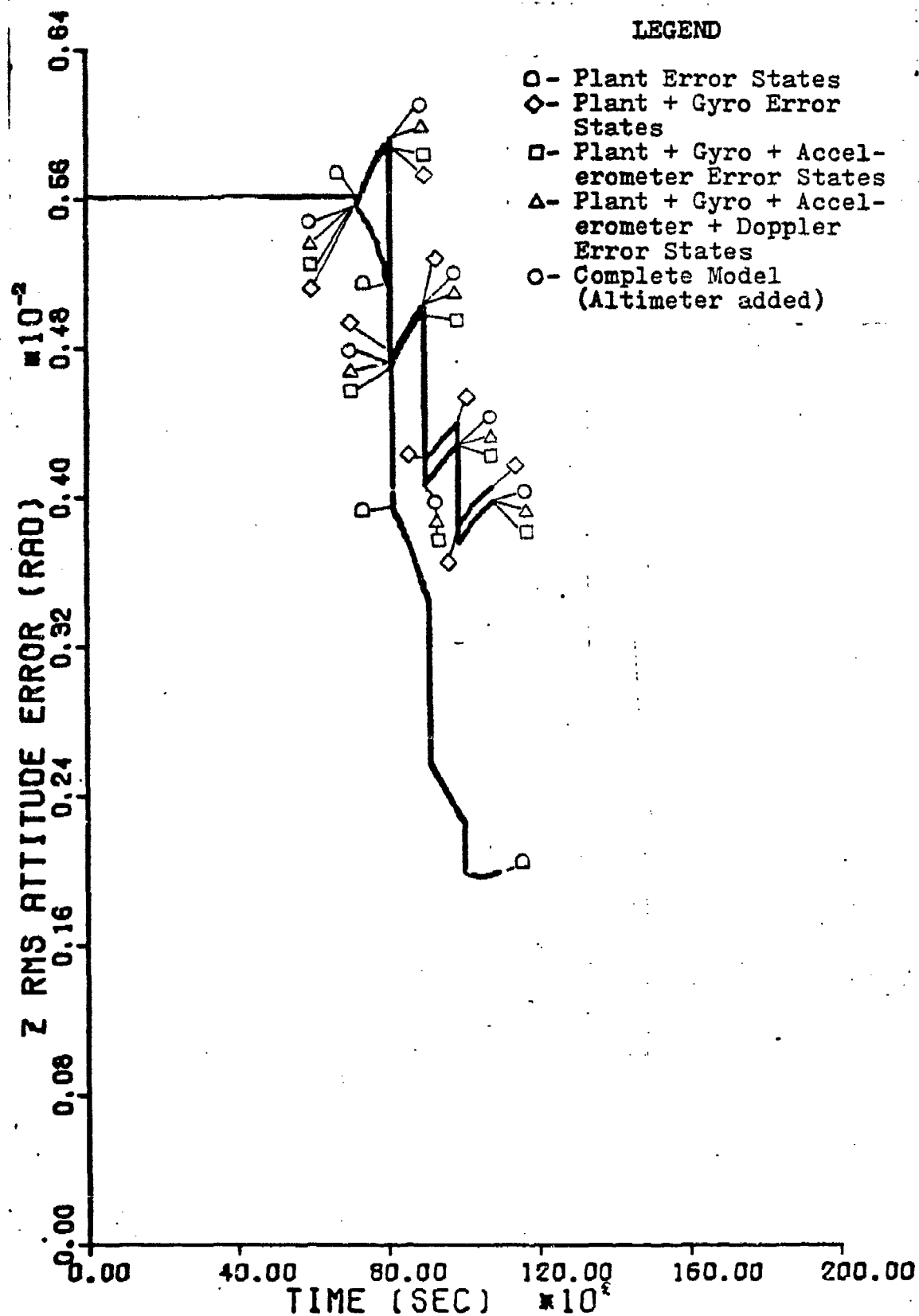


Figure 69. Maneuvering Z RMS Tilt Error Budget



Table XI

Plant Error States Straight and Level RMS Errors

Values labeled H are high values and values labeled L are low values at data time. Initial condition values are taken from the total reference system model.

Variable (units)	Initial Condition (t=7200 sec)	Decoupled 17-State Filter	
		(t=8640 sec)	(t=10,020 sec)
$\delta x$ ft	H - 2616.3 L - 574.6	H - 1152.5 L - 1054.9	H - 1185.4 L - 500.1
$\delta y$ ft	H - 2404.7 L - 537.0	H - 1968.8 L - 1712.6	H - 3528.5 L - 608.4
$\delta z$ ft	H - 259.4 L - 259.4	H - 272.7 L - 268.2	H - 178.0 L - 171.7
$\delta v_x$ ft/sec	H - 4.36 L - 2.09	H - 2.00 L - 2.00	H - 1.75 L - 1.30
$\delta v_y$ ft/sec	H - 4.46 L - 2.45	H - 4.43 L - 4.24	H - 4.02 L - 1.82
$\delta v_z$ ft/sec	H - 0.537 L - 0.537	H - 0.553 L - 0.458	H - 0.013 L - 0.020
$\delta \phi_x$ millirad	H - 0.168 L - 0.165	H - 0.130 L - 0.127	H - 0.085 L - 0.083
$\delta \phi_y$ millirad	H - 0.182 L - 0.180	H - 0.048 L - 0.048	H - 0.055 L - 0.054
$\delta \phi_z$ millirad	H - 6.45 L - 5.61	H - 4.44 L - 4.43	H - 3.38 L - 2.69

Table XII

Plant + Gyro Error States Straight and Level RMS Errors

Values labeled H are high values and values labeled L are low values at data time. Initial condition values are taken from the total reference system model.

Variable (units)	Initial Condition (t=7200 sec)	Decoupled 17-State Filter	
		(t=8640 sec)	(t=10,020 sec)
$\delta x$ ft	H - 2616.3 L - 574.6	H - 958.8 L - 894.6	H - 788.3 L - 478.0
$\delta y$ ft	H - 2404.7 L - 537.0	H - 1751.7 L - 1542.3	H - 3122.9 L - 590.2
$\delta z$ ft	H - 259.4 L - 259.4	H - 379.2 L - 372.8	H - 32.1 L - 32.1
$\delta v_x$ ft/sec	H - 4.36 L - 2.09	H - 1.32 L - 1.25	H - 1.34 L - 1.30
$\delta v_y$ ft/sec	H - 4.46 L - 2.45	H - 4.02 L - 4.15	H - 4.89 L - 2.51
$\delta v_z$ ft/sec	H - 0.537 L - 0.537	H - 0.096 L - 0.095	H - 0.101 L - 0.097
$\delta \phi_x$ millirad	H - 0.168 L - 0.165	H - 0.112 L - 0.111	H - 0.095 L - 0.090
$\delta \phi_y$ millirad	H - 0.182 L - 0.180	H - 0.0027 L - 0.0096	H - 0.063 L - 0.063
$\delta \phi_z$ millirad	H - 6.45 L - 5.61	H - 5.58 L - 5.62	H - 5.76 L - 5.03

Table XIII

Plant + Gyro + Accelerometer Error States  
Straight and Level RMS Errors

Values labeled H are high values and values labeled L are low values at data time. Initial condition values are taken from the total reference system model.

Variable (units)	Initial Condition (t=7200 sec)	Decoupled 17-State Filter	
		(t=8640 sec)	(t=10,020 sec)
$\delta x$ ft	H - 2616.3 L - 574.6	H - 671.9 L - 651.5	H - 674.8 L - 467.3
$\delta y$ ft	H - 2404.7 L - 537.0	H - 1395.1 L - 1227.5	H - 3006.3 L - 575.2
$\delta z$ ft	H - 259.4 L - 259.4	H - 94.2 L - 92.9	H - 103.6 L - 103.6
$\delta v_x$ ft/sec	H - 4.36 L - 2.09	H - 0.097 L - 0.107	H - 1.043 L - 0.257
$\delta v_y$ ft/sec	H - 4.46 L - 2.45	H - 3.16 L - 3.33	H - 4.58 L - 2.25
$\delta v_z$ ft/sec	H - 0.537 L - 0.537	H - 0.365 L - 0.364	H - 0.355 L - 0.354
$\delta \phi_x$ millirad	H - 0.168 L - 0.165	H - 0.184 L - 0.184	H - 0.166 L - 0.164
$\delta \phi_y$ millirad	H - 0.182 L - 0.180	H - 0.137 L - 0.138	H - 0.160 L - 0.159
$\delta \phi_z$ millirad	H - 6.45 L - 5.61	H - 5.55 L - 5.59	H - 5.66 L - 4.94

Table XIV

Plant + Gyro + Accelerometer + Doppler Error States  
Straight and Level RMS Errors

Values labeled H are high values and values labeled L are low values at data time. Initial condition values are taken from the total reference system model.

Variable (units)	Initial Condition (t=7200 sec)	Decoupled 17-State Filter	
		(t=8640 sec)	(t=10,020 sec)
$\delta x$ ft	H - 2616.3 L - 574.6	H - 778.2 L - 743.0	H - 870.3 L - 475.4
$\delta y$ ft	H - 2404.7 L - 537.0	H - 1376.8 L - 1214.1	H - 2987.0 L - 574.7
$\delta z$ ft	H - 259.4 L - 259.4	H - 94.3 L - 93.1	H - 103.4 L - 103.4
$\delta v_x$ ft/sec	H - 4.36 L - 2.09	H - 0.498 L - 0.382	H - 0.947 L - 0.837
$\delta v_y$ ft/sec	H - 4.46 L - 2.45	H - 3.41 L - 3.25	H - 4.60 L - 2.29
$\delta v_z$ ft/sec	H - 0.537 L - 0.537	H - 0.365 L - 0.364	H - 0.355 L - 0.354
$\delta \phi_x$ millirad	H - 0.168 L - 0.165	H - 0.183 L - 0.183	H - 0.166 L - 0.164
$\delta \phi_y$ millirad	H - 0.182 L - 0.180	H - 0.138 L - 0.137	H - 0.155 L - 0.154
$\delta \phi_z$ millirad	H - 6.45 L - 5.61	H - 5.61 L - 5.57	H - 5.67 L - 4.96

Table XV

Plant + Gyro + Accelerometer + Doppler + Altimeter  
Error States Straight and Level RMS Errors

Values labeled H are high values and values labeled L are low values at data time. Initial condition values are taken from the total reference system model.

Variable (units)	Initial Condition (t=7200 sec)	Decoupled 17-State Filter	
		(t=8640 sec)	(t=10,020 sec)
$\delta x$ ft	H - 2616.3 L - 574.6	H - 778.2 L - 743.1	H - 870.3 L - 475.4
$\delta y$ ft	H - 2404.7 L - 537.0	H - 1376.8 L - 1214.1	H - 2987.2 L - 574.7
$\delta z$ ft	H - 259.4 L - 259.4	H - 117.0 L - 116.1	H - 109.0 L - 108.9
$\delta v_x$ ft/sec	H - 4.36 L - 2.09	H - 0.498 L - 0.382	H - 0.947 L - 0.838
$\delta v_y$ ft/sec	H - 4.46 L - 2.45	H - 3.41 L - 3.25	H - 4.60 L - 2.29
$\delta v_z$ ft/sec	H - 0.537 L - 0.537	H - 0.359 L - 0.359	H - 0.359 L - 0.358
$\delta \phi_x$ millirad	H - 0.168 L - 0.165	H - 0.183 L - 0.183	H - 0.166 L - 0.164
$\delta \phi_y$ millirad	H - 0.182 L - 0.180	H - 0.138 L - 0.137	H - 0.155 L - 0.154
$\delta \phi_z$ millirad	H - 6.45 L - 5.61	H - 5.61 L - 5.57	H - 5.67 L - 4.96

Table XVI

Plant Error States Maneuvering RMS Errors

Values labeled H are high values and values labeled L are low values at data time. Initial condition values are taken from the total reference system model.

Variable (units)	Initial Condition (t=7200 sec)	Decoupled 17-State Filter	
		(t=8640 sec)	(t=10,020 sec)
$\delta x$ ft	H - 2616.3 L - 574.6	H - 1680.4 L - 1493.7	H - 2428.7 L - 561.6
$\delta y$ ft	H - 2404.7 L - 537.0	H - 1692.3 L - 1497.8	H - 2009.4 L - 517.4
$\delta z$ ft	H - 259.4 L - 259.4	H - 63.8 L - 62.9	H - 803.4 L - 803.0
$\delta v_x$ ft/sec	H - 4.36 L - 2.09	H - 4.12 L - 3.96	H - 3.76 L - 1.77
$\delta v_y$ ft/sec	H - 4.46 L - 2.45	H - 4.41 L - 4.28	H - 3.37 L - 1.91
$\delta v_z$ ft/sec	H - 0.537 L - 0.537	H - 0.325 L - 0.324	H - 0.325 L - 0.325
$\delta \phi_x$ millirad	H - 0.168 L - 0.165	H - 0.095 L - 0.093	H - 0.058 L - 0.055
$\delta \phi_y$ millirad	H - 0.182 L - 0.180	H - 0.130 L - 0.129	H - 0.072 L - 0.069
$\delta \phi_z$ millirad	H - 6.45 L - 5.61	H - 3.74 L - 3.71	H - 2.26 L - 1.99

Table XVII

Plant + Gyro Error States Maneuvering RMS Errors

Values labeled H are high values and values labeled L are low values at data time. Initial condition values are taken from the total reference system model.

Variable (units)	Initial Condition (t=7200 sec)	Decoupled 17-State Filter	
		(t=8640 sec)	(t=10,020 sec)
$\delta x$ ft	H - 2616.3 L - 574.6	H - 1322.5 L - 1201.9	H - 1434.8 L - 507.4
$\delta y$ ft	H - 2404.7 L - 537.0	H - 1497.6 L - 1341.1	H - 1626.5 L - 509.6
$\delta z$ ft	H - 259.4 L - 259.4	H - 63.8 L - 62.1	H - 80.2 L - 80.2
$\delta v_x$ ft/sec	H - 4.36 L - 2.09	H - 2.93 L - 2.88	H - 3.17 L - 1.98
$\delta v_y$ ft/sec	H - 4.46 L - 2.45	H - 4.07 L - 3.98	H - 3.59 L - 2.27
$\delta v_z$ ft/sec	H - 0.537 L - 0.537	H - 0.324 L - 0.324	H - 0.325 L - 0.324
$\delta \phi_x$ millirad	H - 0.168 L - 0.165	H - 0.059 L - 0.057	H - 0.067 L - 0.065
$\delta \phi_y$ millirad	H - 0.182 L - 0.180	H - 0.056 L - 0.053	H - 0.091 L - 0.090
$\delta \phi_z$ millirad	H - 6.45 L - 5.61	H - 4.91 L - 4.89	H - 4.40 L - 3.88

Table XVIII

Plant + Gyro + Accelerometer Error States  
Maneuvering RMS Errors

Values labeled H are high values and values labeled L are low values at data time. Initial condition values are taken from the total reference system model.

Variable (units)	Initial Condition (t=7200 sec)	Decoupled 17-State Filter	
		(t=8640 sec)	(t=10,020 sec)
$\delta x$ ft	H - 2616.3 L - 574.6	H - 1120.7 L - 1027.8	H - 1347.1 L - 496.6
$\delta y$ ft	H - 2404.7 L - 537.0	H - 1227.5 L - 1112.0	H - 1581.2 L - 502.7
$\delta z$ ft	H - 259.4 L - 259.4	H - 95.0 L - 93.7	H - 103.1 L - 103.1
$\delta v_x$ ft/sec	H - 4.36 L - 2.09	H - 2.67 L - 2.60	H - 2.77 L - 1.61
$\delta v_y$ ft/sec	H - 4.46 L - 2.45	H - 3.68 L - 3.59	H - 3.32 L - 2.06
$\delta v_z$ ft/sec	H - 0.537 L - 0.537	H - 0.365 L - 0.364	H - 0.352 L - 0.352
$\delta \phi_x$ millirad	H - 0.168 L - 0.165	H - 0.159 L - 0.158	H - 0.156 L - 0.155
$\delta \phi_y$ millirad	H - 0.182 L - 0.180	H - 0.158 L - 0.157	H - 0.166 L - 0.166
$\delta \phi_z$ millirad	H - 6.45 L - 5.61	H - 4.88 L - 4.86	H - 4.28 L - 3.78



Table XIX

Plant + Gyro + Accelerometer + Doppler Error States  
Maneuvering RMS Errors

Values labeled H are high values and values labeled L are low values at data time. Initial condition values are taken from the total reference system model.

Variable (units)	Initial Condition (t=7200 sec)	Decoupled 17-State Filter	
		(t=8640 sec)	(t=10,020 sec)
$\delta X$ ft	H - 2616.3 L - 574.6	H - 1181.4 L - 1078.7	H - 1482.4 L - 505.2
$\delta Y$ ft	H - 2404.7 L - 537.0	H - 1245.9 L - 1127.0	H - 1593.8 L - 503.6
$\delta Z$ ft	H - 259.4 L - 259.4	H - 95.0 L - 93.7	H - 103.1 L - 103.1
$\delta V_x$ ft/sec	H - 4.36 L - 2.09	H - 2.77 L - 2.69	H - 2.89 L - 1.65
$\delta V_y$ ft/sec	H - 4.46 L - 2.45	H - 3.69 L - 3.60	H - 3.33 L - 2.05
$\delta V_z$ ft/sec	H - 0.537 L - 0.537	H - 0.365 L - 0.364	H - 0.353 L - 0.352
$\delta \phi_x$ millirad	H - 0.168 L - 0.165	H - 0.159 L - 0.159	H - 0.156 L - 0.155
$\delta \phi_y$ millirad	H - 0.182 L - 0.180	H - 0.158 L - 0.158	H - 0.167 L - 0.167
$\delta \phi_z$ millirad	H - 6.45 L - 5.61	H - 4.90 L - 4.88	H - 4.29 L - 3.78

Table XX

Plant + Gyro + Accelerometer + Doppler + Altimeter  
Error States    Maneuvering    RMS    Errors

Values labeled H are high values and values labeled L are low values at data time. Initial condition values are taken from the total reference system model.

Variable (units)	Initial Condition (t=7200 sec)	Decoupled 17-State Filter	
		(t=8640 sec)	(t=10,020 sec)
$\delta x$ ft	H - 2616.3 L - 574.6	H - 1181.4 L - 1078.7	H - 1482.4 L - 505.2
$\delta y$ ft	H - 2404.7 L - 537.0	H - 1245.9 L - 1127.0	H - 1593.8 L - 503.6
$\delta z$ ft	H - 259.4 L - 259.4	H - 117.5 L - 116.6	H - 108.7 L - 108.5
$\delta v_x$ ft/sec	H - 4.36 L - 2.09	H - 2.77 L - 2.69	H - 2.89 L - 1.65
$\delta v_y$ ft/sec	H - 4.46 L - 2.45	H - 3.69 L - 3.60	H - 3.33 L - 2.05
$\delta v_z$ ft/sec	H - 0.537 L - 0.537	H - 0.359 L - 0.359	H - 0.357 L - 0.356
$\delta \phi_x$ millirad	H - 0.168 L - 0.165	H - 0.159 L - 0.159	H - 0.156 L - 0.155
$\delta \phi_y$ millirad	H - 0.182 L - 0.180	H - 0.158 L - 0.158	H - 0.167 L - 0.167
$\delta \phi_z$ millirad	H - 6.45 L - 5.61	H - 4.90 L - 4.88	H - 4.29 L - 3.78

the plots for each of the nine basic plant error states as the complexity of the system reference model is increased to include the gyro errors, accelerometer errors, Doppler errors, and the altimeter error. Tables XI through XV give the data for straight and level flight while Tables XVI through XX pertain to the maneuvering flight profile. The high values on the initial conditions are given only as a reference to aid in visualizing the trend of the average values between the high and low data points. This means that an indication of the general shape of the plots can be obtained by connecting the average values at each data point listed. An example of this technique is shown in Figure 70 below.

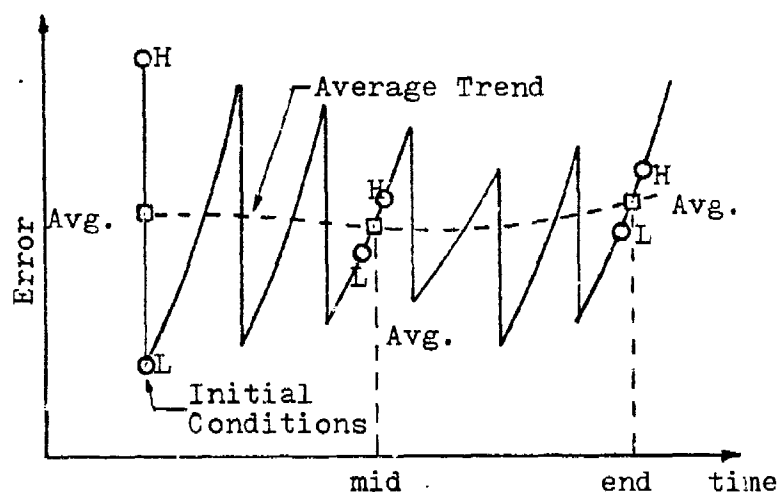


Figure 70. Average Error Trend

Tables XXI and XXII show the error budget for straight and level and maneuvering flight respectively. The error budget is shown as the percentage contribution to the total error for each system reference model configuration. An

Table XXI

Percent Contribution to Variable Error (Straight and Level Flight)  
(t = 10,020 seconds)

Values labeled H are high values and values labeled L are low values at data time.

System Configuration	Variable									
	$\delta X$	$\delta Y$	$\delta Z$	$\delta V_x$	$\delta V_y$	$\delta V_z$	$\delta \phi_x$	$\delta \phi_y$	$\delta \phi_z$	
Plant	H	136.33	118.13	163.35	137.25	87.25	3.56	51.48	35.41	59.61
	L	105.18	105.86	157.72	208.72	79.69	5.66	50.51	34.96	54.23
Plant + Gyro	H	-45.74	-13.58	-133.88	-.11	18.89	24.72	5.94	5.61	42.04
	L	-4.66	-3.17	-128.22	-48.65	30.13	21.45	4.15	5.90	47.20
Plant + Gyro + Accelerometer	H	-13.05	-3.90	65.55	-26.93	-6.67	70.54	42.64	62.28	-1.90
	L	-2.23	-2.61	65.68	-129.84	-11.36	71.69	45.45	62.08	-1.83
Plant + Gyro + Accelerometer + Doppler	H	22.46	-.64	-.16	-10.21	.53	.11	-.06	-3.30	.25
	L	1.71	-.08	-.16	69.78	1.54	.10	-.11	-2.94	.40
Complete System Reference Model	H	0.00	0.00	5.14	0.00	0.00	1.07	0.00	0.00	0.00
	L	0.00	0.00	4.98	0.01	0.00	1.10	0.00	0.00	0.00
Total Error Basis	H	870.30	2987.20	109.00	0.947	4.60	0.359	0.166	0.155	5.67
	L	475.40	574.70	108.90	0.838	2.29	0.358	0.164	0.154	4.96

Table XXII

Percent Contribution to Variable Error (Maneuvering Flight)  
(t = 10,020 seconds)

Values labeled H are high values and values labeled L are low values at data time.

System Configuration	$\delta x$	$\delta y$	$\delta z$	$\delta v_x$	Variable $\delta v_y$	$\delta v_z$	$\delta \phi_x$	$\delta \phi_y$	$\delta \phi_z$
Plant	H	163.83	126.08	73.90	130.11	101.38	91.05	37.36	43.16
	L	111.17	102.74	74.05	107.31	93.24	91.25	35.18	41.29
Plant + Gyro	H	-67.05	-24.03	-.13	-20.37	6.61	-.20	5.34	11.46
	L	-10.75	-1.55	-.14	12.87	17.84	-.18	6.49	12.66
Plant + Gyro + Accelerometer	H	-5.91	-2.84	21.07	-14.01	-8.15	7.97	57.23	45.08
	L	-2.13	-1.37	21.09	-22.79	-10.45	7.75	58.27	45.71
Plant + Gyro + Accelerometer + Doppler	H	9.13	.79	.01	4.27	.16	.11	.07	.30
	L	1.71	.18	.01	2.61	-.63	.09	.06	.34
Complete System Reference Model	H	0.00	0.00	5.15	0.00	0.00	1.07	0.00	0.00
	L	0.00	0.00	4.99	0.00	0.00	1.09	0.00	0.00
Total Error Basis	H	1482.40	1593.80	103.10	2.89	3.33	0.353	0.156	0.167
	L	505.20	503.60	103.10	1.65	2.05	0.352	0.155	0.167

increase in the error is shown as a positive percentage and a reduction in the error is shown as a negative percentage. For example, referring to Table XXI, the plant model alone contributes 136.33% of the high value of position error based on a complete system reference model error of 870.3 feet at 10,020 seconds. By adding the gyro models the error is reduced 45.74% and addition of the accelerometer models reduces to error another 13.05%. When the Doppler model is added the error is increased by 22.46% and the altimeter model has negligible affect on the x position error. The total x position error is then 100% of the 870.3 feet used as a base value.

These tables show no real consistency in the error contributions between the straight and level case and maneuvering case with one exception. The Doppler generally contributes a larger portion of the total error during maneuvering flight than it does in straight and level flight.

VII. Conclusions and RecommendationsConclusions

Based on the material presented in this thesis, as well as knowledge gained throughout the study, the following conclusions are drawn:

1. The decoupled 17-state filter provides adequate performance during straight and level flight over land but allows the x and y velocity and the heading errors to reach values approximately twice those of the optimal filter.

2. Although level channel velocity errors increase about twofold during a maneuvering flight profile, the decoupled 17-state filter performance is not significantly degraded in this environment.

3. The separate contributions of the various error sources to the total error budget cannot be readily determined as a function of the flight environment. However, the Doppler error contribution appears to be greater during maneuvering flight.

4. Finally, it should be emphasized again that this type of covariance analysis is very sensitive to (a) the initial conditions of the covariance matrix,  $P(0)$ , (b) erroneous system reference models, and (c) the dynamics of the flight profile.

Recommendations

The following recommendations are made for continued

study in the subject area of this thesis and for improvement in the existing computer programs:

1. A terrain following flight profile should be investigated with the associated variations in g loading.

2. Filter performance should be investigated during partial siding system failures such as Doppler and/or position fix radar inoperative.

3. The filter effectiveness should be tested for various values of Q matrix and R matrix noises. This is especially necessary with the trend toward underestimation of certain errors after  $1\frac{1}{2}$  hours of flight, indicating that some Q terms are too small, and that the proposed design used a large P(0) rather than an increased Q to tune the filter. Longer flight times will demonstrate the proper tuning values.

4. Another area of interest would be the effect of staggered measurement updates rather than regular intervals. This would more closely approach an actual flight environment.



# Bibliography

1. Kayton, M. and W. Fried. Avionics Navigation Systems. New York: John Wiley and Sons, Inc., 1969.
2. Maybeck, P. S. The Kalman Filter, An Introduction for Potential Users. TM - 72-3. Wright-Patterson Air Force Base, Ohio: Air Force Flight Dynamics Laboratory, 1972.
3. Meditch, J. S. Stochastic Optimal Linear Estimation and Control. New York: McGraw-Hill, 1969.
4. Maybeck, P. S. Kalman Filtering Applied to Inertial Systems. Course Notes from EE 7.65, Air Force Institute of Technology, Wright-Patterson Air Force Base, Ohio, 1974.
5. "A Short Course on Kalman Filter Theory and Application." The Analytic Science Corporation, Reading, Massachusetts, 1971.
6. Wrigley, W. et. al. Gyroscopic Theory, Design and Instrumentation. Massachusetts: The M.I.T. Press, 1969.
7. Musick, S. A Users Guide to Profgen, A Flight Profile Generator. Unpublished. Wright-Patterson Air Force Base, Ohio: Air Force Avionics Laboratory, 1973.
8. Leondes, C. T. Guidance and Control of Aerospace Vehicles. New York: McGraw-Hill, 1963.
9. Brockstein, A. J. Analytical Differences Between Pinson and Raides Inertial System Error Models. File AJB - 6903-032. Litton Industries, Calif: Guidance and Control Systems Division, 1969.
10. Asher, R. B. and R. M. Reeves. Performance Evaluation of Suboptimal Filters. Unpublished. Wright-Patterson Air Force Base, Ohio: Air Force Avionics Laboratory, 1972.
11. Clarke, A. B. and R. L. Disney. Probability and Random Processes for Engineers and Scientists. New York: John Wiley and Sons, Inc., 1970.
12. Brockstein, A. J. and J. T. Kouba. Derivation of Free Inertial, General Wander Azimuth Mechanization

Equations. Publication No. 9176A, Litton Systems, Inc., June 1969.

13. Maybeck, P. S. Filter Design for a Tacon-Aided Bore-Inertial System with ILS Smoothing Capability.  
AFFDL - TM - 74 - 52. Wright-Patterson Air Force Base, Ohio: Air Force Flight Dynamics Laboratory, 1974.

Vita

Jerry Edward Hammett was born on 29 September 1940 in Shawnee, Oklahoma to Thomas E. and Helen A. (Sawyer) Hammett. He graduated from Northwest Classen (Oklahoma City) Highschool in 1958 and received a Bachelor of Science degree in Electrical Engineering from Oklahoma University in 1963. He was commissioned a 2/Lt. in the United States Air Force through the AFROTC program upon graduation and was assigned as a Research and Development Electronics Engineer to the Flight Test Division of Aeronautical Systems Division at Wright-Patterson AFB, Ohio for four years. He then completed both Undergraduate Navigator Training and Navigator/Bombardier Training and was assigned to the 416th Bomb Wing (SAC) at Griffiss AFB, New York for five years. He was a Stan/Eval navigator for two years and flew 160 combat missions in SEA as a B-52 Radar Navigator. Major Hammett entered the Air Force Institute of Technology Resident School of Engineering in pursuit of a Master's Degree in Electrical Engineering, Guidance and Control in June 1973. Major Hammett is married and has two sons.

Permanent Address: 3405 N.W. 42nd  
Oklahoma City, Oklahoma

This thesis was typed by Martha Hammett.